

Synthesis, Characterization and Surface Group Quantification of Functionalized Polymer Particles for Signal Amplification Strategies

INAUGURAL-DISSERTATION

to obtain the academic degree
DOCTOR RERUM NATURALIUM (DR. RER. NAT.)

submitted to
The Department of Biology, Chemistry, and Pharmacy
OF FREIE UNIVERSITÄT BERLIN

by
NITHIYA NIRMALANANTHAN-BUDAU
from BERLIN-SPANDAU

2019

This work was prepared under supervision of
DR. UTE RESCH-GENGER
(BUNDESANSTALT FÜR MATERIALFORSCHUNG UND -PRÜFUNG BERLIN)

in the time frame of
MARCH 2015 TO APRIL 2019

at the
BUNDESANSTALT FÜR MATERIALFORSCHUNG UND -PRÜFUNG

I hereby declare that this doctoral studies was prepared autonomously and that no illegal help was used. Contributions of others, e.g., content, quotes, or figures are indicated by referring to the original work.

Berlin, April 2019 _____ (Nithiya Nirmalananthan-Budau)

1 st Reviewer	DR. UTE RESCH-GENGER
2 nd Reviewer	PROF. DR. SIEGFRIED EIGLER
Date of Defence	29.07.2019

Danksagung

An dieser Stelle möchte ich meinen Dank an diejenigen richten, die mir geholfen haben diese Arbeit anzufertigen. Beginnen möchte ich hier mit Dr. Ute Resch-Genger für die Vergabe des spannenden Forschungsthemas, für die vielen Möglichkeiten meine Arbeit auf unterschiedlichsten Konferenzen als Poster- oder sogar als Vortragsbeiträge zu präsentieren, für ihre Unterstützung beim Publizieren der Ergebnisse und auch für die vielen spannenden Kooperationspartner und -themen. Ebenso danke ich ihr für die Möglichkeit, dass ich während meiner Doktorarbeit Weiterbildungen in der Qualitätssicherung und in der Nutzung von Origin machen konnte. Einen sehr großen Dank möchte ich an sie richten für ihren Rat, ihre konstruktiven Kritiken, ihre unermüdliche Unterstützung bei der Anfertigung dieser Arbeit und für ihr Vertrauen kleinere organisatorische Aufgaben, sowie Betreuungsaufgaben an mich zu übergeben.

Herrn Prof. Dr. Siegfried Eigler möchte ich für die schnelle und unkomplizierte Übernahme der Zweitbegutachtung meiner Arbeit und die fachliche Unterstützung bei der Anfertigung der Doktorarbeit danken.

Ein besonderer Dank gilt meinen direkten Betreuern Herrn Dr. Thomas Behnke, Frau Dr. Katrin Hoffmann und Herrn Dr. Daniel Geißler sowie Dipl.-Chem. Marko Moser und Dr. Bastian Rühle, die mich mit sehr viel Engagement, fachlichen Erklärungen und Diskussionen in den letzten vier Jahren bei der Anfertigung dieser Arbeit und teilweise auch vor dieser Zeit während der Masterarbeit schon unterstützten. Bei Rückschlägen ermutigten und unterstützten sie mich beim Lösen der Probleme und standen mir tagtäglich mit Rat und Tat zur Seite. Dr. Daniel Geißler und Dr. Bastian Rühle danke ich zusätzlich für die Korrektur einzelner Abschnitte dieser Arbeit.

Frau Maria Richter, Frau Dr. Jutta Pauli, Herrn Arne Güttler und Herrn Thomas Schneider danke ich für die Geräte-Einweisungen, Chemikalienbestellungen, Geräte-Kalibrierungen, Laborsicherheit, Qualitätssicherung, also im Prinzip für die gesamte Laborinfrastruktur, die ein analytisch akkurates Arbeiten erst ermöglichte.

Ein weiterer großer Dank gilt meinen Kollegen und mittlerweile guten Freunden Lorena D., Maysoon S., Sebastian R., Daniel K., Marko M., Norman S., Pablo Q. und Marco K. Euch danke ich nicht nur für die tollen Frühstücks-, Cafe- und Mittagspausen, sondern auch für eure Ratschläge, Ideen und Lösungsansätze. Ihr habt es mir ermöglicht mit viel Spaß und Freude diese Zeit zu erleben. An dieser Stelle möchte ich ebenfalls der gesamten Arbeitsgruppe 1.2 (ehemals 1.10) Biophotonik meinen Dank für die gute Arbeitsatmosphäre aussprechen. Meinen Auszubildenden/Hilfswissenschaftlern Christopher, Maurice, Martin und Marvin,

meiner Bachelorstudentin Ella und meiner Praktikantin Shreya möchte ich nicht nur meinen Dank für die Unterstützung im Labor aussprechen, sondern auch für die Erfahrungen, die ich mit euch zusammen sammeln konnte.

Für die vielen tollen und spannenden internen Zusammenarbeiten danke ich weiterhin Dipl.-Chem. Marko Moser, Dr. Alexander Roloff, Dr. Marc Wegmann und Dr. Harald Tschiche. Darüber hinaus danke ich Prof. Dr. Thomas J.J. Müller, Dr. Charlotte Gers-Panther, Dr. Melanie Denßen von der Heinrich-Heine-Universität, Dr. Andreas Schäfer und Prof. Dr. Beate Paulus von der Freien Universität und Prof. Dr. Anke Krüger, Johannes Ackermann MSc. von der Universität Würzburg für stimulierende Zusammenarbeiten.

Für einen regelkonformen, flüssigen und reibungslosen Ablauf der bürokratischen und technischen Angelegenheiten während meiner Arbeit danke ich Frau Christin Heinrich, Frau Grit Ostermann, Frau Julianne Schäfer und Frau Anka Kohl.

Last but not least möchte ich meiner Familie danken. Insbesondere meinen Eltern, die mir von den ersten Schritten als kleines Kind bis heute den Rücken stärken und mir mit Rat und Tat bei Tag und Nacht zur Seite stehen, die mich lehrten nie aufzugeben und immer ein Ziel vor Augen zu haben. Ganz besonders danken möchte ich meinem Freund, meiner besseren Hälfte, meinem Mann Johannes Horst für seinen unermüdlichen und selbstlosen Beistand während meiner gesamten bisherigen akademischen Laufbahn, für seine ruhige Art (mein Ruhepol), für seinen Durchblick, für seine ehrlichen Worte, und natürlich auch für die Durchsicht meiner gesamten Arbeiten während meiner chemischen Laufbahn.

VIELEN HERZLICHEN DANK EUCH ALLEN!!!

Contents

Abstract	vii
Kurzzusammenfassung	ix
1 Introduction & Motivation	1
1.1 Introduction to nanoparticles	1
1.2 Application relevant properties of PNP	3
1.2.1 Composition of PNP	3
1.2.2 Size and size distribution of PNP	3
1.2.3 Shape of PNP	4
1.2.4 Optical properties of PNP (fluorescent PNP)	4
1.2.4.1 Aggregation induced property changes and aggregation-induced emission (AIE) PNP	6
1.2.5 Surface functional groups (FGs) of PNP	7
1.2.5.1 Stability of PNP	7
1.2.5.2 Functionalization of PNP	8
1.2.5.3 Biocompatibility of PNP	8
1.2.5.4 Toxicity of PNP	9
1.3 Motivation and objectives	10
2 Synthesis, Characterization and Quantification Methods for PNP	11
2.1 Synthesis of PNP	11
2.1.1 Preparation of fluorescent PNP and AIE-PNP	13
2.2 Characterization of PNP	15
2.2.1 Characterization of size, size distribution and shape	15
2.2.1.1 Scanning electron microscopy (SEM)	15
2.2.1.2 Dynamic light scattering (DLS)	16
2.2.2 Surface charge	17
2.2.3 Optical properties	17
2.2.3.1 Absorption	18
2.2.3.2 Emission	18
2.2.3.3 Fluorescence quantum yield (ϕ_f)	19
2.2.3.4 Fluorescence lifetime (τ)	19
2.2.4 Surface FGs	20
2.2.4.1 Conductometric titration	21
2.2.4.2 Optical assays	23
2.2.4.3 BCA assay for protein quantification	24
2.2.4.4 Inductively coupled plasma optical emission spectroscopy (ICP-OES)	25
2.2.4.5 Quantitative nuclear magnetic resonance (qNMR)	26

3	Results: Publications and Manuscripts	29
3.1	Major contributions	29
3.1.1	Crystallization and Aggregation-Induced Emission in a Series of Pyrrolidinylnylvinylquinoxaline Derivatives	29
3.1.2	Multimodal Cleavable Reporters vs Conventional Labels for Optical Quantification of Accessible Amino and Carboxy Groups on Nano- and Microparticles	41
3.1.3	Multimodal Cleavable Reporters for Quantifying Carboxy and Amino Groups on on Organic and Inorganic Nanoparticles	63
3.2	Minor contributions	90
3.2.1	3-Piperazinyl propenylidene indolone merocyanines: consecutive Three-component Synthesis and Electronic Properties of Solid-state Luminophores with AIE Properties	90
3.2.2	Quantification of Aldehydes on Polymeric Microbead Surfaces via Catch and Release of Reporter Chromophores	149
4	Synopsis of the Results, Conclusion & Outlook	171
5	Reference	177
A	Appendix	187
A.1	Publications and planned publications	187
A.2	Conference contributions	188

Abbreviations and Glossary

N-APPA *N*-(aminoethyl)-3-(pyridin-2-yl)disulfanylpropanamide

ACQ aggregation-caused quenching

AFM atomic force microscopy

AIE aggregation-induced emission

APTES (3-aminopropyl)triethoxysilane

BCA bicinchoninic acid

BDP-hzd BODIPY-hydrazide

CLSM confocal laser scanning microscope

DCC dicyclohexylcarbodiimide

DIC diisopropylcarbodiimide

DLS dynamic light scattering

EDC 1-ethyl-3-(3-dimethylaminopropyl)carbodiimide

FDA Food and Drug Administration

FG functional group

FLIM fluorescence lifetime imaging microscopy

FRET fluorescence resonance energy transfer

FTIR Fourier-transform infrared spectroscopy

IC internal conversion

ICP-MS inductively coupled plasma mass spectrometry

ICP-OES inductively coupled plasma optical emission spectroscopy

IS internal standard

ISC intersystem crossing

MSN mesoporous silica nanoparticles

NHS *N*-hydroxysuccinimide
NMR nuclear magnetic resonance
NP nanoparticle
NTA nanoparticle tracking analysis
PAA polyacrylic acid
PDPH 3-(2-pyridyldithio)propionyl hydrazide
PGA poly(glycolic acid)
PLA poly(lactic acid)
PMMA poly(methyl methacrylate)
PNP polymer nanoparticles
PSP polystyrene particles
PVC poly(vinyl chloride)
RAFT reversible addition-fragmentation chain transfer
ROS reactive oxygen species
SAXS small-angle X-ray scattering
SEM scanning electron microscopy
SPDP *N*-succinimidyl-3-(2-pyridyldithio) propionate
sulfo-NHS *N*-hydroxysulfosuccinimide
TCEP tris(2-carboxyethyl)phosphine hydrochloride
TCSPC time-correlated single-photon counting
TEM transmission electron microscopy
TSEM transmission scanning electron microscopy
XPS X-ray photoelectron spectroscopy
XRD X-ray diffraction

Abstract

Polymer nanoparticles (PNP) are increasingly used as tools in (bio)analytics. Typical applications of PNP include carriers for drugs, carriers for dye molecules for signal amplification in optical assays, nanosensors and targeted probes for bioimaging studies. These applications in life sciences impose stringent requirements on particle size, size distribution, morphology, colloidal stability, biocompatibility, optical properties, and ease of surface functionalization with, for example, targeting ligands, sensor molecules, and linkers.

PNP, including the polystyrene particles (PSP) which are in the focus of this work, are non-fluorescent by nature but can be made fluorescent with the aid of luminophores such as organic dyes. Fluorescent PNP can be obtained by coupling reactive fluorophores to the surface groups of the PNP or by encapsulation of fluorophores into the PNP matrix. The latter approach is particularly attractive due to its versatility since the encapsulation into preformed PNP does not require luminophores with reactive functional groups (FGs), but rather only requires hydrophobic luminophores. Moreover, the fluorophores are protected from the potentially fluorescence quenching environment surrounding the PNP matrix and the reactive groups on the PNP surface can be exclusively used for the attachment of targeting ligands. Dye loading of PNP typically requires a dye-specific optimization of the loading concentration with respect to signal strength as conventional dyes commonly form barely emissive or even non-fluorescent aggregates at high loading concentrations. Exceptions exist, which are dyes with propeller-like groups that show aggregation-induced emission (AIE). These dyes can be loaded with high concentrations into PNP without detrimental fluorescence quenching effects and can even exhibit fluorescence and hence signal amplification upon aggregation. Due to these attractive properties, AIE dyes for use in PNP were investigated. The spectroscopic properties of different AIE dye derivatives were systematically studied in organic solvents, solvent–water mixtures, and in the solid state. Dyes with optimal performance were entrapped in PSP. The staining of PSP with these AIE dyes resulted in a considerable increase in the dye fluorescence quantum yield and lifetime, reflecting the combined influence of the restricted molecular motion and the reduced polarity of the dye microenvironment.

Functionalization of undoped and dye loaded PNP with, for example, targeting ligands requires knowledge of the chemical nature and total amount of the surface groups as well as the amount of surface FGs accessible for coupling reactions such as the conjugation of biomolecules. These numbers can differ considerably depending on factors including particle morphology and sterical constraints. Ideal methods for surface group quantification should

be robust, reliable, and fast. Moreover, they should not require expensive instrumentation and should be versatile to enable the characterization of a broad variety of particle systems independent of their optical properties, including systems that scatter or include systems with encoded dyes. For this respect, we studied a variety of optical assays for the quantification of carboxy and amino surface groups commercial and custom-made particles with varying surface group densities. We performed these studies using both conventional reporters such as fluorescein derivatives, Fluram, or IR 797 as well as synthetically customized cleavable labels. Special emphasis was dedicated to the development of a platform of cleavable and multimodal labels which consist of a suitable reactive group such as NHS-esters or amine, a quantitatively cleavable linker such as disulfide, and an optically active moiety such as 2-thiopyridone for optical assays. Conventional reporters are measured when bound to the particle surface, which renders the resulting optical signals prone to distortions by scattering and interferences from encoding dyes. In contrast, these cleavable labels can be detected photometrically or fluorometrically in the supernatant after quantitative cleavage of the linker. Moreover, the linker unit is designed in such a way that the products of the cleaved linkers remaining at the particle surface can also be detected optically. In addition, the presence of a heteroatom such as sulfur, nitrogen or fluorine in the reporter and/or the linker can be detected by an analytical method relying on a different measurement principle. This allows for straightforward validation by method comparison with, for instance, ICP-OES. Thereby, FGs on a broad variety of different particles such as PNP, silica nanoparticles (NPs), and metal particles can also be quantified.

Kurzzusammenfassung

Polymernanopartikel (PNP) werden in der Bioanalytik zunehmend als Trägermaterial für Medikamente oder Farbstoffmoleküle, die als Reporter zur Signalverstärkung in optischen Assays, als Nanosensor oder als Zielsonden für die Bildgebung eingesetzt werden, verwendet. Partikelanwendungen in der Material- und Lebenswissenschaft hängen stark von der Größe, Größenverteilung, Form, Dispersionsstabilität, Bioverträglichkeit, optischen Eigenschaften sowie der Oberflächenfunktionalisierung mit beispielsweise Zielliganden, Sensormolekülen und Linkern, ab.

PNP, im speziellen hier in dieser Arbeit Polystyrolpartikel (PSP), sind von Natur aus nicht emissiv, durch Anbindung von reaktiven Farbstoffen an den Oberflächenfunktionsgruppen oder durch Einlagerung von Farbstoffen in die Polymermatrix können dennoch fluoreszierende Partikel realisiert werden. Letztere Methode wird vorallem dadurch attraktiv, dass keine reaktiven Gruppen an den hydrophoben Farbstoffen notwendig sind. Außerdem können die Farbstoffe in der Polymermatrix vor der Partikelumgebung und vor Emissionsauslöschungen geschützt werden und die Oberflächenfunktionsgruppen stehen für anderweitige Anbindungen von Zielliganden zu Verfügung. Die Einlagerung von Farbstoffen benötigt eine farbstoffspezifische Optimierung der Beladungskonzentration, um ein optimales Emissionssignal zu erhalten. Während konventionelle Farbstoffe beim Einlagern von hohen Konzentrationen wenig bis nicht fluoreszierende Aggregate bilden, können verdrillte bzw. Farbstoffe mit propellerartigen Gruppen (AIE Farbstoffe), in hohen Konzentrationen in PNP eingelagert werden. Dabei kommt es statt Auslöschungseffekten zu einer Emissionssignalverstärkung. Aus diesem Grund wurden in dieser Arbeit verschiedene AIE Farbstoffderivate systematisch spektroskopisch in organischen Lösemitteln, in Lösemittel-Wasser Gemischen und als Feststoff untersucht und Farbstoffe mit optimalen Eigenschaften in PSP eingelagert. Eingelagerte Farbstoffe in PSP zeigen eine erhöhte Quantenausbeute und eine verlängerte Lebensdauer, was durch die Kombination der Einschränkung der Molekülbewegung und der Reduzierung der Polarität in der Farbstoffumgebung erreicht wird.

Die Funktionalisierung von sowohl unbeladenen, als auch mit Farbstoffen beladenen Partikeln mit zum Beispiel Biomolekülen, benötigt die Kenntnis der chemischen Natur, der Gesamtanzahl an Funktionsgruppen (FGs), sowie der tatsächlich zugänglichen FGs, die für anschließende Kupplungsreaktionen wichtig sind. Diese Anzahl hängt stark von der Partikelform und der sterischen Einschränkung ab. Idealerweise sind die Analysemethoden robust, vertrauenswürdig, schnell, mit kostengünstigen Instrumenten durchführbar und für eine breite Vielfalt an Partikelsystemen einsetzbar, unabhängig von deren optischen Eigenschaften wie Streu-

ung oder die Anwesenheit von eingelagerten Farbstoffen. In diesem Zusammenhang haben wir verschiedene konventionelle Reporter wie Fluoresceinderivate, Fluram oder IR797 und synthetisch angepasste spaltbare Linker für die Quantifizierung von käuflich erworbenen sowie selbsthergestellten Partikeln mit unterschiedlichen Carboxy und Amin Funktionsdichten untersucht. Dabei wurde der Fokus auf die Entwicklung spaltbarer multimodaler Linker mit reaktiven Gruppen wie NHS-Ester oder Amin zur Anbindung an Partikeln, quantitativ abspaltbaren Linkern wie Disulfidbrücken und optisch auslesbarer Einheiten wie 2-Thiopyridon gesetzt. Im Vergleich zu den konventionellen Reportern, deren direkte Quantifizierung an Partikeln durch Partikelstreuung und der eingelagerten Farbstoffe gestört wird, können die spaltbaren Reporter nach der quantitativen Abspaltung von der Partikeloberfläche im Überstand ohne jegliche Störung optisch vermessen werden. Außerdem können die optischen Ergebnisse der spaltbaren Linker, wenn sie Heteroatome wie beispielsweise Schwefel, Stickstoff oder Fluor tragen, mit Hilfe einer etablierten Methode wie ICP-OES validiert werden. Mit der spaltbaren Linker Methode können auch farbstoffbeladene Partikel problemlos quantifiziert werden. Weiterhin ist diese Methode nicht nur auf PNP begrenzt, sondern eignet sich auch für die Funktionsgruppenquantifizierung an Silikapartikeln oder Metallpartikeln.

1 Introduction & Motivation

1.1 Introduction to nanoparticles

In general, nanoparticles (NPs) are defined as materials with dimensions smaller than 100 nm.¹ One nanometer is one billionth of a meter or equal to ten hydrogen atoms or five silicon atoms lying in a line.² The history of NPs dates back to thousands of years ago, when Chinese artists used gold NPs as pigments. The first colloiddally stable gold NPs that are stable for almost a century were prepared and reported by Faraday in 1857.³ Nowadays, there is a vast variety of NPs. This demands a way of NP classification. Basically, NPs comprise (i) inorganic materials (e.g. metals, metal chalcogenides and other metal salts, alloys, or semiconductors), (ii) organic materials (polymers, amphiphilic systems such as micelles or liposomes, or carbon allotropes),⁴ and (iii) hybrid materials consisting of both inorganic and organic materials. A more detailed classification of (i) and (ii) is given in ??.

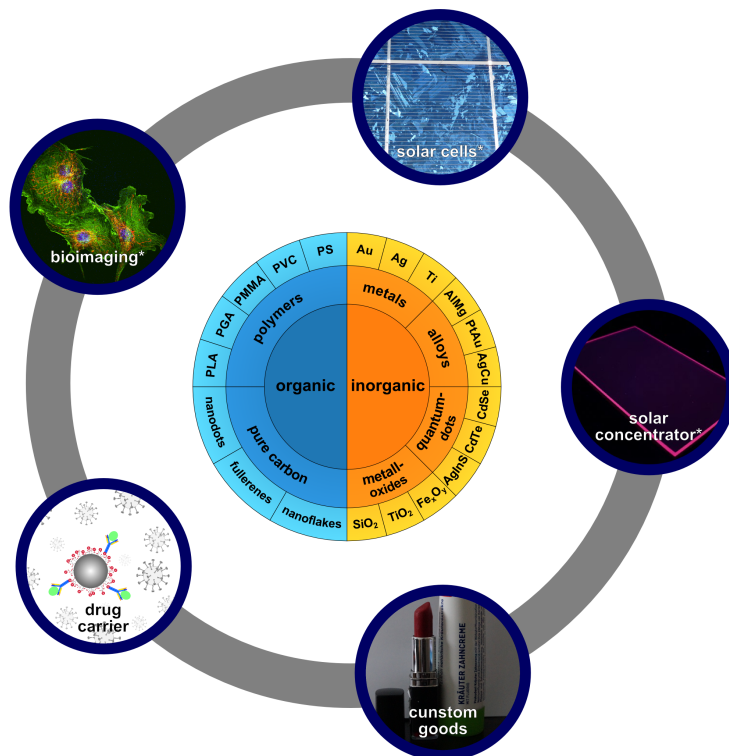


Figure 1: Classification of organic and inorganic NPs and some famous examples and their applications;¹ poly(vinyl chloride) (PVC), poly(methyl methacrylate) (PMMA), poly(lactic acid) (PLA), poly(glycolic acid) (PGA) *Copyright by Bundesanstalt für Materialforschung und -prüfung.

Advanced syntheses make it possible to prepare not only (quasi) spherical NPs,⁵ which is the most common shape, but also various other shapes such as rods,^{6,7} cages,⁸ cubes,^{9,10} disks,¹¹ hexagons,^{12–14} prisms,^{15,16} wires,¹⁷ or tubes,¹⁸ etc. The interest in these systems arises from the combination of nanoscale size with the unique diversity of physical properties and chemical functionality. NPs can be described as intermediates between bulk materials and molecules. While micrometer-sized particles show properties that are similar to the respective bulk materials, NPs can exhibit unique properties that are not found in their bulk forms.¹⁹ This includes high surface-to-volume ratios, enabling surface modification with many different molecules to impart a variety of functionalities and for some materials, also unique mechanical, thermal, electrical, magnetic, and optical properties. This versatility provides the basis for a broad range of applications in different areas, such as material sciences, life sciences, and medicine.¹ Depending on the desired application, the NP composition can be chosen to fit its purpose. Particularly, there is a choice between single and multi-composition to build up NPs. The most common multi-composition material is a spherical core/shell system, which consists of a core (inner material) and a shell (outer layer material). Typically, the core particles are completely coated by a shell of a different material. Different combinations are possible for such systems. The most interesting organic ones are inorganic/organic and organic/organic materials. Inorganic/organic core/shell NPs are made of a metal, a metallic compound, a metal oxide, a semiconductor, or a silica core with a surface stabilizing polymer shell. An organic shell on an inorganic core has a lot of advantages as it can reduce unspecific adsorptions, provide stabilization in the suspension media, and increase the biocompatibility for bioapplications.^{20–22} Organic/organic core/shell NPs are made of a polymer core and a polymer shell.

The majority of organic NPs are made from polymers. Simple non-crosslinked polymer nanoparticles (PNP) are considered as agglomerates of polymer chains with nanoscale dimensions and represent the most common organic NP structures used nowadays.¹ A growing area of application of PNP is in life sciences. This includes their use as carriers for e.g., analyte-responsive ligands, drugs^{23–25} as well as dye molecules for their use as multichromophoric reporters for signal enhancement in optical assays^{26–28} or the fabrication of nanosensors²⁹ and targeted probes in bioimaging studies.^{30,31} One of the main reasons for such a broad area of application is their design flexibility which results from the polymer diversity and enables a plethora of different sizes, morphologies, and surface functionalities, as well as the synthesis of NPs with structural stability even at dilute concentrations, low production cost, high resistance and of course low/non-toxicity.^{24,32}

Particularly, polystyrene particles (PSP) present an attractive example for an organic/organic core/shell NPs. PSP can be easily synthesized at low costs with high monodispersity and good reproducibility. As PSP are non-functionalized NPs, they need functional groups (FGs) on their surface for their aqueous dispersibility and subsequent functionalization. This can be done easily by grafting with a polymer shell with functional groups.^{33,34} Nowadays, or-

ganic/organic core/shell **PSP** are commercially available with various surface chemistries and narrow size distributions in different sizes from 15 nm up to several micrometers and they are considered as inert and commonly non-toxic.^{35–37} Therefore, **PSP** are attractive materials, for example, for their use as fluorescent reporters for imaging or bioanalytics.³¹

1.2 Application relevant properties of PNP

PNP offer a great versatility. Hence, these particles have various applications in different areas as described in detail in ???. Depending on their specific application, differently designed **PNP** are desired. **PNP** composition, size, shape, surface properties including surface **FGs**, and surface charge, as well as optical properties can have a considerable impact on their performance.³⁸

1.2.1 Composition of PNP

PNP can be classified into natural **PNP** such as chitosan, alginate, gelatin, and albumin and synthetic **PNP** such as poly(lactides), poly(lactide-co-glycoside), poly(methyl methacrylate) (**PMMA**), polyacrylamide, **PSP**. While natural **PNP** vary in purity and have often lack of consistence that make them less reproducible, synthetic **PNP** show good purity and batch-to-batch reproducibility. This characteristic of synthetic polymers favors them clearly for different **PNP** applications.³⁹ Synthetic **PNP** can be divided again into two chemical composition types. **PNP** with heteroatomic ($-C-X-$) backbones such as poly(lactides), poly(lactide-co-glycoside) copolymers, poly(ϵ -caprolactones), and poly(amino acids) are easily hydrolysable, and thus, biodegradable.^{40,41} Polymers with carbon-only ($-C-C-$) backbones such as **PMMA**, polyacrylamide, **PSP**, and polyacrylates are stable in the body and non-biodegradable.³⁹ Both synthetic **PNP** compositions are commonly used as carriers for small molecules, drugs, dyes or biomolecules by incorporating them into the **PNP** matrix or attaching them onto the particle surface.⁴²

1.2.2 Size and size distribution of PNP

Two key parameters of **PNP** are particle size and size distribution, which determine the basic physiochemical behavior of the particles (e.g. sedimentation rate) and their surface area.⁴³ The size of **PNP** can be influence by material selection and different synthesis methods. Different examples show that the size of **NPs** has also a large impact on biological applications. One example for this was reported by Kulkarni and Feng.⁴⁴ They studied the uptake of **PSP** in kidney cells and focused on the size by using non-deformable **PSP**. While the uptake of 100-200 nm-sized **PSP** has the highest efficiency, 500 nm **PSP** are poorly internalized and small particles are cleared rapidly from the blood via extravasation. Thus, the size of the **PSP** influences in this example the uptake. This example shows that 50–200 nm-sized **PNP** have the highest potential for *in vivo* applications, due to their ability to circulate in the

blood for long periods of time without uptake in the liver while also being small enough to avoid filtration in the spleen.^{38,45,46} An ideal NP size for biological applications cannot be generalized. It is not only size dependent. Additionally, it depends on the cell line, NP material, surface properties, complexity of the area.³⁸

1.2.3 Shape of PNP

Typically, PNP are synthesized in a spherical shape, due to physical facts such as surface tension. However, the synthesis of discs, rods, fibers, and elliptical disks were also reported and studied for different applications.^{47,48} The uptake of PNP carriers by target cells and their degradation are also influenced by their shape.⁴⁷ Champion and Mitragotri showed that worm-like particles exhibit insignificant phagocytosis compared to traditional spherical particles. Thus, due to the change of the particle curvature the application of such biological processes can be inhibited.⁴⁸

1.2.4 Optical properties of PNP (fluorescent PNP)

Depending on particle size, particle concentration and particle refractive index, all kind of particles can exhibit Raleigh and Mie scattering by interaction with electromagnetic radiation.⁴⁹ While for the small particles the Rayleigh scattering dominate, for the bigger ones the Mie scattering affects more. In ?? absorbance spectra with the specific scattering profile of 25 nm – 1 μ m-sized PSP in water with identical mass concentrations are depicted.

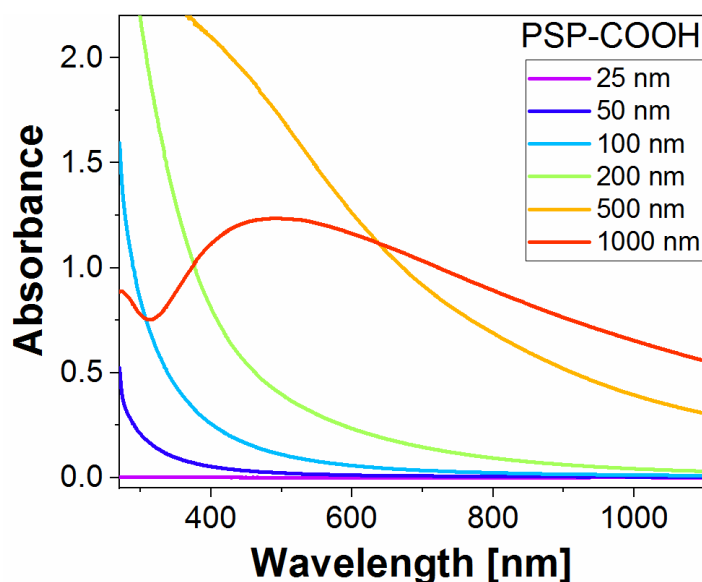


Figure 2: Absorption spectra of differently sized PSP with their typical scattering profiles with identical 0.17 mg/mL mass concentration.

Fluorescence-based techniques are promising tools for the analysis of complex biological systems and processes. While commonly used fluorescent organic dye molecules and flu-

orescent proteins are small and biocompatible, fluorescent NPs have the potential to be 10-1000 times brighter and more photostable than the former. Additionally, they can be surface-functionalized with biocompatible molecules,⁵⁰ and stay in the blood circulation for an extended period of time, which can be important for specific bioimaging and/or drug delivery applications. The advantages of fluorescent NPs strongly attract scientists from biological research fields, but not all NPs are suitable for biological applications.^{51,52} For example, quantum dots are perfect candidates for multiplex imaging due to their photostability and narrow emission band; their optical properties are tightly linked to their core composition and size.^{53,54} Up-conversion NPs can be excited with a low energy, near-infrared light source and emit higher energy photons in the visible range, which can be beneficial for deep tissue imaging.⁵⁵ However, their relatively low brightness in water and possible toxicity (release of fluoride and lanthanide ions) needs to be considered.⁵⁵⁻⁵⁷ PNP, in turn, exhibit a remarkable stability in biological environments, a well-controlled surface chemistry, and biocompatibility. Compared to inherently fluorescent quantum dots and up-conversion NPs, PNP are non-fluorescent, yet can be made emissive by combining them with, for example, organic dyes.

Non-fluorescent PNP can be used as nm-sized matrices for organic dyes to generate fluorescent NP-based emitters as well as to stabilize less photochemically and chemically stable NIR dyes to increase their quantum yield. Such a system provides an enormous flexibility in synthesis, in matrix-dye combinations, and in optical properties which also allows the control of brightness, absorption and emission wavelength, size (ranging between 15-500 nm), surface chemistry, etc.⁵⁸ Furthermore, it offers the opportunity to synthesize multiple excitation/emission PNP by encapsulating more than one type of dye.²⁹

Fluorescent PNP can be made by attaching reactive fluorophores to the surface FGs of the PNP or by encapsulation of the fluorophores into the PNP matrix. The advantages, disadvantages and different synthesis approaches are described in ???. For the application of fluorescent PNP, the brightness which is proportional to the absorption coefficient, quantum yield, and number of dyes per molecule is a relevant aspect. Important parameters that influence the brightness are the number of dye molecules, the brightness of the dye itself, and quenching effects such as reabsorption, dye-dye interactions, and dye-matrix interactions. Encapsulation of conventional dyes such as rhodamines, cyanines, Nile Red, etc. in high concentrations leads to self-quenching due to dye-dye interactions and is called aggregation-caused quenching (ACQ). One example, given by Behnke *et al.*,²⁷ exhibits the decrease of quantum yield from 76% to 22% by an increase of the dye loading from 0.05 wt% to 0.8 wt%.^{27,59,60}

1.2.4.1 Aggregation induced property changes and aggregation-induced emission (AIE) PNP

Conventional hydrophobic dyes are often highly fluorescent as monomeric species in organic dilute solutions. In cases of dye-dye-interactions, which are encouraged in concentrated solutions and in hydrophilic surroundings,^{61,62} through close attachment of several dyes to a biomolecule⁶³ or to functional groups on the surface of NPs,^{64,65} or high dye concentrations in a polymer matrix,²⁷ the dyes can become less or even non-emissive. The main reason for ACQ is π - π stacking interactions of the chromophores with their extended π -conjugated systems⁶⁶ favoring the formation of H-type dimers and aggregates that are barely or non-emissive. These dimers can then act as energy sinks for fluorescence resonance energy transfer (FRET) processes between monomeric dyes and aggregated dyes (so called homo-FRET between chemically identical dyes).⁶⁷ Additionally, hydrogen-bonding interactions can also lead to intermolecular fluorescence quenching, particularly in the case of charge transfer dyes.⁶⁸⁻⁷⁰

π - π stacking of conventional dyes can be prevented or at least reduced by introducing bulky aromatic substituents such as diarylamino or tetraphenylethylene groups,⁶² which prevent strong π - π interactions due to steric hindrance. Tang and coworkers observed a strong emission enhancement upon dye aggregation behavior for the twisted dye 1-methyl-1,2,3,4,5-pentaphenylsilole in 2001.⁷¹ This opposite phenomenon to ACQ is called aggregation-induced emission (AIE) and was observed for many dyes with a twisted skeleton conformation and propeller-like moieties.^{70,72} In diluted solution, particularly in polar solvents, the monomeric AIE dyes show very low or even no emission, as non-radiative relaxation processes are favored due to intramolecular rotations and vibrations of the bulky substituents. Aggregation, however, results in a rigidization of the dye's intramolecular conformational flexibility and the packing structure of the molecule's propeller blade-like substituents. The completely or at least partly blocked intramolecular motions of the substituents and the prevented direct π - π stacking lead to a blocking of the nonradiative decay pathways of the excited singlet state,⁷³⁻⁷⁶ and thus, increase the dye's emission.

Since the AIE concept was proposed in 2001, these kinds of dyes received great attention. Consequently, a variety of AIE dyes have been developed in recent years (see some famous examples in ??). They can be classified in several categories according to their skeletons: i) heterocycles such as siloles,⁷⁶ tetraphenylpyrazines,⁷⁷ and quinoline-malononitriles;⁷⁸ ii) pure carbon aromatics such as distyrylanthracene⁷⁹ and hexaphenylbenzenes; as well as iii) ethylene derivatives such as tetraphenylethenes and cyanostilbenes.⁸⁰

Fluorophores showing AIE are promising candidates for novel signal enhancement strategies in bioassays or improved NP-based bioimaging approaches as such dyes enable higher dye loading densities than conventional ACQ dyes.⁸¹

AIE dyes already found a wide range of applications, and thus the varied reported AIE NPs syntheses are summarized in ?. They are used in bioimaging to visualize cells, organelles,

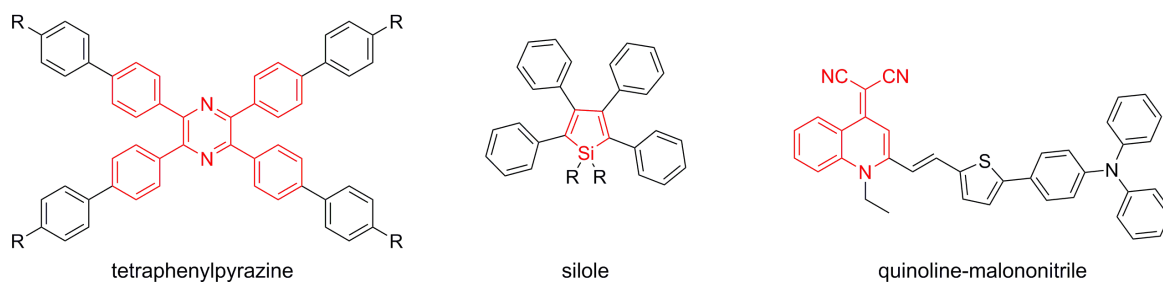


Figure 3: Recently reported AIE dye skeletons.^{76–78}

tissues, and biological processes in living systems by rapid, noninvasive, sensitive, and inexpensive fluorescence imaging.^{82–84} Due to their brightness, biocompatibility, and photostability, AIE-based PNP are also applied as contrast agents for long-term staining and as reporters for cancer cell tracking.^{66,85,86} They enable the monitoring of cells, depending on the chosen dye, for up to 42 days. Some selected AIE PNP are also used in photodynamic therapy due to their reactive oxygen species (ROS) generation efficiency and high *in vitro* photocytotoxicity.⁸⁷ Various *in vivo* and *in vitro* studies reported about the successful use of AIE NPs as drug delivery systems, for example, for doxorubicin.⁸⁸

1.2.5 Surface functional groups (FGs) of PNP

One of the key parameters which have to be considered for the synthesis of stable and biocompatible core-shell NPs is their surface chemistry.^{64,89–91} FGs play a pivotal role in colloidal stability (aggregation tendency), reactivity (special attention biochemical reactivity), biocompatibility, pharmacodynamics, biodistribution, etc. They build the interface between the particle and their environment, and thus, the first point of contact and first interaction point.⁹²

1.2.5.1 Stability of PNP

The stability of a NP suspension depends on the van der Waals forces, Coulomb forces, and on the distance between neighboring NPs. If attractive forces dominate, the NPs can aggregate while a dominance of repulsive forces leads to NP stabilization. NPs can be stabilized in different ways: electrostatic repulsion, steric repulsion, and entropic stabilization. For electrostatic repulsion, the NPs must be charged by surface FGs, which need to be introduced by covalent attachment or adsorption on the NP surface. Thus, the same surface charge of neighboring NPs leads to NP repulsion and stabilization. Steric repulsion can be obtained by covalent attachment or adsorption of long chain polymers to the NPs and increase the distance between the NPs. Electrosteric stabilization, the combination of both effects, can also be used for the stabilization of NP dispersions.^{93,94}

1.2.5.2 Functionalization of PNP

Many applications of NPs require further surface functionalization, for example, with biomolecules such as proteins, DNA, and antibodies or other target-specific molecules or stimuli-responsive dyes such as fluorescein for the preparation of nanosensors. The terminal surface functionalities on the NPs, which can be formed by co-polymerization of a co-monomer, can act as anchoring points for further surface functionalization.^{1,95} Such molecules can be covalently attached by traditional organic chemistry reactions or by using small cross-linking molecules.²⁸

The most commonly used FGs are carboxy and amino groups, as they can be easily introduced on polymer core NPs and can be further modified with many established (bio)functionalization reactions known from protein chemistry.^{28,95}

The carboxy groups give the PNP a negative zeta potential at neutral pH. As carboxy groups have only a limited reactivity in amide formation, they need to be activated prior to reaction, for example, using a carbodiimide such as 1-ethyl-3-(3-dimethylaminopropyl)carbodiimide (EDC), dicyclohexylcarbodiimide (DCC), or diisopropylcarbodiimide (DIC). One disadvantage of the formed O-acylisourea intermediate is the rapid hydrolysis. In consequence, a high excess is used to achieve a complete activation, but this can cause a loss of colloidal stability due to poor solubility of O-acylisourea. This in turn can be mitigated by converting the O-acylisourea to a more stable intermediate by using *N*-hydroxysulfosuccinimide (sulfo-NHS) or *N*-hydroxysuccinimide (NHS). The formed active ester can undergo an addition-elimination reaction with amino groups. Biomolecules, small molecules, or dyes with amino functions can be coupled to the carboxylated PNP surface by formation of an amide bond.^{96–98}

The second common terminal functions are amino groups, which yields PNP with a positive zeta potential at neutral pH. They can undergo an addition-elimination reaction with active esters, as described above. Biomolecules, small molecules, or dyes with active ester groups can be used as reactants for the coupling to amino groups.^{99,100}

Thiol, maleimide, aldehyde, azide, and vinyl groups are also often used for PNP surface modification and extend the possible reactions and reagents on PNP surfaces. Thiol groups can undergo an oxidation reaction with another thiol function and generate a disulfide bond, but it can also perform an exchange reaction with a disulfide and generate a new asymmetric disulfide bond.^{101–103} Aldehyde PNP are used to attach hydrazides to the surface by the formation of a hydrazone, but also amino groups can undergo a (reductive) amination with carbonyls.^{104,105}

An overview of FGs and their subsequent reaction possibilities that are important for this work are shown in ??.

1.2.5.3 Biocompatibility of PNP

A surface modification is a useful strategy to make NPs more biocompatible. Since biomolecules often have ϵ -amino groups as found, for example, on the lysine side chains as well

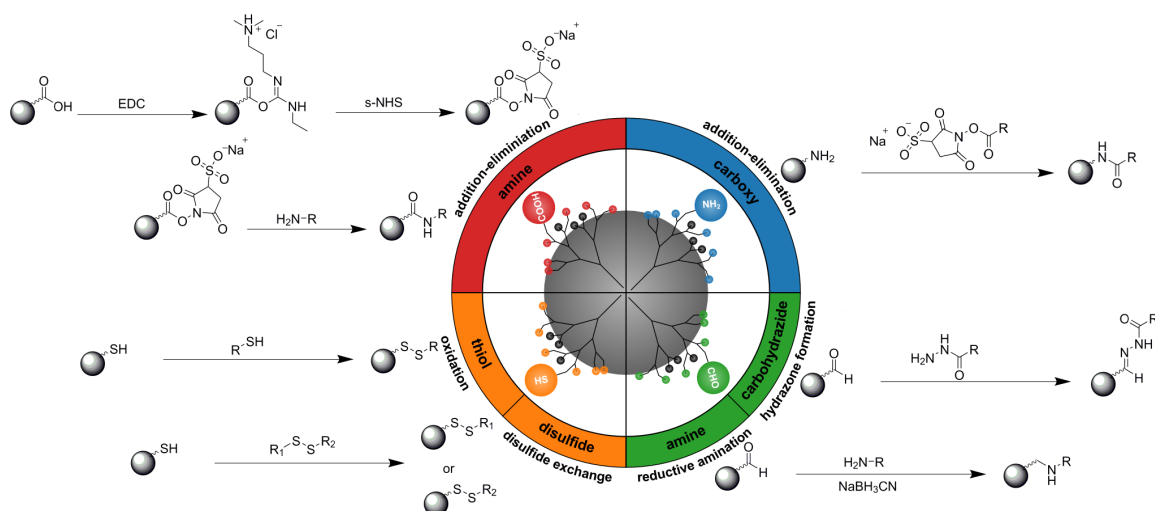


Figure 4: FGs and the further reactions possibilities: carboxy and amino FGs can undergo addition-elimination reactions (blue and red), thiol functions oxidation or disulfide exchange reactions (yellow), and aldehyde functions hydrazine formation or reductive amination reactions (green), respectively.

as N-terminal primary amines of proteins, an addition-elimination reaction is often used to couple biomolecules to the activated carboxy PNP surface. Additionally, the carboxy groups in aspartic acid, glutamic acid, or the C-terminus of biomolecules can also be used to couple proteins, peptide, or antibodies to aminated PNP surfaces.¹⁰⁶ Such bioconjugation or also, for example, PEGylations are used to coat the surface and enhance their hydrophilicity and biocompatibility. PEG is a hydrophilic, biologically inert polymer that has been approved by the U.S. Food and Drug Administration (FDA) for internal use. PEG-coated PNP show significant differences compared to non-coated ones in blood circulation times, it prevents the aggregation of NPs, and hinders the non-specific interactions with cells by forming a neutral stabilizing interface.^{107,108} Such a surface modification can have a large influence on the biological transport, mediating interactions with cellular membranes and proteins, kinetics and mechanism of uptake into cells, diffusion through various biological barriers, and biodistribution to specific tissues, cells, or organelles.¹⁰⁹

1.2.5.4 Toxicity of PNP

The surface chemistry stands out as the main parameter of biological performance as the NP surface is the first point of exposure, thus, it has also a major impact on the toxicity. Free reactive groups on NPs can lead to toxicity. NPs with high cationic surface charge and hydrophobic character can more strongly interact with anionic functions on the cellular membranes than NPs with anionic or neutral FGs.^{109–111}

1.3 Motivation and objectives

Fluorescent PNP with high brightness and accurately characterized properties, especially a complete knowledge about the type and amount of the surface chemistry, are prerequisites for sophisticated and versatile applications in the material and life sciences and in particular as signal amplification systems in bioanalytics. Knowledge of these fundamental properties is also necessary for a sustainable and resource efficient application of surface functionalized fluorescent PNP, which is a major goal in today's research. The aim of this work is

- (i) development of signal enhancement strategies
- (ii) development of methods for the precise FG quantification on PNP surfaces

The former is addressed by loading preformed PNP with different organic dyes with special emphasis on AIE emitters. In this respect the understanding of AIE behavior of dye derivatives with different substitution patterns on optical properties in solution and in preformed PNP is essential. Since no standardized methods for the FG analysis and no reference materials with known FG densities are currently available, the latter is addressed to the determination of the accessible amount of FGs on simple and dye-loaded PNP. The main objectives of this thesis are summarized in ??.

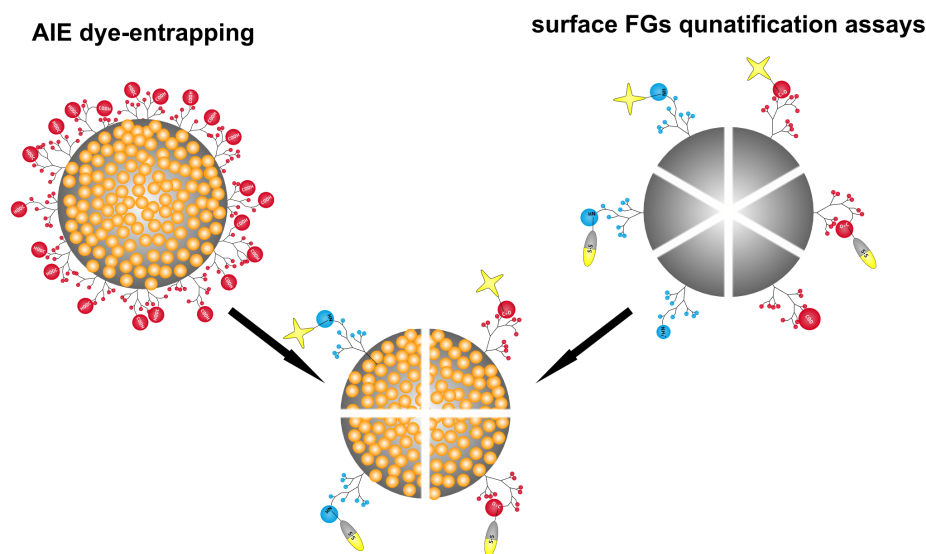


Figure 5: Objectives of the doctoral thesis a) development of signal enhancement strategies by AIE dye entrapping b) development of surface FG quantification assays.

2 Synthesis, Characterization and Quantification Methods for PNP

2.1 Synthesis of PNP

The synthesis of monodisperse, uniformly shaped and chemically homogeneous PNP cannot be simply generalized. PNP can be prepared either by “top-down” synthesis approaches, starting from a preformed polymer and shape the “bulk material” into to the desired structure, or via a “bottom-up” synthesis, where the chemical properties of the monomers are exploited to polymerize monomer-by-monomer and create the desired NPs.^{2,43} Procedures belonging to the top-down and bottom-up approaches are summarized in ???. With the above mentioned techniques not only simple NPs, but also different types of core/shell NPs can be synthesized.

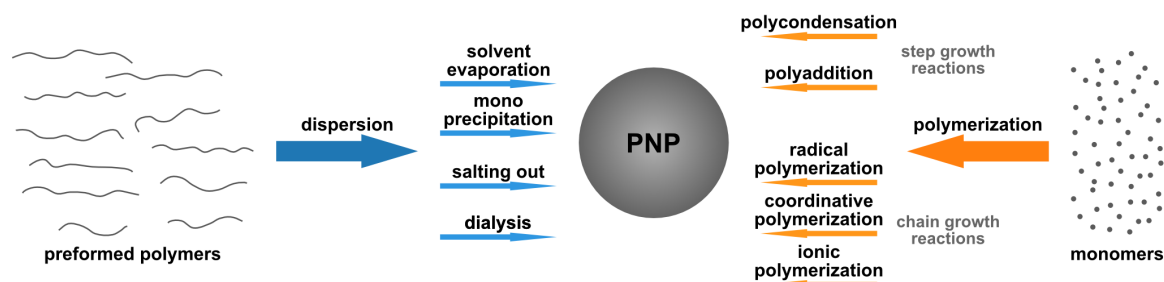


Figure 6: Various top-down and bottom-up approaches for the preparation of PNP.

The progress in controlled polymerization enables the engineering of multifunctional PNP with precise control over chemical composition, shape, size, shell thickness, surface charge, and functionality. The conventional radical emulsion polymerization is the most common way to synthesize PNP. Herein, the monomer is added stepwise in the presence of a suitable initiator, which starts the polymerization reaction by forming free radicals and interacting with the monomers in two immiscible liquids, e.g., water and oil. Hence, the carefully controlled emulsion polymerization needs additional surface modifiers, emulsifying agents, or surfactants. These molecules can significantly reduce the interfacial tension and form nanometer-sized micelle droplets of oil-in-water emulsions (nanoreactors/nanocavities), which serve as centers for nucleation and growth and protect the nonpolar monomers. Additionally, they also work as a steric stabilizer to prevent the aggregation of the reacting species during the reaction period. Such an emulsion polymerization can also be done surfactant free, but in that case the monomer must be soluble in water and stabilized by using ionic co-monomers

or ionizable initiators. In most cases, a mini-emulsion polymerization with an initiator in the organic phase or a micro-emulsion polymerization with a water-soluble initiator is performed. Due to the water insolubility of the monomer, a surfactant is necessary in both polymerizations.^{33,43,112,113}

During the polymerization synthesis, different factors can influence the size and the shape of formed particle, such as the stirring speed and temperature conditions. Also, the applied surfactant and the water-to-surfactant ratio are of great importance, as they control the polymer chain length as well as the size and shape of the final PNP via the formed reaction cavity that depends additionally on the surfactant's hydrophilic-lipophilic balance value. Finally, the reactant concentration is important for the amount of formed nuclei and the period of particle growth, because only the monomers remaining in the reaction solution are available for a collision with the formed nuclei and for deposition on the surface of nuclei.¹¹⁴ The coating of the synthesized core PNP can be performed by using the *in-situ* polymerization method. In this method, after the synthesis of the core particles, a co-monomer is added to the particle nuclei, which has the desired FG (see ??).^{115,116}

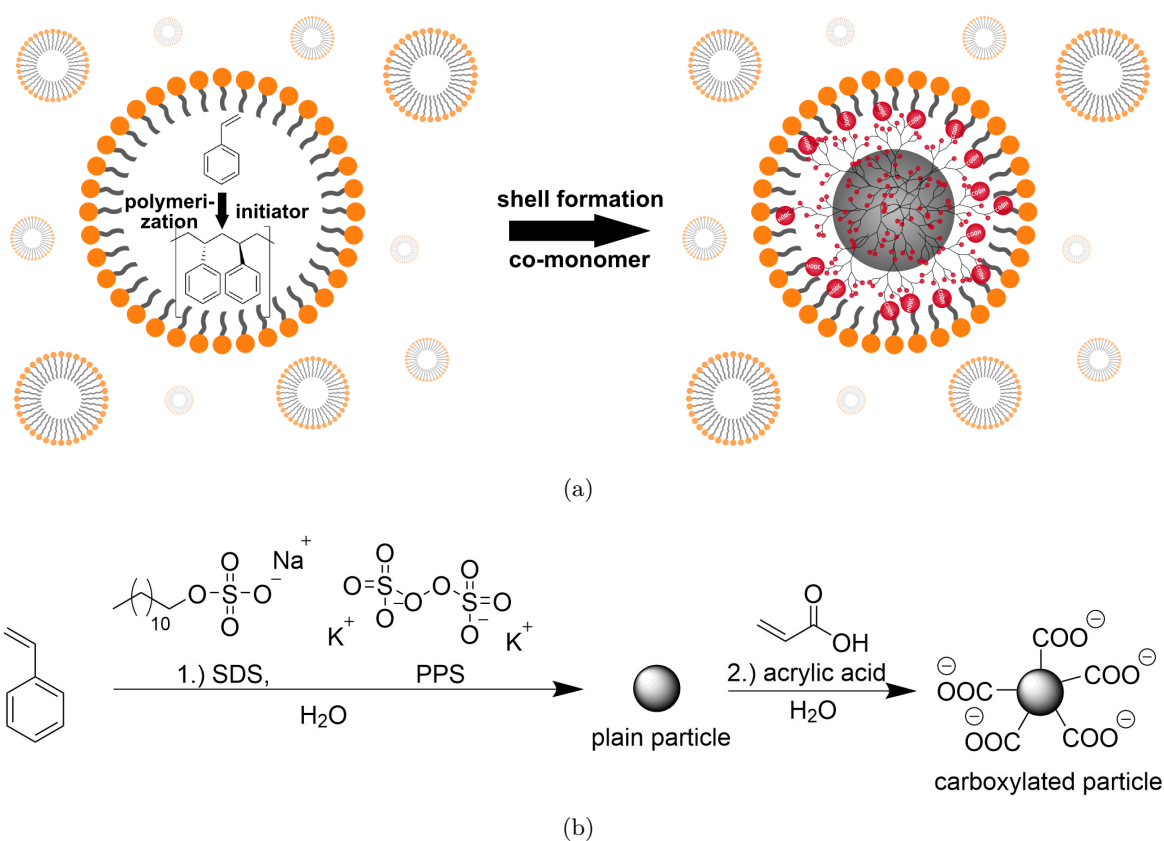


Figure 7: Emulsion polymerization of styrene to polystyrene, and *in-situ* addition of acrylic acid to achieve the formation of a carboxy shell in micelles.^{33,34}

The shell formation reaction can be challenging as particle agglomeration and formation of shell particles have to be prevented. Agglomeration of the particles in the reaction media

can be controlled via stabilization with surfactants. The separate formation of shell material particles can be inhibited by adjusting the stirring speed, the co-monomer concentration, and the co-monomer addition rate. An incomplete coverage of the core can be prevented by using a sufficient amount of co-monomer molecules to fully cover the surface of the PNP cores. Some common shell-forming molecules (co-monomers) are listed in ??.

Table 1: Co-monomers with reactive functionalities for the surface functionalization of PNP, especially interesting for PSP cores.

Co-monomers	Functional groups
4- <i>N</i> -Boc-vinylaniline ¹¹⁷	amino
aminoethyl methacrylate hydrochloride ³³	amino
acrylic acid ³³	carboxy
methyl methacrylate ¹¹⁸	carboxy
vinylbenzaldehyde ¹¹⁹	aldehyde
vinyl aryl azide ¹²⁰	azide

2.1.1 Preparation of fluorescent PNP and AIE-PNP

Fluorescent PNP can be made via different approaches. One way is attaching reactive fluorophores to the surface FGs of the PNP. The disadvantages of this strategy are that only reactive dyes with suitable functionality can be coupled covalently to the surface, only accessible FGs can be modified, and the dyes are located at the interface between PNP and the surrounding medium, which makes them accessible for quenchers present in the solution.¹²¹ This strategy is often used for the preparation of nanosensors using stimuli-responsive dyes.¹²² Another elegant way is to encapsulate the dyes into the PNP matrix, either during the polymerization reaction or after the synthesis of preformed PNP. The dye can be added during the synthesis in the reaction mixture as dye monomers, which are then incorporated covalently in the PNP matrix or through physical trapping.¹²³ The incorporation of dyes during the synthesis can impact particle properties such as size, size distribution, and shape. Additionally, this requires the synthesis of fluorophore-modified monomers, which can be tedious, and dyes, which survive the sometimes stringent polymerization conditions. The advantage of such a dye polymerization into the PNP matrix is that it prevents leaking. The other approach is the simple swelling procedure studied, for example, by Behnke *et al.*^{26,27} using preformed PSP and conventional water-insoluble dyes without reactive groups (see ??). In this case, hydrophobic organic dyes are dissolved in an organic solvent, for example, THF or DMF, and added to the aqueous PNP suspension. The organic solvent leads to a swelling of the particles. Depending on their $\log D$ value (see ??), the hydrophobic organic dyes are distributed preferentially within the hydrophobic polymer matrix and can then be entrapped by reducing the organic solvent content. This leads to a deswelling of the PNP back to their original size and shape. The excess dye is removed by several washing steps.^{26,27} In this way,

PNP can act as carriers for water-insoluble materials such as hydrophobic dyes and provide long-term chemical stability and protection against chemical species which can lead to photo- or chemical degradation.

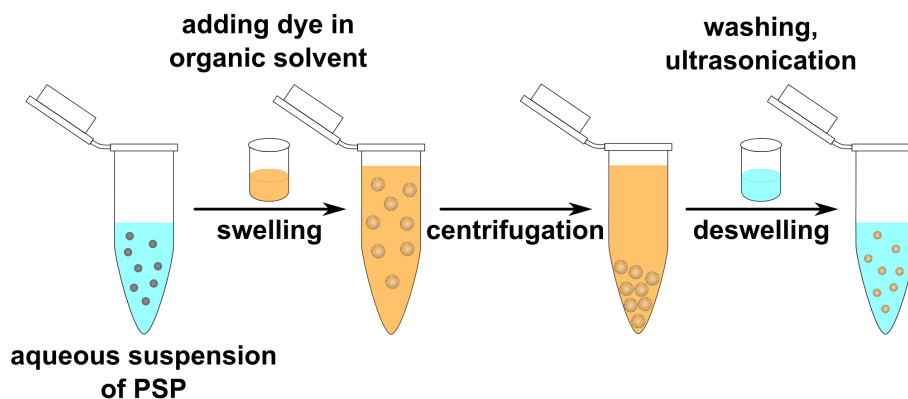


Figure 8: Simple encapsulation procedure for producing fluorescent PNP with hydrophobic dyes.

An important aspect for the application of dye-loaded particles is to prevent dye leaking. Leaking of dyes into the environment leads to a decrease of the NP brightness, increases the background signal and can have toxic effects. In order to avoid dye release and achieve high dye loading efficiencies, sufficiently hydrophobic dyes that can be entrapped within the hydrophobic polymer matrix are required.^{124,125} For every dye the degree of hydrophobicity can be calculated. The $\log D$ is the logarithm of the ratio of the concentration sums of all i species in water and in octanol as a measure for the hydrophobicity or hydrophilicity of the dye:

$$\log D = \log \frac{\sum_1^i \cdot c_{okt}^i}{\sum_1^i \cdot c_{water}^i}. \quad (1)$$

The higher the $\log D$ value, the higher the hydrophobicity of the dye.

A special form of fluorescent NPs are AIE PNP. Different synthesis methods for producing them were reported in the recent years. Examples involve the covalent attachment of AIE dyes to the polymer or the entrapment of the dyes in PNP. For example, Wei and co-workers used cross-linkable/polymerizable AIE dyes for the preparation of NPs in a reversible addition-fragmentation chain transfer (RAFT) polymerization,^{126,127} emulsion polymerization,^{128,129} radical polymerization,^{130,131} and redox polymerization.¹³² Another synthesis of AIE PNP is based on the nanoprecipitation with an amphiphilic polymer such as 1,2-distearoyl-sn-glycero-3-phosphoethanolamine-PEG (DSPE-PEG) as encapsulating or coating agent, which additionally enables further functionalization of the PNP.⁸⁵ Another study reports the synthesis of AIE PNP by an emulsion solvent evaporation method.¹³³ The amount of emulsifier is one of the important aspects for this kind of synthesis, because the lower the amount, the higher the aggregation state of the AIE dye. A high amount of emulsifier encourages a homogeneous dye distribution in the polymer matrix, and thus, no

aggregation takes place, leading to a reduced quantum yield. The generation of AIE PNP by a simple swelling procedure followed in this work has not been reported yet.

2.2 Characterization of PNP

To obtain a complete picture about size, size distribution, shape, shell thickness, and surface charge of the synthesized NPs, suitable analytical methods are required. Several techniques are established for the characterization of NPs.

- (i) microscopic analyses^{134–137} such as atomic force microscopy (AFM), scanning electron microscopy (SEM), transmission electron microscopy (TEM)
- (ii) spectroscopic analyses^{136,138–140} such as UV-Vis spectroscopy, fluorescence spectroscopy, X-ray photoelectron spectroscopy (XPS), Fourier-transform infrared spectroscopy (FTIR)
- (iii) scattering analyses^{141,142} such as dynamic light scattering (DLS), nanoparticle tracking analysis (NTA), small-angle X-ray scattering (SAXS)

For the determination of the NP properties, the characterization method must be suitable for both, the core and the shell material. In the case of core/shell PSP, both materials are organic polymers. Methods that are suitable for the core are also suitable for the shell but distinguishing between core and shell could be challenging.

2.2.1 Characterization of size, size distribution and shape

2.2.1.1 Scanning electron microscopy (SEM)

SEM is the most common and reliable technique for visualization of different types of NPs and for their size and shape analysis (see ??).

Compared to a conventional light microscope, which is typically working with a visible light source in a wavelength range of 400 to 800 nm, the resolution of an electron microscope is several orders of magnitude higher, down to the sub-nanometer region. The generated electron beam at a tungsten cathode is focused by condenser lenses. Subsequently, the focused electron beam passes through deflector plates and interacts with the sample line by line in a raster pattern. Different processes can take place when the beam hits the sample. The collimated electrons can be deflected by elastic scattering or they can ionize the sample and generate secondary electrons with lower energy, that can be detected. With a CCD detector, the resulting image is obtained by mapping the intensity of the detected signal.^{143,144} For the measurement, the samples are in a dried form, fixed on a substrate, and measured under high vacuum. Instead of detecting secondary electrons, SEM can also be used in transmission mode in the so-called transmission scanning electron microscopy (TSEM). In this special

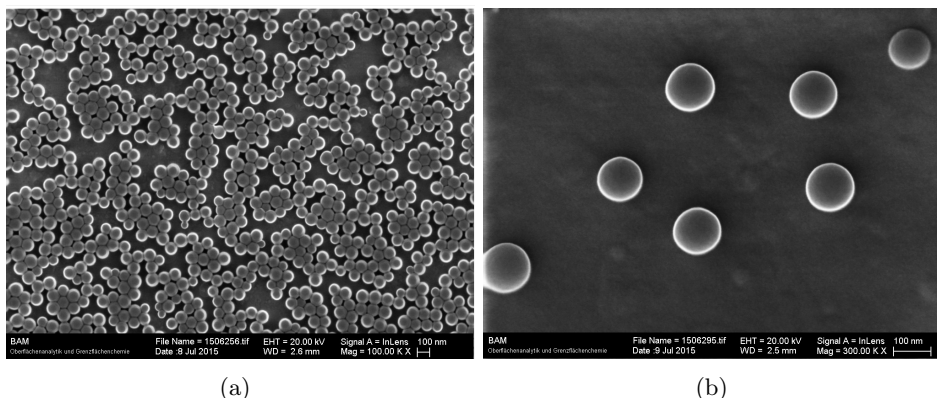


Figure 9: SEM images of 100 nm-sized PNP. (a) overview image of 100 nm-sized PNP; (b) zoomed-in image of 100 nm-sized PNP.

mode a detector below the sample collects the transmitted electrons.¹⁴⁵

2.2.1.2 Dynamic light scattering (DLS)

DLS is another widely used, simple and fast technique for the determination of the hydrodynamic radius of NPs in a colloidal suspension. The method is based on measuring the intensity fluctuation of a coherent laser source by a detector. NPs in suspension are constantly moving (Brownian motion) and thus, the relative distances of the particles change continuously. Simultaneously, the condition for constructive and destructive interferences changes as well, which results in time dependent intensity fluctuations of the light scattered by the NPs.

Application of monochromatic and coherent laser light allows to observe interference changes and measure the intensity fluctuations, and thus, offers access to the diffusion coefficient D of the particles at a constant temperature T . Via the Stokes-Einstein equation (see ??), the hydrodynamic diameter d_h of the particles can be calculated with the Boltzmann constant k and the viscosity η of the used solvent.

$$D = \frac{k \cdot T}{6 \cdot \pi \cdot \eta \cdot r}. \quad (2)$$

The resulting hydrodynamic diameter depends on the temperature and the viscosity of the solvent. The hydrodynamic diameter describes the whole particle diameter including the core, shell(s), and the surface-bound solvent layer(s) and is consequently larger than the diameter measured with SEM. Since the diffusion of small NPs is faster than that of larger NPs, the intensity fluctuations of the scattered light changes faster for small NPs than for larger NPs. The larger the particle, the slower the movement and the lower the diffusion coefficient D of the particle.

The method is limited to a particle size range of typically 1-10000 nm. Exemplarily, measurements of 100 nm-sized PSP and a mixture of 100 and 200 nm-sized PSP are shown in ?? ^{144,146}

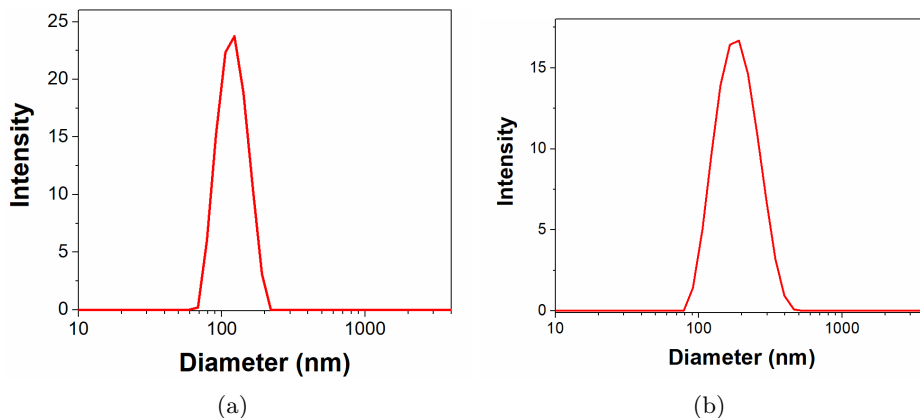


Figure 10: Hydrodynamic diameter of PSP measured by DLS; 100 nm-sized PSP (a), 100 and 200 nm-sized PSP (50/50 w/w, b).

2.2.2 Surface charge

Electrophoretic light scattering determines the surface charge of NPs, which also influences the colloidal stability of the NP dispersion. Around the surface charge, ions of opposite charge are attracted and an ionic double layer is formed. The ζ potential is the electric potential at the slipping plane on the NP surface (including the NP surface charge, and the diffuse Stern layer) and the bulk solvent solution. It can be determined by measuring the electrophoretic mobility. The ζ potential of a sample depends on ionic strength, pH (when (de)protonatable groups are on the surface), and composition and dielectric constant of the solvent. A surface charge above 20 mV or below -20 mV usually leads to a good colloidal stability of NP dispersions due to electrostatic repulsion.¹⁴⁷

2.2.3 Optical properties

Optical spectroscopy exploits the interaction of materials with electromagnetic radiation covering the UV-VIS-IR spectral region. Absorption-, luminescence- (emission, fluorescence quantum yield, fluorescence lifetime, fluorescence anisotropy), IR-, and Raman spectroscopy also belong to the optical spectroscopy methods. In these optical methods the excitation and relaxation of molecules in rotational, vibrational, and electronic states can be studied to obtain information about the concentration, energy levels, and the structure of the analyte.

2.2.3.1 Absorption

When electromagnetic radiation interacts with a sample, it can be absorbed, reflected, scattered, and/or transmitted. In the absorption process, sample molecules absorb electromagnetic radiation with a defined energy, which causes an excitation from an electronic ground state S_0 to higher electronic and vibronic states S_1 or S_2 (see ?? blue and green arrows). From the ratio of the incident radiation intensity I_0 and the weaker transmission radiation intensity I the absorbance A can be determined (in the absence of scattering/reflection). The measured $A(\lambda)$ depends on the concentration c of the material in the solution, the material and wavelength specific absorption coefficient ϵ_λ , and the optical pathlength d , as defined by the Beer-Lambert law:^{148–150}

$$A(\lambda) = \log\left(\frac{I_0}{I}\right) = c \cdot \epsilon_\lambda \cdot d. \quad (3)$$

When ϵ_λ of the material is known and d is constant, the change of $A(\lambda)$ is proportional to the change of c of the sample. This law is only valid for transparent, diluted samples with an absorbance ≤ 1 and for samples where scattering and reflection can be neglected.¹⁴⁸ That's why, the Beer-Lambert law is not valid for dispersions of particles with sizes exceeding approximately 50 nm.

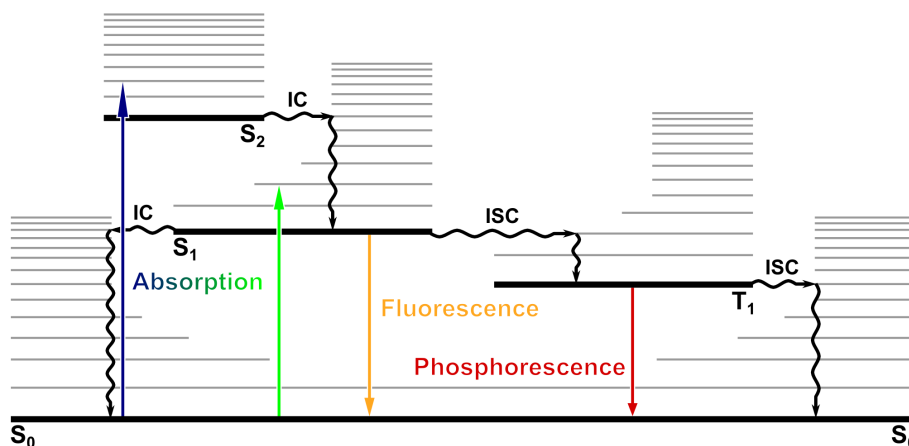


Figure 11: Simple Jablonski diagram with absorption, fluorescence and phosphorescence.

2.2.3.2 Emission

After the electrons relax into the vibronic ground state of the electronically excited state S_1 by radiationless internal conversion (IC), they emit in most cases a photon with lesser energy than the absorbed photon and relax back into the ground state S_0 (see ?? yellow and red arrow).¹⁵⁰ This allowed fast relaxation process is called fluorescence (yellow arrow). In some cases the electrons relax back into S_0 without emitting photons (non-radiative relaxation).

Some systems can also change from the excited singlet electronic state to an excited triplet state (spin flip) due to intersystem crossing (ISC). This spin-forbidden relaxation from T₁ back in the ground state is called phosphorescence (red arrow).

2.2.3.3 Fluorescence quantum yield (ϕ_f)

ϕ_f and fluorescence lifetime (τ) are the two key parameters for the characterization and comparison of fluorescent samples such as dyes.¹⁵⁰

ϕ_f is defined as the ratio between the radiative rate constant k_r and the sum of the radiative k_r and nonradiative rate constant k_{nr} (depopulating the excited state) or the ratio of the number of emitted photons and the number of absorbed photons (see ??).^{151,152}

$$\phi_f = \frac{k_r}{k_r + k_{nr}} = \frac{N_{em}(\lambda)}{N_{abs}(\lambda)}. \quad (4)$$

ϕ_f can be determined relatively or absolutely. For the relative $\phi_{f;rel}$ determination, the sample's emission intensity is measured relative to the emission intensity of a reference dye with known ϕ_f at constant instrument settings (see ??).

$$\phi_{f;rel} = \phi_{f;st} \cdot \frac{F_x}{F_{st}} \cdot \frac{f_{st}(\lambda_{ex})}{f_x(\lambda_{ex})} \cdot \frac{n_x^2}{n_{st}^2}. \quad (5)$$

$\phi_{f;st}$ is the fluorescence quantum yield of the standard, F is the integral photon flux, f is the absorption factor and n is the refractive index of the solvent; subscripts x and st denote the sample and standard, respectively.

The absolute ϕ_f determination can be done with an integrating sphere setup by directly measuring the number of emitted photons (N_{em}) and the number of absorbed photons (N_{abs}) without the need for a reference dye. Only this absolute method should be used for scattering samples such as NP suspensions, solid samples, films, and powder samples, as light scattering can affect the optical pathway and absorption of the sample.^{151–153}

2.2.3.4 Fluorescence lifetime (τ)

The second important parameter is τ which is the average time that the fluorophore is present in the excited state before it relaxes back to the ground state by emitting light (radiative decay) or via non-radiative decay pathways such as IC or ISC.¹⁵⁰

$$\tau = \frac{1}{k_r + k_{nr}}. \quad (6)$$

τ can be determined by using the time-correlated single-photon counting (TCSPC) method with a pulsed light source and a fast reacting detector.¹⁵⁰

2.2.4 Surface FGs

The wide-spread usage of PNP and the importance of surface chemistry for their applications make it mandatory to quantify the amount of surface groups on the particles. Without an accurate characterization and thorough quantification of the surface chemistry, it becomes very challenging to perform subsequent (bio)functionalizations efficiently and in a controlled fashion. Ideal methods for FG quantification should be fast in readout, easy in handling, inexpensive even for industrial routines, robust, reliable, and should have been validated.^{64,89,154} Additionally, it is important for the quantification method to distinguish between the total amount of functionalities on the PNP surface and the accessible amount, which can be utilized for coupling of small molecules, drugs, or biomolecules such as antibodies, peptides, and DNA to the NP surface. There are methods that are able to quantify the total amount of FGs, others quantify the application-relevant accessible amount, and yet other methods are able to quantify both amounts depending on special requirements such as the presence of method-relevant chemical elements or traceable groups. The various methods and techniques for FG quantification are summarized and divided into quantification methods for total amount, for accessible amount, and for both by color and grouping in ??.

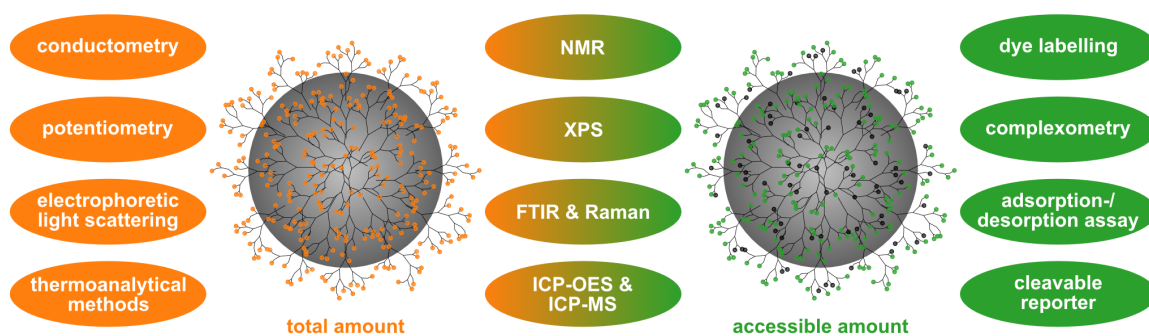


Figure 12: Quantification methods for total, accessible or both FG amounts.

Furthermore, the choice of a suitable quantification method requires knowledge of the method's general properties, including

- (i) Is a reporter necessary for signal generation or is the method label-free?
- (ii) Can the reporter size influence the quantification?
- (iii) Is the reporter covalently attached to the particle surface?
- (iv) Is a calibration required?
- (v) Does the method quantify the total or accessible amount of FGs?
- (vi) Is a penetration/deformation depth known?

Established analytical techniques such as nuclear magnetic resonance (NMR), inductively coupled plasma optical emission spectroscopy (ICP-OES), and inductively coupled plasma mass spectrometry (ICP-MS) can in principle be used for label-free FG determination, provided that relevant elements or traceable groups are present. Nevertheless, they require expensive and complicated instrumentation and elaborate data analysis. Simple and inexpensive methods are electrochemical titration methods such as conductometry¹⁵⁵ or potentiometry⁹⁴ which need only (de)protonatable FGs (label-free method) and label requiring optical methods.^{64,89}

2.2.4.1 Conductometric titration

Conductometric titration is a simple, fast, and inexpensive analytical method for the determination of the total/overall (de)protonatable FGs, for example, amino or carboxy groups on NPs, and enables also distinction between strongly and weakly acidic groups.¹⁵⁶ Sample preparation and analysis for this method are fast, and the instrumentation is simple and inexpensive (see ?? left).¹⁵⁷ In this technique the change of the electric conductivity in the analysis solution is measured during the successive addition of a base or acid. The addition of NaOH or HCl induces a (de)protonation or neutralization reaction in the solution and increases or decreases the conductivity with the changing concentrations of the two most highly conducting ions, the hydrogen (H^+) and hydroxyl ions (OH^-).¹⁵⁸ ?? (right) shows a typical conductometric titration curve of PNP after addition of excess NaOH deprotonating all FGs. This curve shows the change in conductivity plotted against the amount of added titrant volume.

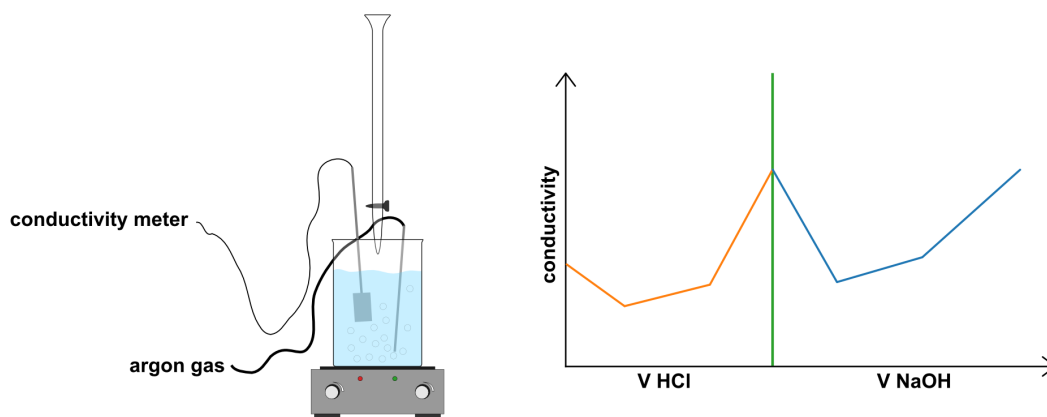


Figure 13: Schematic representation of the experimental setup for conductometric titration (left), and typical conductometric curve obtained for back and forth titration of aminated or carboxylated PNP with HCl and NaOH.

The titration with HCl and the back titration with NaOH consists of three sections each. Addition of HCl in the first section causes a decrease in conductivity due to the neutralization of OH^- in the solution with the H^+ from the titrant. Due to the neutralization reaction,

OH^- ions with higher equivalent conductivity ($\Lambda=199 \text{ Scm}^2$)¹⁵⁹ are replaced by Cl^- ions with a lower equivalent conductivity ($\Lambda=76 \text{ Scm}^2$).¹⁵⁹ The slope of this part of the curve is only affected by remaining Na^+ ($\Lambda=50 \text{ Scm}^2$)¹⁵⁹ and the added Cl^- . In the second section, further addition of HCl leads to a protonation of the ionized FGs. Only the Cl^- ions will increase the conductivity. The change in the slope between sections 2 and 3 indicates the end of the protonation of the analyte. The steep increase in conductivity in section 3 is due to the increase of free H^+ ions and Cl^- ions. The back titration with NaOH is in principle similar. The first section of the back titration is the neutralization reaction of the excess H^+ ions. In the second section, the analyte is deprotonated and in the last section an excess of OH^- and Na^+ remain in the solution.

The volume between the equivalence points, i.e. the intersections of the linear parts of the conductometric titration curves, which should be the same for the titration with HCl and NaOH, is proportional to the amount of (de)protonatable FGs in the solution.¹⁶⁰

$$\text{amount of FG} \left[\frac{\mu\text{mol}}{\text{g}} \right] = \frac{c_{\text{titrant}} \cdot V_{\text{titrant}}}{m_{\text{analyte}}} . \quad (7)$$

Due to the simplicity of this basic method, a lot of different materials have been quantified with it. Beck *et al.* used this method for the surface group quantification of cellulose nanocrystals.¹⁵⁷ Fras *et al.* applied it for the determination of FGs on cellulose fibers.¹⁵⁸ Martín-Domínguez quantified acidic groups of humic substances.¹⁵⁹ These are only some of the examples. The application of this method on PNP was also reported by Wen *et al.* in 2017¹⁵⁵ and a quantification and validation of this approach was also done in our group by Hennig *et al.* in 2015.⁸⁹

The simplicity of this method also entails some limitations. For the quantification of FGs, a large sample quantity is needed (typically at least FG density of 1000 nmol), which is however not a big obstacle for the typical synthesis scale of PNP.¹⁶¹ More importantly, the method does not distinguish between sample and additives such as salts, initiator or surfactant and is hence not selective, as all (de)protonatable functionalities in the analysis solution will be quantified.¹⁵⁵ For an accurate result, several washing steps of the analyte before the measurements are necessary. In the case of weak acids, the method is severely limited, because the dissociation degree can be too low to be measured accurately.¹⁶⁰ In ?? some pK_a values of commonly used FGs are listed.

Table 2: pK_a values of some surface FGs which are relevant for this work.

Functional groups	pK _a values
$-\text{H}_2\text{SiOH}$ ¹⁶²	4.5-5.5
$-\text{COOH}$ ¹⁶³	4.8
$-\text{NH}_3^+$ ¹⁶⁴	8-10
$-\text{SH}$ ¹⁶⁵	10.6

An additional source of interference can be dissolved CO_2 in the sample solution, forming carbonic acid. This can be avoided by working under an inert atmosphere.¹⁶⁶ Depending on the sample material, additional problems may occur. The method needs to be validated individually for different analyte materials.

2.2.4.2 Optical assays

Optical assays based on spectrophotometric or fluorometric readouts are simple, inexpensive, robust, fast, and can be performed with routine laboratory instrumentation. These methods are used to quantify accessible FGs on PNP. They require a spectrophotometrically or fluorometrically active label such as a colored product or a fluorescent dye that absorbs and/or emits in the UV, VIS or NIR region to be measured with common UV-VIS absorption or emission spectrometer.

For **dye labeling assays**, emissive dyes with reactive FGs can be attached covalently to the terminal surface FGs of NPs. A large variety of different dye classes for fluorophore labelling strategies are used in the quantitative analysis of surface FGs on different types of nanomaterials. One example was published recently by Felbeck *et al.*⁹⁹ They quantified amino functions on laponite disks with differently charged fluorescent dyes (see ??).

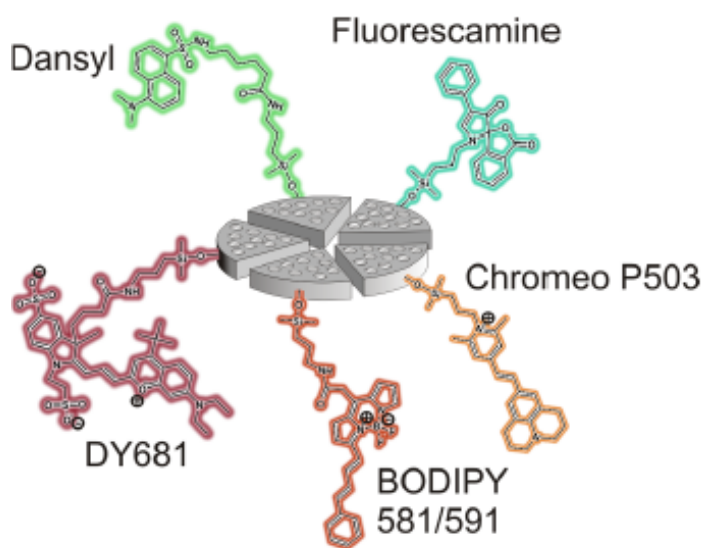


Figure 14: Schematic presentation of the different fluorescent labels covalently linked to the rim of laponite disks via 3-aminopropyldimethylsilane. Adapted with permission from Felbeck *et al.* Copyright 2015, American Chemical Society.

Other examples have been reported by Hennig *et al.*^{64,65} describing the fluorophore labelling of PMMA particles grafted with polyacrylic acid (PAA), where carboxy groups were conjugated with a 1,6-diaminohexane derivative of fluorescein-5-isothiocyanate. However, the simplicity of this conventional dye labelling quantification method also has some disadvan-

tages. The use of organic solvents for the organic dye labelling can lead to particle swelling and nonselective incorporation of fluorescent dyes or at worst dissolution of the particles. Furthermore, the direct determination of PNP-bound dyes is hampered by the NP scattering in spectrophotometric or fluorometric measurements and by dye-dye interactions at high local dye concentrations which can lead to self-quenching and prevent a reliable quantification.^{64,65} To mitigate these problems, the indirect quantification of unbound dye can be used.

Felbeck *et al.*⁹⁹ also used dye precursors that become strongly absorptive and/or emissive upon reaction with the respective FGs (“turn-on” or activatable labels). Related dye labels are so-called chameleon dyes^{167–169} which are color changing dyes. However, like the “always on” dyes, these dyes also show the same disadvantages, and additionally, require a calibration with a model system.

For the **multimodal cleavable linker labelling strategies**, structures with a binding part, cleavable part and a reporter part are necessary. Different cleavable units which are shown in ?? could be used for the linkers design.



Figure 15: Possible cleavable linkers for quantification of FGs on PNP.¹⁷⁰

The reporter part could be a dye that absorbs and emits in the UV-Vis range and bear additional traceable groups such as F, Eu, or S. The advantage of this method compared to the direct dye labelling method is that the reporter can be detected optically in solution after cleavage and a dissolution of the particles is not needed.

2.2.4.3 BCA assay for protein quantification

The bicinchoninic acid (BCA) assay is a spectrophotometric assay and is commonly used for the quantification of the total amount of proteins in aqueous solutions. The assay is based on the reduction of a Cu^{2+} complex to a Cu^+ complex under basic conditions and in the presence of biomolecules.¹⁷¹ At room temperature cysteine, cystine, tryptophan, and tyrosine amino acids of the proteins are responsible for the reduction reaction. At higher temperature, such as 37 °C or 60 °C, the peptide bond of the proteins is also accountable for the color changing reaction.¹⁷² Due to the reduction, the green colored Cu^{2+} complex becomes violet (see ??). This color change can be quantified spectrophotometrically at around 562 nm.^{28,171} The higher the absorption, the higher the amount of protein in the analyzed solution.

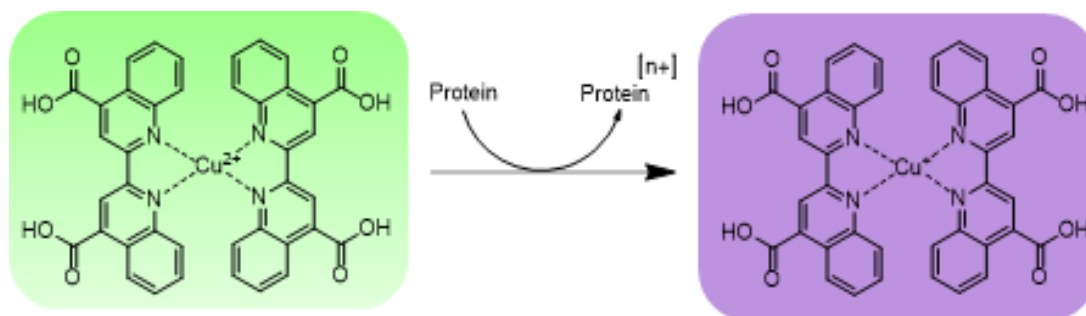


Figure 16: Schematic presentation of the **BCA** assay: reduction reaction of green Cu^{2+} complex to violet Cu^{+} complex in the present of the peptide-bound of proteins.

A disadvantage of the **BCA**-Assay is the time and temperature dependence of the reaction and the lack of an easily identifiable endpoint. Moreover, the **BCA** assay can respond to other redox-active species. In addition, the quantification of an unknown sample requires a calibration curve from the investigated protein. The calibration must be done under the same experimental conditions as the quantification of the analyzing sample.

While the **BCA** assay is suitable for the quantification of pure protein solutions, quantification on **NPs** or dye loaded **NPs** turns out to be more challenging due to the **NP** scattering or the spectral overlap. Therefore, it is important to adjust the **BCA** assay conditions to these circumstances.

2.2.4.4 Inductively coupled plasma optical emission spectroscopy (ICP-OES)

Since 1985 **ICP-OES** is established in routine laboratory analyses for the qualitative and quantitative determination of elements in solid, liquid, and gaseous samples. A schematic representation of an **ICP-OES** device is shown in ???. For the analysis, the sample is atomized, ionized, and excited by spraying it into an argon plasma of 6000-12000 K. The excited atoms of the sample emit light with element-specific wavelengths, which can be detected. These emission spectra give insights into the sample's chemical composition. **ICP-OES** offers the opportunity to determine almost all elements of the periodic table at trace levels. Nevertheless, the detection of some elements is extremely difficult due to the operating modes, such as Ar in an Ar plasma, air/solvents containing elements such as H, N, O, and C, halogen atoms emitting in the vacuum UV region, or radioactive/short-lived elements. **ICP-OES** has an extremely wide linear range and enables the determination of a multitude of elements simultaneously with proper calibration.^{173,174}

This well-established, highly sensitive, and versatile quantification technique is applied in geoanalysis for the analysis of rocks, soils, and sediments, in agricultural and food samples for the determination of essential nutrients and toxic elements, in biological and clinical samples for the determination of toxic or therapeutic elements, in environmental samples like water for the determination of P, Pd, Hg, Cd, or As, and especially in organic chemistry for the elemental information of analytes.¹⁷⁴ **ICP-OES** can also be used for the quantification

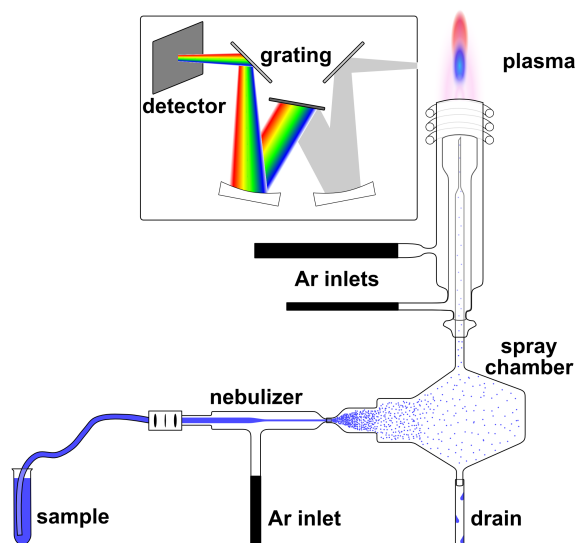


Figure 17: Schematic representation of an ICP-OES device with a nebulizer for the sample aerosol formation, a plasma for atomization, ionization and excitation of the sample, detection of the emitted wavelength with a CCD detector.

of the total or accessible amount of functionalities on PNP surfaces by tracing specifically introduced elements such as S, B, or Eu during the synthesis of the particles or afterwards by attaching it to the respective FGs.

2.2.4.5 Quantitative nuclear magnetic resonance (qNMR)

NMR is a widely used routine analysis technique for the identification and characterization of (newly) synthesized (organic) compounds. Besides the structural information, commonly used $^1\text{H-NMR}$ and $^{13}\text{C-NMR}$ give important information about the purity of the measured compounds. NMR detectable element isotopes have a nuclear spin > 0 and a sufficiently high (natural) abundance.

In the past few years, the use of NMR as a quantitative method (qNMR) received significant attention in academia and industry.¹⁷⁵ The fact that NMR has a short analysis time, simple sample preparation, and each NMR signal is proportional to the number of nuclei contributing to the signal makes qNMR a well suited technique for the quantification of organic molecules such as drug metabolites, capsular polysaccharides, residuals in complex solutions, peptides, and natural products.^{175–177} It has also been used for the analysis of the ligand shell of nanomaterials such as semiconductor quantum dots^{178–180} and for the quantification of FGs on silica nanostructured materials.¹⁸¹ In principal, it can also be used for PNP, directly quantifying the surface FGs or the attached dye labels if the NMR signals of these species appear at frequencies that are not covered by the matrix.

Commonly, qNMR analysis focuses on the measurement of protons (^1H), due to the high sensitivity and omnipresence of these nuclei in organic molecules. Other NMR-sensitive

nuclei such as ^{19}F , which can be specifically introduced into a molecule, can provide clear and single signal NMR spectra for quantification.¹⁷⁶ Alternatively, molecules containing specific isotopes such as ^{13}C can also be used.⁶⁴

For qNMR, parameters such as the longitudinal relaxation time T1, in cases where transversal relaxation time $T2 > T1$ also T2 and the pulse angle (0° - 90°) play an important role and need to be chosen carefully to optimize the quantification results. T1 is a characteristic time for longitudinal relaxation which is required to ensure that 63% relaxation of the corresponding protons. To be sure that 99.9% of the excited nuclei relax back to the ground state, the relaxation delay time must be set at least 7-times the T1 time of the proton with the slowest relaxation. The robustness of the method can be validated by changing one of three parameters, the number of scans, the temperature, or the mass of the internal standard (IS).¹⁷⁶

One of the most important steps in qNMR experiments is the selection of an IS. The IS must be of very high and known purity, well-known concentration, good solubility in the chosen solvent, should not interact or react with the analyte, not be volatile, and have sharp signals that do not overlap with the sample signals in the spectra.^{175,182} The concentration of the IS is then used as a reference peak for the quantification of the sample by comparing the integral of the standard peak with the integral of the analyte peak. In ?? a qNMR evaluation of (3-aminopropyl)triethoxysilane (APTES) functionalized silica NPs with 1,3,5 trioxane as IS is shown. Taking into account the different number of protons contributing to the individual signals, the concentration of aminopropyl groups is about 2.4 times higher than that of the IS.

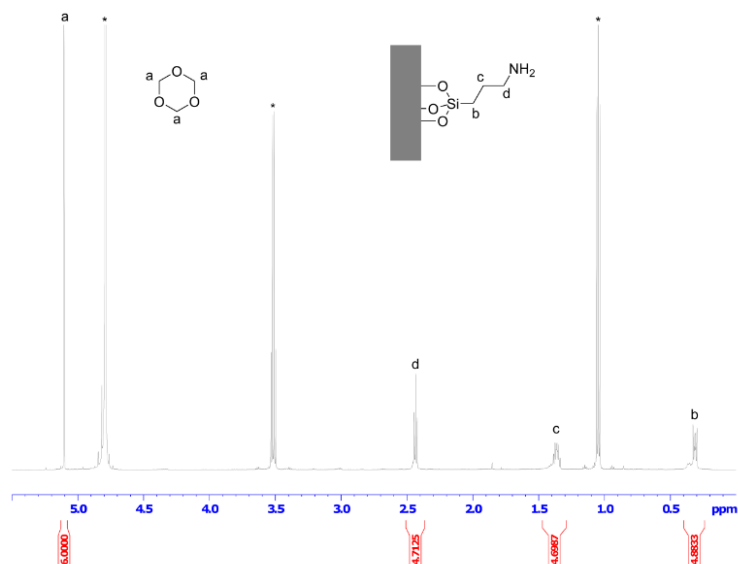


Figure 18: qNMR analysis example of functionalized silica NP with 1,3,5 trioxane as IS.

3 Results: Publications and Manuscripts

In the following section the published articles and submitted manuscripts are listed and the contributions of the author are specified.

3.1 Major contributions

3.1.1 Crystallization and Aggregation-Induced Emission in a Series of Pyrrolidinylvinylquinoxaline Derivatives

Nithiya Nirmalanathan, Thomas Behnke, Katrin Hoffmann, Daniel Kage, Charlotte F. Gers-Panther, Walter Frank, Thomas J. J. Müller, and Ute Resch-Genger*

J. Phys. Chem. C **2018**, *122*, 11119-11127.

DOI: [10.1021/acs.jpcc.8b01425](https://doi.org/10.1021/acs.jpcc.8b01425)

URL: <https://doi.org/10.1021/acs.jpcc.8b01425>

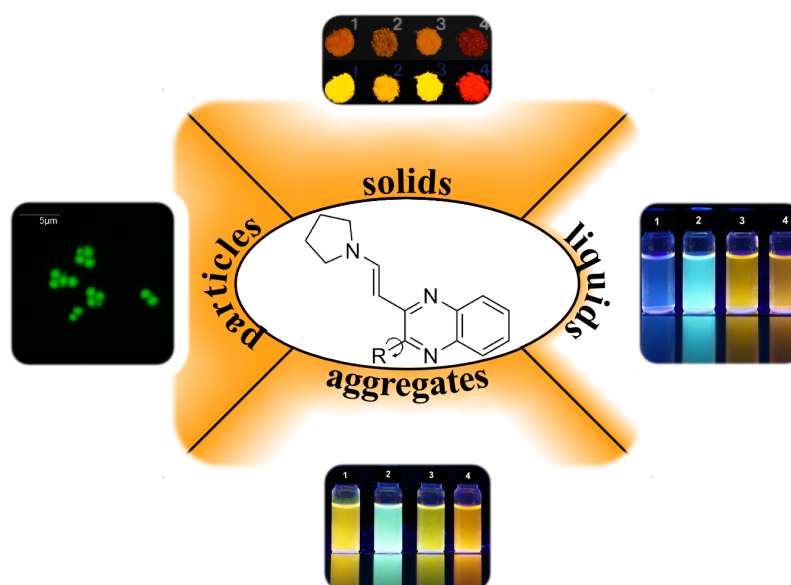


Figure 19: Adapted with permission from N. Nirmalanathan *et al.* Copyright 2018 Journal of Physical Chemistry C.

In this publication N. Nirmalanathan-Budau contributed the spectroscopic studies of the four pyrrolidinylnylquinoxaline derivatives in the solid state, diluted in ethanol, as aggregates in ethanol-water mixtures, and entrapped in preformed carboxylated PSP. She performed all experiments, evaluated and interpreted all data under supervision of Dr. T. Behnke, Dr. K. Hoffmann, and Dr. U. Resch-Genger. Dr. K. Hoffmann and D. Kage made the confocal laser scanning microscope (CLSM) images and the fluorescence lifetime imaging microscopy (FLIM) measurements. Dr. C. F. Gers-Panther synthesized the pyrrolidinylnylquinoxaline derivatives (synthesis is already published separately) and the dye crystals under supervision of Prof. Dr. T. J. J. Müller. Dr. W. Frank performed the X-ray diffraction (XRD) measurements.

The manuscript was mainly written by N. Nirmalanathan-Budau and Dr. U. Resch-Genger.

Estimated own contribution: $\approx 85\%$

3.1.2 Multimodal Cleavable Reporters vs Conventional Labels for Optical Quantification of Accessible Amino and Carboxy Groups on Nano- and Microparticles

Marko Moser,[§] Nithiya Nirmalananthan,[§] Thomas Behnke, Daniel Geißler, Ute Resch-Genger*

Anal. Chem. **2018**, *90*, 5887–5895.

DOI: [10.1021/acs.analchem.8b00666](https://doi.org/10.1021/acs.analchem.8b00666)

URL: <https://doi.org/10.1021/acs.analchem.8b00666>

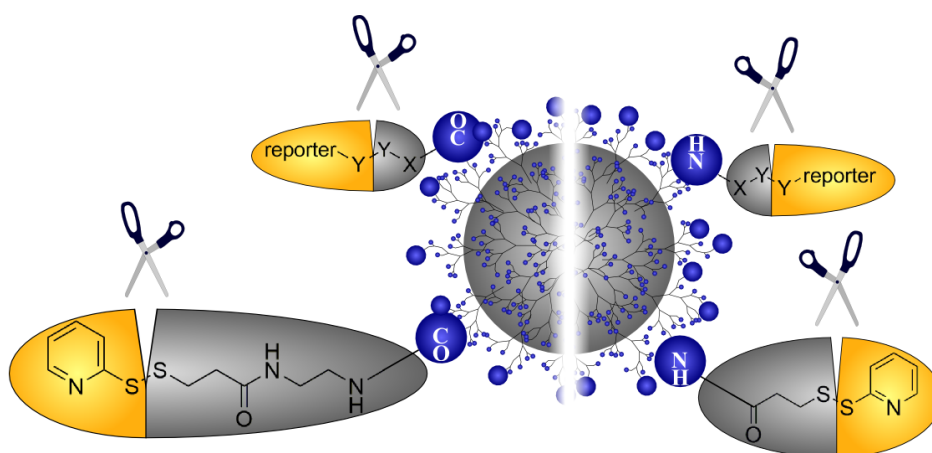


Figure 20: Adapted with permission from M. Moser and N. Nirmalananthan *et al.* Copyright 2018 Analytical Chemistry.

In this publication N. Nirmalananthan-Budau contributed the synthesis of the cleavable linker *N*-(aminoethyl)-3-(pyridin-2-yl)disulfanylpropanamide (*N*-APPA) and the quantification of the total and the accessible carboxy FGs on 100 nm-sized and 1 μ m-sized PSP. Additionally, the quantification of the amino functionalized 100 nm-sized and 1 μ m-sized PSP with the dye IR 797 was performed by N. Nirmalananthan. M. Moser performed the quantification of the total and the accessible amino FGs on 100 nm-sized and 1 μ m-sized PSP. Both authors evaluated and interpreted the obtained data jointly under supervision of Dr. T. Behnke, Dr. D. Geißler, and Dr. U. Resch-Genger.

The manuscript was mainly written by M. Moser, N. Nirmalananthan-Budau, and Dr. U. Resch-Genger.

Estimated own contribution: \approx 45 %

3.1.3 Multimodal Cleavable Reporters for Quantifying Carboxy and Amino Groups on Organic and Inorganic Nanoparticles

Nithiya Nirmalanathan-Budau, Bastian Rühle, Daniel Geißler, Marko Moser, Christopher Kläber, Andreas Schäfer, Ute Resch-Genger*

Sci. Rep. **2019**, *9*, 17577–17587.

DOI: [10.1038/s41598-019-53773-3](https://doi.org/10.1038/s41598-019-53773-3)

URL: <https://doi.org/10.1038/s41598-019-53773-3>

Pre-print version of the journal article submitted to *Sci. Rep.* in 2019. Reproduced with permission.

In this publication N. Nirmalanathan-Budau contributed the synthesis and characterization of carboxy and amino functionalized **PSP** with three different **FG** densities, the quantification of the amount of the total **FGs** of these **PSP** with conductometric titration, and the quantification and validation of the amount of accessible **FGs** on all **PSP** and mesoporous silica nanoparticles (MSN) with the cleavable reporters **N-APPA** and **N-succinimidyl-3-(2-pyridyldithio) propionate (SPDP)**. Additionally, N. Nirmalanathan-Budau encapsulated three different dyes into the **PSP** matrix, functionalized the **PSP** with representative biomolecules and quantified the amount of biomolecules bound to the particles. Also, she evaluated and interpreted the data under the supervision of Dr. D. Geißler and Dr. U. Resch-Genger. Dr. B. Rühle synthesized and characterized the carboxy and amino functionalized **MSN** and evaluated and interpreted the qNMR data which were measured by Dr. A. Schäfer. Christopher Kläber investigated the reproducibility of the obtained results under the supervision of N. Nirmalanathan-Budau and M. Moser established the synthesis of the monodisperse **PSP** core and the accessible amino group quantification with **SPDP** on commercial **PSP**.

The manuscript was mainly written by N. Nirmalanathan-Budau, Dr. B. Rühle, and Dr. U. Resch-Genger.

Estimated own contribution: $\approx 80\%$

Multimodal Cleavable Reporters for Quantifying Carboxy and Amino Groups on Organic and Inorganic Nanoparticles

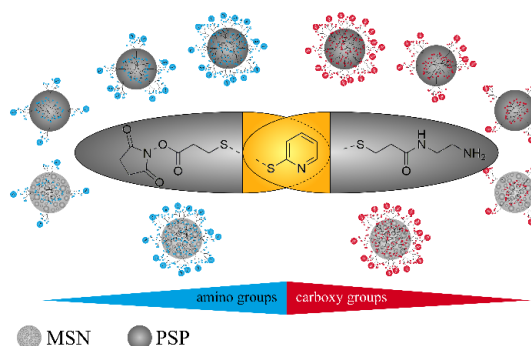
Nithiya Nirmalanathan-Budau,^{1,2} Bastian Rühle,¹ Daniel Geißler,¹ Marko Moser,^{1,2} Christopher Kläber,¹ Andreas Schäfer,² Ute Resch-Genger^{1,*}

¹) Federal Institute for Materials Research and Testing (BAM), Richard-Willstätter-Str. 11, D-12489 Berlin, Germany

²) Institut für Chemie und Biochemie, Freie Universität Berlin, Takustrasse 3, 14195, Berlin, Germany

KEYWORDS quantitative spectroscopy; polystyrene nanoparticle; mesoporous silica nanoparticles; cleavable reporter; functional groups; surface chemistry.

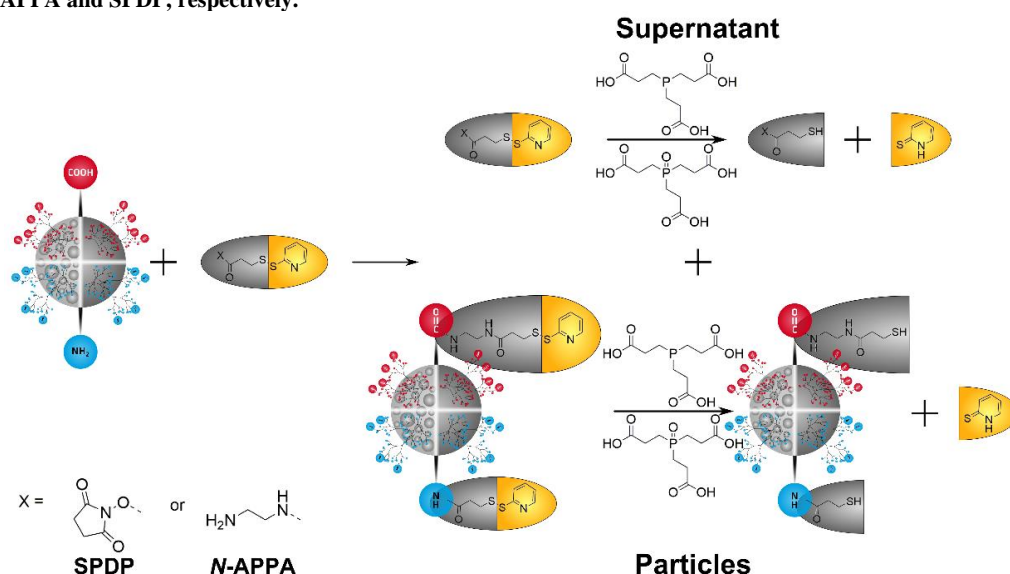
ABSTRACT: Organic and inorganic nanoparticles (NPs) are increasingly used as drug carriers, fluorescent sensors, and multimodal labels in the life and material sciences. These applications require knowledge of the chemical nature, total number of surface groups, and the number of groups accessible for subsequent coupling of e.g., antifouling ligands, targeting bioligands, or sensor molecules. To establish the concept of catch-and-release assays, cleavable probes were rationally designed from a quantitatively cleavable disulfide moiety and the optically detectable reporter 2-thiopyridone (2-TP). For quantifying surface groups on nanomaterials, first, a set of monodisperse carboxy- and amino-functionalized, 100 nm polymer and silica NPs with different surface group densities was synthesized. Subsequently, the accessible functional groups (FGs) were quantified via optical spectroscopy of the cleaved off reporter after its release in solution. Method validation was done with inductively coupled plasma optical emission spectroscopy (ICP-OES) utilizing the sulfur atom of 2-TP. This comparison underlined the reliability and versatility of our probes, which can be used for surface group quantification on all types of transparent, scattering, absorbing and/or fluorescent particles. The correlation between the total and accessible number of FGs quantified by conductometry, qNMR, and with our cleavable probes, together with the comparison to results of conjugation studies with differently sized biomolecules reveal the potential of catch-and-release reporters for surface analysis. Our findings also underline the importance of quantifying particularly the accessible amount of FGs for many applications of NPs in the life sciences.



Surface-functionalized organic, inorganic, and hybrid NPs are increasingly used in the life and material sciences¹⁻⁵ with many foreseeable applications e.g., in medical and consumer products. Amongst the most frequently used NPs are polystyrene particles (PSP) and silica NPs. These NPs can be prepared in different sizes with different surface functionalities and commonly show a high colloidal stability, a remarkable stability in biological environments, and a good biocompatibility.⁶⁻⁹ Moreover, they can be easily doped with functional molecules like fluorescent dyes and the large number of FGs at their surface makes them interesting carriers for stimuli-responsive sensor molecules and releasable drugs.¹⁰ In addition, mesoporous silica nanoparticles (MSN) have the advantage of a particularly large surface-to-volume ratio, with uniform and tunable pore sizes.¹¹⁻¹⁶ These properties paved the road for applications of PSP and MSN as multi-chromophoric reporters for signal enhancement and multiplexing strategies in optical assays, targeted probes in bioimaging studies, and nanoscale sensors.^{9,17-25}

For the majority of NP applications, NP performance depends mainly on particle size, size distribution, shape, surface chemistry, and charge. These features control colloidal stability, subsequent functionalization with ligands or biomolecules, and the interaction with the environment, including biological systems and thereby, biocompatibility and toxicity.^{4,26,27} Thus, important prerequisites for every commercial application of NPs are not only reproducible particle syntheses, but also suitable methods for characterizing these features. Particularly relevant for material processing and for monitoring batch-to-batch variation is the quantification of the total and accessible amounts of functional groups (FGs) at the NP surface.^{26,28,29} This calls for robust, simple, and inexpensive methods that should preferably be validated. Additionally, these methods should be specific, sensitive, fast, and versatile, i.e., useable for characterizing a broad variety of particle systems independent of their chemical composition or optical properties such as scattering, absorption, and emission. Meanwhile, there exists a large toolbox of methods for FG analysis to choose from. Principally suited techniques range from X-ray photoelectron spectroscopy (XPS),^{26,30} (quantitative) nuclear magnetic resonance spectroscopy (NMR),^{28,30}

Scheme 1. Mechanism for quantifying the accessible amount of carboxy and amino groups on PSP and MSN with the cleavable reporters *N*-APPA and SPDP, respectively.



thermogravimetric analysis (TGA) detecting mass losses during heating, sometimes in conjunction with Fourier Transform infrared spectroscopy (FTIR) or mass spectrometry (MS), as well as inductively coupled plasma optical emission spectroscopy (ICP-OES) and mass spectrometry (ICP-MS).³¹ These methods need, however, expensive instrumentation and are commonly operated by specifically trained personnel. Only very few methods can provide the total number of FGs. Examples are very versatile quantitative NMR (qNMR) requiring special measurement conditions and specific signals distinguishable from those of the NP matrix, and inexpensive electrochemical titration methods like conductometry for (de)protonatable FGs like carboxyl and amino groups. The latter methods require, however, a relatively large amount of substance and detect all (de)protonatable species present in solution which have comparable pK_a values unspecifically, including initiators, stabilizers, and surfactants remaining from the particle preparation, or other (de)protonatable surface groups such as silanols.³²⁻³⁵ Also, not all methods are suitable for all types of nanomaterials. For example, TGA with mass loss detection can only be used to determine the number of organic ligands, and thus, indirectly also the number of FGs for one type of surface ligand, on inorganic particles such as metal NPs, semiconductor quantum dots, and upconversion nanocrystals.³⁶

Elegant and frequently used methods to quantify the number of accessible surface groups are optical assays with spectrophotometrical or fluorometrical readout. These assays typically require a labeling step, i.e., the covalent binding of an optically detectable reporter bearing a reactive group. Quantification can be done with commonly used and widely available laboratory instrumentation such as spectrometers or microplate readers using a calibration curve obtained with a calibrant with known optical features closely matching those of the species detected in the respective assay. Optical measurements, however, can be affected by the absorption and fluorescence properties of the

(nano)material to be analyzed, dye-dye interactions leading to fluorescence quenching, and the inherent environment sensitivity of the spectroscopic features of the optical reporters used for quantification, namely the reporter's molar absorption coefficient or its fluorescence quantum yield. The consideration of these effects can impose challenges on assay calibration. To overcome some of these challenges, we recently presented the versatile concept of catch-and-release reporters, utilizing as first examples Ellman's reagent-related *N*-(aminomethyl)-3-(pyridin-2-yl)disulfanyl)propanamide (*N*-APPA) and *N*-Succinimidyl-3-(2-pyridyldithio) propionate (SPDP, NHS-PDP) for quantifying carboxy and amino groups on nano- and microparticles.³⁷ These cleavable probes consist of reactive groups for the coupling to surface functionalities via established conjugation chemistries, a quantitatively cleavable unit like in our case a reductively cleavable disulfide moiety, and an optically detectable reporter. Here, 2-thiopyridone (2-TP) was chosen containing a sulfur heteroatom that can also be quantified by complementary analytical techniques such as ICP-OES or ICP-MS. Cleavage of the disulfide unit releases 2-TP which can then be detected in the supernatant photometrically or with ICP-OES. Thereby, the distortion of optical signals by particle scattering is avoided and simple method validation by method comparisons and mass balances can be obtained.^{37,38}

To demonstrate the potential of our reductively cleavable probes for the quantification of some of the most frequently used particles and surface FGs in life science applications, we prepared a series of PSP and MSN, surface modified with varying densities of carboxyl and amino groups. These FGs were then quantified with conductometry, qNMR, and optical assays using the custom-designed cleavable probes *N*-APPA and SPDP shown in Scheme 1. To underline the versatility of our catch-and-release reporter concept, we also performed similar studies with dye-loaded PSP. Additionally, the results were cor-

related with data from PSP conjugation to differently sized biomolecules. Here, the proteins bovine serum albumin (BSA) and streptavidin (Sav), as well as wheat germ agglutinin (WGA) and concanavalin A (ConA), two lectins often used for the design of bioconjugates for bacteria detection,^{39,40} were chosen exemplarily due to their different protein size ranging from 25 to 67 kDa.

Materials and Methods

Materials. Styrene, potassium persulfate (PPS), sodium dodecyl sulfate (SDS), acrylic acid (AA), tetraethyl orthosilicate (TEOS), (3-aminopropyl)triethoxysilane (APTES), cetyltrimethylammonium bromide (CTAB), ammonium nitrate (NH_4NO_3), 4-morpholine-ethanesulfonic acid monohydrate (MES), 1-ethyl-3-(3-dimethylaminopropyl)carbodiimide (EDC), *N*-sulfohydroxysuccinimide (sulfo-NHS), *N*-hydroxysuccinimide (NHS), tetrahydrofuran (THF), dimethyl sulfoxide (DMSO), methanol (MeOH), ethanol (EtOH), sodium phosphate, *N*-Boc-ethylendiamine (EDA), sodium hydroxide (NaOH), and hydrochloric acid (HCl) were purchased from Sigma Aldrich Co. (Germany), *N*-Succinimidyl-3-(2-pyridyldithio) propionate (SPDP, NHS-PDP), tris(2-carboxyethyl) phosphine hydrochloride (TCEP) were obtained from Thermo Fisher Scientific Germany BV & Co KG (Germany), 2-cyanoethyltriethoxysilane (CETES) was obtained from abcr (Germany). All solvents used in optical assays were of spectroscopic grade. All solutions and buffers were prepared with Milli-Q water (Millipore).

Synthesis of functionalized PSP and MSN. The detailed synthetic procedures for the formation of the carboxy PSP and MSN as well as the aminated PSP is described in the Supporting Information (SI) together with the basic characterization of the produced particles regarding particle size / size distribution, surface charge, nitrogen sorption data, and thermogravimetric analysis (TGA).

Activation of carboxy groups on PSP and MSN. 120 μL of EDC (150 mM) and 60 μL of NHS (300 mM) in phosphate buffer (0.01 M; pH 5.5) were added to 100 μL of carboxy PSP or MSN (5 wt-%) in phosphate buffer. The mixture was shaken at 700 rpm for 1 h at RT, followed by one washing step using 300 μL of phosphate buffer (0.01 M, pH 8 for PSP and pH 7.4 for MSN).

Quantification of carboxy groups on PSP and MSN with *N*-APPA. 580 μL of the activated carboxy particle suspension (0.86 wt-%) were added to a solution of 1.65 μmol (for PSP) or 2.5 μmol (for MSN) *N*-APPA dissolved in 20 μL of methanol. The reaction mixture was shaken at 700 rpm for 16 h at RT, followed by centrifugation at 16,000 g for 40 min for PSP and 10,000 g for 5 min for MSN. The supernatant was removed, and the labeled particle suspension was washed three times with 400 μL of phosphate buffer (0.01 M, pH 8 for PSP and pH 7.4 for MSN). 50 μL of a TCEP stock solution (40 mM) in phosphate buffer were added to the combined supernatant fractions with unreacted *N*-APPA (pH of the resulting solution 6.8) and shaken at 600 rpm for 45 min at RT. The amount of 2-TP was quantified spectrophotometrically at $\lambda_{\text{abs}} = 343 \text{ nm}$ ($\epsilon = (8000 \pm 100) \text{ M}^{-1}\text{cm}^{-1}$).

Additionally, 50 μL of a TCEP stock solution were added to the washed particles (PSP, MSN), which were resuspended in 350 μL of phosphate buffer (pH of the resulting suspension

3.8). After shaking at 700 rpm for 45 min at RT, the particle suspension was washed twice with phosphate buffer. The amount of 2-TP in the combined supernatant fractions was determined spectrophotometrically. The formed thiol groups in the supernatants were also quantified with ICP-OES.

Quantification of amino groups on PSP and MSN with SPDP. Aminated PSP or MSN (0.86 wt-%) suspended in 580 μL of phosphate buffer (0.01 M, pH 8 for PSP and pH 7.4 for MSN) were added to a solution of 2 μmol of SPDP dissolved in 20 μL of DMSO and shaken at 700 rpm for 45 min at RT, followed by centrifugation at 16,000 g for 40 min for PSP and 10,000 g for 5 min for MSN. The supernatant was removed, and the particle suspensions were washed three times with 400 μL of phosphate buffer (0.01 M, pH 8 for PSP and pH 7.4 for MSN). The combined supernatant fractions containing unreacted SPDP were mixed with 50 μL of a TCEP stock solution (40 mM) in phosphate buffer to cleave the disulfide bond of SPDP. The reaction mixture was shaken at 700 rpm for 45 min at RT. The amount of 2-TP was quantified spectrophotometrically at $\lambda_{\text{abs}} = 343 \text{ nm}$ ($\epsilon = (8000 \pm 100) \text{ M}^{-1}\text{cm}^{-1}$).

Additionally, 50 μL of a TCEP stock solution were added to the washed particles (PSP and MSN) resuspended in 350 μL of phosphate buffer. After shaking at 700 rpm for 45 min at RT, the NP suspension was washed twice with phosphate buffer. The amount of 2-TP in the combined supernatant fractions was determined spectrophotometrically.

Dye staining of PSP. Carboxy-functionalized PSP with a high FG density (PSP-COOH-Hi) were stained exemplarily with the hydrophobic dyes phenyl-pyrrolidinylnylquinoline (PVQ), coumarin 153, and Nile Red following a previously described procedure from Behnke *et al.*¹⁹ For this purpose, 400 μL of a 6 mM dye solution in THF were added to 2400 μL of an aqueous suspension of 12 mg of PSP (0.5 wt-%). After shaking for 30 min at RT, the dye-loaded particles were washed three times with Milli-Q water to remove excess dye and subsequently resuspended in Milli-Q water under sonication. Then, the particles were washed with an ethanol–water mixture (50/50 v/v) to remove dye molecules adsorbed on the particle surface and larger dye aggregates. Subsequently, the particles were suspended in phosphate buffer (0.01 M; pH 5.5).

The quantification of the accessible amount of FGs on the dye-loaded PSP was done following the procedure for undoped carboxy PSP and MSN described above (see sections on *Activation of carboxy groups on PSP and MSN* and *Quantification of carboxy groups on PSP and MSN with N-APPA*).

Biomolecule coupling. After the activation of PSP-COOH-Hi (see section on *Activation of carboxy groups on PSP and MSN*), 275 μL of a bovine serum albumin (BSA), streptavidin (SAv), wheat germ agglutinin (WGA), or concanavalin A (ConA) in phosphate buffer (pH 7.4) containing 50 nmol of protein were added to 125 μL of a suspension of 5 mg of carboxy PSP (4 wt%) in phosphate buffer. The reaction mixture was shaken at RT overnight, followed by centrifugation. The supernatant was removed, the carboxy PSP were washed four times with 300 μL of phosphate buffer, all supernatants were combined, and then used for quantifying the amount of unreacted biomolecules.

BCA assay. The amount of biomolecules covalently bound to the carboxy PSP and unreacted biomolecules in the supernatant were determined with the BCA assay, using 25 μL of the 2.5-

fold diluted supernatant and 25 μL of a 2.5-fold diluted 5 wt-% suspension of biomolecule-labeled PSP. 200 μL of BCA reagent were added to these biomolecule-containing solutions at RT, and shaken for 120 min. To avoid signal distortions from particle scattering, the samples were centrifuged and 225 μL of the supernatants were added to a microtiter plate. The amount of biomolecules in all wells was quantified photometrically at $\lambda_{\text{abs.}} = 562 \text{ nm}$ by comparison with the results from the calibration curve, obtained with nine biomolecule standards (25 μL each) in a concentration range of 0 to 2000 $\mu\text{g}\cdot\text{mL}^{-1}$. The average biomolecule labeling density per mg of particles was calculated from the results of the BCA assay and the amount of particles used in the assay.

Instrumentation.

Dynamic light scattering (DLS) and Zeta Potential Measurements. The measurements were done with a Zetasizer Nano ZS instrument from Malvern Instruments Ltd. and the data were analyzed with the Zetasizer Software v7.02. All samples were measured at $T = 25^\circ\text{C}$ using PS-semi-micro cuvettes from ratiolab.

Scanning electron microscopy (STEM). STEM images were acquired on a Hitachi SU8030 EM. Images were taken with an acceleration voltage of 30 kV, in transmission electron (TE) mode. STEM images were used for the size analysis of the particles using the program FIJI.

Absorption measurements. The absorption spectra of the solutions were measured with a double beam spectrophotometer Specord 210plus from Analytik Jena (Germany) at RT in (10x10) mm quartz cuvettes from Hellma GmbH (Germany). For the BCA assay, absorption spectra were measured with a Microplate Reader Infinity M200 Pro from Tecan Inc. (Austria) at RT in microtiter plates from Fischer Scientific GmbH (Germany).

ICP-OES measurements. Quantitative ICP-OES analysis of the sulfur concentration of the suspended PSP was performed with a 5110 ICP-OES from Agilent Technologies. The sulfur signal was detected at 180.669 nm.

All relative standard deviations of the optical assays were derived from measurements of six independent samples. In the case of the ICP-OES measurements, the relative standard deviations were obtained from three independent measurements.

Conductometric titration. Conductivity measurements providing the maximum (or "total") number of (de)protonatable FGs were performed with a Modul 856 conductometer (Metrohm). For complete protonation/deprotonation of the FGs on the PSP surface, the conductivity of the PSP suspensions was adjusted to 100 $\mu\text{S}/\text{cm}$ with either HCl or NaOH prior to FG titration. The samples containing 10 mg of PSP-COOH or 5 mg of PSP-NH₂ in 80 mL of Milli-Q water were titrated with base (10 mM NaOH) or acid (10 mM HCl) in 20 μL steps under argon atmosphere to exclude CO₂ from air.

qNMR. Solution ¹H NMR spectra were collected at RT on a JEOL JNM-ECZ600R/M1 spectrometer operated at 600 MHz or on a Bruker Avance III HD 500 operated at 500 MHz. The MSN samples were prepared by drying a known amount (approximately 20 mg) at 80°C for 24 h, adding a known amount (approximately 1-2 mg) of 1,3,5 trioxane as an internal standard, and dissolving the mixture in 1 mL of NaOD in D₂O (1 M, pH 14) under sonication for 30 min at RT.⁴¹ Prior to collecting qNMR spectra, the T1 times of the components were measured using a series of inversion-recovery experiments. For the

qNMR spectra, single 90° pulses with an interpulse delay of at least seven times the longest T1 proton relaxation time (9.2 s for the methylene protons of trioxane in 1 M NaOD) and 128 scans (for samples with high FG density) or 512 scans (for samples with low FG density) were used. Prior to fast Fourier transformation (FFT), the free induction decays (FIDs) were multiplied with an exponential window function (line broadening 0.1 Hz). Transformed spectra were referenced to the residual solvent proton signal centered at 4.79 ppm (broad singlet),⁴² the phase was adjusted manually, and baseline-corrected integral values for the methylene protons of the silane groups and the internal standard were calculated. The purity of the internal standard was determined to be 96% by measuring it against 1,3,5-trimethoxybenzene of known purity (99%) in CDCl₃ (known amount of approximately 5 mg each in 1 mL of CDCl₃, 4 scans, 90° single pulse, interpulse delay of 20 s, other data processing parameters as described above).

Nitrogen sorption measurements. Nitrogen adsorption and desorption isotherms were recorded on an ASAP 2020 from micromeritics at liquid nitrogen temperature (77 K). Approximately 20 mg of sample were degassed for 16 h at 120°C under vacuum. BET surface areas were calculated from the linear part of the BET plots (typically in a partial pressure range from ~0.1-0.3), giving correlation coefficients of at least 0.999. BJH and NLDFT pore size distributions were calculated from the desorption branch, using an equilibrium model for N₂ on silica for NLDFT, as implemented in the Quantachrome ASiQwin software v 3.01.

Thermogravimetric analysis (TGA). The measurements were carried out on a Perkin-Elmer TGA 7 in synthetic air using approximately 5 mg of sample. The samples were heated from room temperature to 120 °C with a heating rate of 5 K/min, held at 120 °C for 60 min, and then heated from 120 °C to 700 °C with a heating rate of 5 K/min. The weight loss is normalized to the sample weight obtained after 60 min at 120 °C.

Results and discussion

Synthesis and characterization of carboxyl and amino PSP and MSN. Carboxy PSP with different FG densities were synthesized by an emulsion polymerization reaction following a slightly modified procedure from Holzapfel *et al.*⁴³ by adding different amounts of co-monomer AA. The size of the particles was determined with DLS to be between 100 nm and 150 nm (intensity-weighted harmonic mean diameter, so-called Z-average). The monodisperse, spherical, ~100 nm-sized particles have a zeta potential (in Milli-Q water, pH 7) of -25 mV and -48 mV for the samples with low functionalization density (PSP-COOH-Lo) and high functionalization density (PSP-COOH-Hi), respectively. The aminated PSP were synthesized by derivatization of PSP-COOH-Hi with three different amounts of EDA. This derivatization, which is also used in the synthesis of many commercialized aminated particles, results in an increase in PSP diameter by approximately 15 nm and an increase of the zeta potential from -48 mV for PSP-COOH-Hi to -25 mV for PSP-NH₂-Hi.

Carboxylated and aminated MSN were prepared according to the literature,^{44,45} by a slightly modified surfactant-templated (CTAB) sol-gel method using the co-condensation of TEOS and different amounts of CETES or APTES (10 mol% or 0.1 mol% with respect to TEOS). The resulting particles have intensity-weighted Z-average hydrodynamic diameters of 200

nm and 320 nm, respectively. The carboxy MSN have negative zeta potential values of -25 mV (MSN-COOH-Lo) and -15 mV (MSN-COOH-Hi) in Milli-Q water (pH 7). The respective aminated MSN have positive zeta potentials of +34 mV (MSN-NH₂-Lo) and +41 mV (MSN-NH₂-Hi). All synthesis procedures and characterization results of all particles used in this study are given in detail in the Supporting information (SI) in Figures S1-S7 and in Tables S1-S3.

Quantification of total carboxy and amino groups on PSP by conductometric titration. This method was previously validated by us for the quantification of carboxy groups on differently sized, surface modified polymethylmethacrylate (PMMA) micro- and nanoparticles grafted with poly(acrylic acid) by comparison with qNMR²⁸ and for aminated particles by a Fluram assay.³⁷ The results obtained for the carboxylated and aminated PSP are summarized in Table 1. This table reveals that the increasing volume of the co-monomer AA which was added during the in-situ co-polymerization leads to an increase of the carboxy FG density on the PSP surface.

The aminated PSP which were made by derivatization of PSP-COOH-Hi with different amounts of EDA all show similarly high amounts of FGs, with the measured values being comparable to the total amount of carboxy FGs on unmodified PSP-COOH-Hi. Since during the derivatization process only a few accessible carboxy groups are aminated, these particles bear a mixture of carboxy and amine FGs on their surface, and the conductometric titration is not sensitive enough to distinguish between the (de)protonation of carboxy and amino groups. Hence, only a sum of all (de)protonatable FGs can be obtained (see Figure S8). The corresponding value does not reflect the increase in amino FG density or the total amount of amino groups but can solely be used for the comparison of different PSP batches. Similarly, the quantification of the total amount of carboxy and amino FGs on MSN by conductometric titration is impeded by the presence of (de)protonatable silanol groups on the silica surface. The pK_a value of the silanol groups is about 4.5-5.5⁴⁶ and the pK_a values for the carboxy and amino FGs are estimated to be at around 4.8 and 9-11, respectively. Additionally, the silica framework of the MSN can be hydrolyzed under basic conditions under the consumption of hydroxide ions. Both effects

lead to an overestimation of the actual FG density (see Figure S9). Therefore, the total amount of carboxy and amino FGs on MSN was quantified by qNMR rather than conductometry.

Quantification of total carboxy and amino groups on MSN with qNMR. For the determination of the total number of FGs by qNMR, the MSN were dissolved in 1 M NaOD in D₂O together with a known amount of an internal standard, here 1,3,5 trioxane, and the amount of carboxy and amino groups was determined from the ratio of the integrals of the methylene protons of trioxane and the methylene protons of the alkyl silane bearing the respective FGs (see SI, Figure S10-S13). This procedure assumes that each alkyl chain corresponds to one FG.^{41,47}

The total amount of NH₂ FGs determined by qNMR agrees well with the expected amount of FGs calculated from the molar ratios of TEOS to APTES that were used for MSN synthesis. Assuming a stoichiometric reaction of TEOS and APTES and complete hydrolysis and condensation of the precursors, we expect FG densities of 1413 μmol/g and 17 μmol/g for samples MSN-NH₂-Hi and MSN-NH₂-Lo, respectively. The values measured by qNMR were 1532 μmol/g and 44 μmol/g for MSN-NH₂-Hi and MSN-NH₂-Lo (see Table 1). For carboxyl functionalized MSN, the difference between the expected and found amounts of FGs is somewhat larger. Under the same assumptions as above, as well as assuming a quantitative hydrolysis of nitrile groups to carboxy groups (which appears to be a good presumption given the very weak cyanoethylsilane signals visible in the ¹H NMR spectra in Figures S12 and S13), the expected FG densities are 1382 μmol/g and 17 μmol/g for samples MSN-COOH-Hi and MSN-COOH-Lo, while the amounts obtained from qNMR are 860 μmol/g and 65 μmol/g, respectively. A reason for the higher discrepancies could be – besides the simplifying nature of the assumptions – that some functional groups are hydrolyzed off and dissociate from the silica framework under the rather harsh nitrile hydrolysis conditions (5 h reflux in 9M HCl). Interestingly, the carboxylated MSN samples also show lower BET surface areas, lower pore volumes, and smaller pore diameters than the aminated MSN samples (see Table S3 and Figure S6). This observation could be attributed to different effects of APTES and CETES during the

Table 1. Quantification of Total and Accessible Amount of Surface FGs on PSP and MSN

	Surface density	Total FGs [μmol/g]	Accessible FGs [μmol/g]	(Accessible / Total) *100 [%]
PSP-COOH	Low	185 ± 36	27 ± 5	15
	Medium	393 ± 5	61 ± 6	16
	High	642 ± 14	85 ± 8	13
PSP-NH₂	Low	621 ± 44	38 ± 4	6
	Medium	671 ± 60	52 ± 2	8
	High	686 ± 45	65 ± 1	10
MSN-COOH	Low	65	19 ± 4	29
	High	860	50 ± 5	6
MSN-NH₂	Low	44	21 ± 7	46
	High	1532	219 ± 13	13

synthesis by co-condensation. While the differences are noteworthy, a more thorough investigation is beyond the scope of the current work. TGA data confirms a higher weight loss of the samples with high FG density as compared to the samples with low FG density. Due to an unknown (and also variable) amount of volatiles such as H₂O and EtOH present in the highly porous samples, an exact quantification of the FG density from TGA proved challenging. However, the differences in weight loss between the samples with high and low FG density were found to be similar for aminated and carboxylated MSNs, i.e., 3.5 and 3.7 wt-%, respectively.

Quantification of accessible carboxy and amino groups on PSP. *Carboxy PSP.* The amount of FGs on carboxy PSP with varying FG densities was quantified spectrophotometrically after reductive cleavage of the multimodal cleavable reporter *N*-APPA with TCEP and validated by quantifying the amount of sulfur by ICP-OES. First, *N*-APPA was coupled to the NHS activated carboxy PSP via its primary amino group. The 2-TP reporter, formed upon reductive cleavage of the disulfide bond with TCEP was used to quantify both the initially PSP-bound and the unreacted *N*-APPA molecules in the supernatant. The amount of carboxy groups accessible for *N*-APPA equals the amount of 2-TP cleaved off from the PSP surface. The results of the optical assays are summarized in Figure 1 and in Table 1.

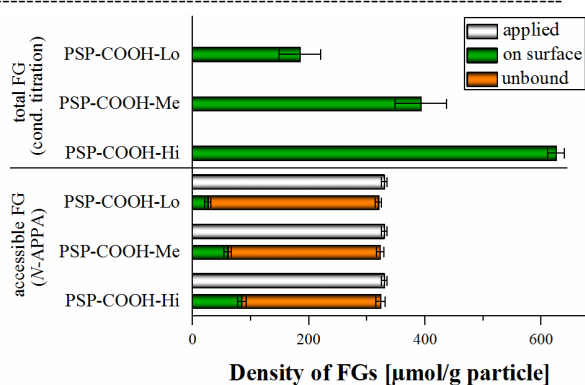


Figure 1. Quantification of FGs on PSP with different carboxy groups densities, of the total FG amount with conductometry and of the accessible FG amount with cleavable reporters. FG density differences are clearly detectable with both methods.

This method reveals that 15% (27 ± 5 μmol/g), 16% (61 ± 6 μmol/g) and 13% (85 ± 8 μmol/g) of the total amount of carboxy groups of PSP-COOH-Lo, PSP-COOH-Me, and PSP-COOH-Hi can be labeled with *N*-APPA, and thereby quantified. As expected, while the absolute amount of carboxy FGs on PSP-COOH-Hi is highest, the relative percentage of the accessible FGs is lower than that of PSP samples with lower FG densities. This underlines that a high FG density – albeit beneficial for the colloidal stability of the particles – must not necessarily be equally advantageous for the number of derivatizable FGs, where also steric effects and the size and charge of the molecules to be covalently attached come into play.

The results of our spectrophotometric detection of 2-TP are in good agreement with those obtained with ICP-OES (see Figure 2 and SI, Figure S14).

Amine PSP. Quantification of amino groups was done with the cleavable reporter SPDP closely related to *N*-APPA, that bears an active NHS-ester group for the coupling reaction with the

surface amino groups. The optical measurements of the reductively cleaved 2-TP reporter yielded 6%, 8%, and 10% of accessible amino groups (see Table 1 and Figure S15) for PSP-NH₂-Lo, PSP-NH₂-Me, and PSP-NH₂-Hi, respectively. Hence, an increase in the amount of EDA reacted with the PSP-COOH-Hi clearly leads to the introduction of an increasing number of amino groups accessible for our cleavable probe. This number is, however, most likely lower than the total number of amino groups which was not determined here due to the previously discussed problems of conductometry to distinguish between carboxy and amino FGs.

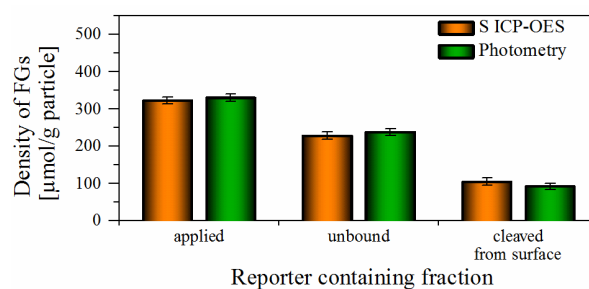


Figure 2. Validation of optical surface group analysis with *N*-APPA using ICP-OES exemplarily for PSP-COOH-Hi. A good correlation of both methods is observed.

In summary, the results obtained with carboxylated and aminated PSP underline the suitability of our custom-made multimodal cleavable reporters *N*-APPA and SPDP for reliably quantifying the amount of accessible FGs on polymer nanoparticles.

Quantification of accessible carboxy and amino groups on MSN. Next, our cleavable reporters *N*-APPA and SPDP were used for quantifying the amount of accessible carboxy and amino groups on another broadly used nanomaterial, MSN. For MSN, the assays with *N*-APPA and SPDP were performed in a less basic phosphate buffer at pH 7.4 to avoid particle etching or dissolution during the assay. As for PSP-COOH, the validation of the optical results for MSN-COOH was done by quantifying the amount of cleaved off 2-TP and the amount of unbound 2-TP in the supernatant with sulfur ICP-OES.

Carboxy MSN. The results obtained for the two carboxy MSN are summarized in Figure 3 and in Table 1. As expected, the overall amount of accessible FGs in sample MSN-COOH-Hi is higher than in MSN-COOH-Lo. The percentage of accessible FGs on MSN-COOH-Hi and MSN-COOH-Lo was measured to be 6% and 29% of the total amount of FGs on MSN-COOH-Hi and MSN-COOH-Lo, respectively. The validation of optical results by ICP-OES (see SI, Figure S16) also correlates well with the results from our optical assays for MSN.

This result trend is attributed to steric effects limiting the number of covalently attachable probe molecules at high FG densities. It is also obvious from these results that the total amount of FGs as determined by qNMR is much higher than the amount of accessible FGs derived from the catch-and-release assay. Since a co-condensation approach was used to synthesize the functionalized MSN, we expect the FGs to be evenly distributed throughout the particle surface. It is, however, possible that some FGs point into the silica pore walls rather than into the void of the mesopores or away from the outer surface, and hence, are not accessible for functionalization. Furthermore, while the pore size of the MSN is large enough to accommodate the cleavable reporter molecules, we assume that the reporters encounter first the FGs on the NP surface or the orifices of the

mesopores and then react preferentially with those. This can lead to a diffusional barrier that prevents or at least significantly slows down the diffusion of further probe molecules deeper into the mesopores where they could react with further FGs.

Amino MSN. Reaction of MSN-NH₂-Hi and MSN-NH₂-Lo with SPDP yielded 13% and 46% of accessible amino groups (see Table 1 and Figure S17). Here, again, the same trend is observed as for the other particles studied before. The well-matching mass balances, i.e., the fact that almost 100% of the initially used amount of the probe can be recovered either in its unbound form after the attachment step in the supernatant or after reductive cleavage from the particles, demonstrates that only a negligible amount of the reporter dye remains adsorbed to the large surface area of the porous structure and hence that our assays are also well-suited for porous host materials.

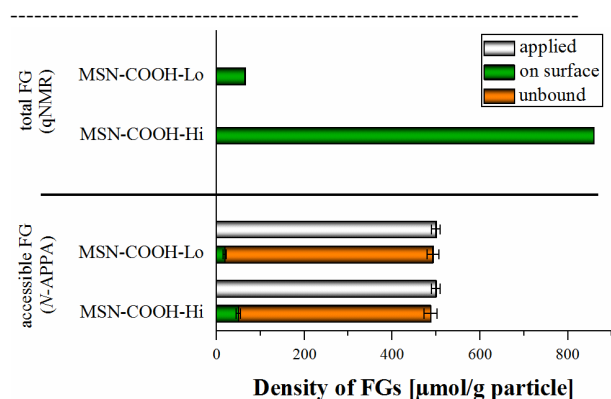


Figure 3. FG quantification on MSN-COOH-Lo and MSN-COOH-Hi using qNMR for the determination of the total amount and cleavable reporters for the quantification of the accessible amount of FGs. FG density differences are clearly detectable with both methods.

Quantification of accessible carboxy groups on fluorescent PSP with *N*-APPA. NPs used in the life sciences are often colored or fluorescent. Since conventional FG quantification methods that rely on dye labeling of NP surface FGs are hampered by light scattering or other optical interferences from the particles as well as possible fluorescence quenching interactions between neighboring reporters at the NP surface, a complete dissolution of the PSP matrix can be necessary prior to quantifying the FG-bound reporter dyes.³⁷ However, for stained particles this simultaneously leads to the release of the dyes encapsulated in the NP. This can result in spectral interferences in absorption and/or emission with the reporter dye used for FG quantification, and thus, limiting the versatility of this approach (see SI, Figure S18). In contrast, our versatile concept of catch-and-release assays is not affected by such interferences, as the quantification of both the unbound and the bound reporter are done in the supernatant after cleavage and particle separation. To demonstrate this absence of influence, we incorporated different hydrophobic fluorophores into PSP-COOH-Hi by a simple swelling/deswelling staining procedure that is also used for the fabrication of commercialized colored and fluorescent particles. This included frequently used dyes such as coumarin 153 and Nile Red^{20,48} as well as the PVQ derivative phenyl-pyrrolidinyl-vinylquinoxaline, a new dye revealing aggregation-induced emission (AIE).⁴⁹ As shown in Figure 4, the accessible amount of carboxy groups could be still determined with *N*-APPA for

the three dye-loaded PSP-COOH-Hi, and the obtained FG densities agree reasonably well with the FG density determined for the corresponding undoped (blank) PSP-COOH-Hi.

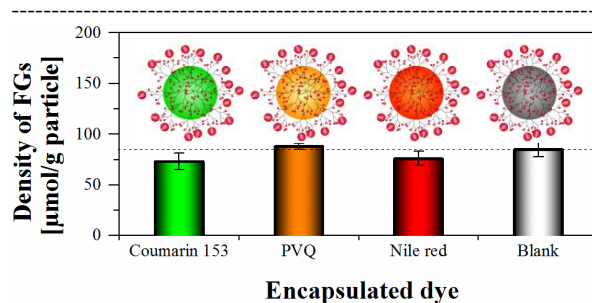


Figure 4. Accessible FG quantification of dye encoded carboxy PSP with cleavable reporter *N*-APPA.

Correlation with bioconjugation studies. Four differently sized biomolecules were coupled to the surface of 100 nm-sized PSP-COOH-Hi via the amine groups of their lysine residues or the N-terminus after activation of the PSP with EDC/sulfo-NHS. The exemplarily chosen proteins were BSA (67 kDa), often used as a model protein, SA_v (53 kDa), employed for the directed conjugation of biotinylated molecules to nanoparticles, and the smaller lectins WGA (36 kDa) and ConA (25 kDa) that are used, for example, for the staining of bacteria in conjunction with fluorescent labels.^{39,40} The BCA assay was used to quantify the amount of PSP-bound proteins and the amount of unreacted biomolecule in the supernatant after particle removal. The amount of FGs accessible for the covalent binding of such large and sterically demanding biomolecules is typically below 1% of the total FG amount on PSP with a high FG density. The results of our bioconjugation studies are shown in Figure 5. The mass balances, obtained from measurements of the unreacted biomolecules in the supernatant and the bound biomolecule on the PSP, and the coupling efficiencies of the biomolecules are detailed in the SI, Figure S19.

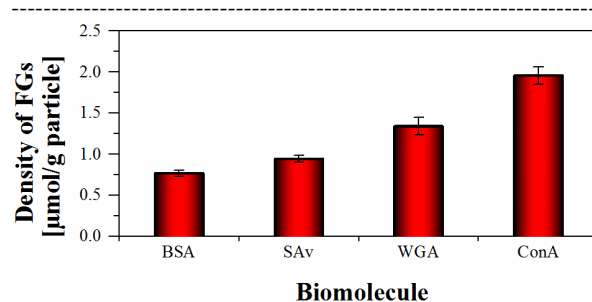


Figure 5. Amount of carboxy FGs accessible for bioconjugation of the differently sized proteins BSA, SA_v, WGA, and ConA.

As shown in Figure 5, the amount of NP-bound biomolecules, and hence, the amount of carboxy surface FGs accessible for bioconjugation clearly depends on biomolecule size. For example, while 1.9 $\mu\text{mol/g}$ of ConA could be bound to the particle surface, only 0.7 $\mu\text{mol/g}$ of the largest biomolecule BSA are coupled to the surface, i.e., 2.9 times less. Moreover, the total amount of carboxy functions is 338 times and the accessible amount as determined with *N*-APPA is 42.5 times higher than the amount of FGs available for the binding of the smallest protein of this series, ConA. For the synthesis of surface function-

alized particles, apparently optimization of the surface functionalization with respect to colloidal stability and minimal non-specific interactions appears to be more important than strategies to maximize the FG density as the latter does not necessarily correlate directly with a higher number of surface-attached biomolecules.

Conclusion and Outlook

In summary, with SPDP and *N*-APPA, we have a set of cleavable probes for the quantification of accessible amino and carboxyl surface groups on different types of particles at hand. The straightforward and versatile catch-and release assays with these probes allow for the quantification of unbound reporters in the supernatant and reporters cleaved off from the particle surface, thereby preventing the distortion of optical signals by particle scattering and fluorescence quenching via reporter-reporter interactions. Validation of the results from the optical assays can be elegantly achieved by comparison of the optical assays with the determination of sulfur in the different supernatants using ICP-OES. Surface group quantification utilizing *N*-APPA and SPDP is not limited to PSP matrices, but can be extended to inorganic porous systems such as MSN.

Our results underline the reliability and versatility of our probe design and the catch-and-release strategy. Our versatile concept can be used for surface group quantification on all types of transparent, scattering, absorbing, and/or fluorescent particles. The cleavable probes can be easily expanded to the determination of other bioanalytically relevant functional groups like maleimide or alkyne functionalities by the choice of the reactive group. Additionally, they can be adapted to other analytical techniques requiring different reporters, or to different types of linkers that can be quantitatively cleaved thermally, photochemically, or by pH, utilizing well-established chemistry, e.g. from drug delivery systems.

AUTHOR INFORMATION

Corresponding Author

* U.R.-G.: e-mail, ute.resch@bam.de; phone, ++49(0)30-8104-1134; fax, ++49(0)30-8104-71134.

ACKNOWLEDGMENT

This project has received funding from the Federal Ministry for Economic Affairs and Energy (BMW-i-10/12). We thank Dr. Charlotte Gers-Panther for the AIE dye PVQ, Dr. Johannes Horst Budau for help with the artwork, MSc. Maysoon Saleh for the acquisition of SEM images, Annett Zimathies and Carsten Prinz for nitrogen sorption measurements, Dr. Rainer Müller and Dr. Thomas Hirsch from the University of Regensburg for TGA measurements. We acknowledge the assistance of the Core Facility BioSupraMol supported by the DFG.

REFERENCES

- (1) Huhn, J.; Carrillo-Carrion, C.; Soliman, M. G.; Pfeiffer, C.; Valdeperez, D.; Masood, A.; Chakraborty, I.; Zhu, L.; Gallego, M.; Yue, Z.; Carril, M.; Feliu, N.; Escudero, A.; Alkilany, A. M.; Pelaz, B.; del Pino, P.; Parak, W. J. *Chem. Mater.* **2017**, *29*, 399-461.
- (2) Ghosh Chaudhuri, R.; Paria, S. *Chem. Rev.* **2012**, *112*, 2373-2433.
- (3) Kim, J.; Green, P. F. *Macromolecules* **2012**, *45*, 3496-3502.
- (4) Sapsford, K. E.; Tyner, K. M.; Dair, B. J.; Deschamps, J. R.; Medintz, I. L. *Anal. Chem.* **2011**, *83*, 4453-4488.
- (5) Stark, W. J.; Stoessel, P. R.; Wohlleben, W.; Hafner, A. *Chem. Soc. Rev.* **2015**, *44*, 5793-5805.
- (6) Banik, B. L.; Fattahi, P.; Brown, J. L. *Nanomed. Nanobiotechnol.* **2016**, *8*, 271-299.
- (7) Hetemi, D.; Pinson, J. *Chem. Soc. Rev.* **2017**, *46*, 5701-5713.

- (8) Rühle, B.; Davies, M.; Bein, T.; Bräuchle, C. *Zeitschrift für Naturforschung B* **2013**, *68*, 423-444.
- (9) Wang, Y.; Zhao, Q.; Han, N.; Bai, L.; Li, J.; Liu, J.; Che, E.; Hu, L.; Zhang, Q.; Jiang, T.; Wang, S. *Nanomedicine* **2015**, *11*, 313-327.
- (10) Reisch, A.; Klymchenko, A. S. *Small* **2016**, *12*, 1968-1992.
- (11) de Barros, A. L.; de Oliveira Ferraz, K. S.; Dantas, T. C.; Andrade, G. F.; Cardoso, V. N.; Sousa, E. M. *Mater. Sci. Eng. C Mater. Biol. Appl.* **2015**, *56*, 181-188.
- (12) Alarcos, N.; Cohen, B.; Ziolk, M.; Douhal, A. *Chem. Rev.* **2017**, *117*, 13639-13720.
- (13) Ellison, P. A.; Chen, F.; Goel, S.; Barnhart, T. E.; Nickles, R. J.; DeJesus, O. T.; Cai, W. *ACS Appl. Mater. Interfaces* **2017**, *9*, 6772-6781.
- (14) Huang, M.; Liu, L.; Wang, S.; Zhu, H.; Wu, D.; Yu, Z.; Zhou, S. *Langmuir* **2017**, *33*, 519-526.
- (15) Moreira, A. F.; Dias, D. R.; Correia, I. J. *Microporous Mesoporous Mater.* **2016**, *236*, 141-157.
- (16) Rosenholm, J. M.; Gulin-Sarfraz, T.; Mamaeva, V.; Niemi, R.; Ozlisesli, E.; Desai, D.; Antfolk, D.; von Haartman, E.; Lindberg, D.; Prabhakar, N.; Nareoja, T.; Sahlgren, C. *Small* **2016**, *12*, 1578-1592.
- (17) Quevedo, P. D.; Behnke, T.; Resch-Genger, U. *Anal. Bioanal. Chem.* **2016**, *408*, 4133-4149.
- (18) Napp, J.; Behnke, T.; Fischer, L.; Würth, C.; Wottawa, M.; Katschinski, D. M.; Alves, F.; Resch-Genger, U.; Schäferling, M. *Anal. Chem.* **2011**, *83*, 9039-9046.
- (19) Behnke, T.; Würth, C.; Laux, E.-M.; Hoffmann, K.; Resch-Genger, U. *Dyes Pigm.* **2012**, *94*, 247-257.
- (20) Behnke, T.; Würth, C.; Hoffmann, K.; Hübner, M.; Panne, U.; Resch-Genger, U. *J. Fluoresc.* **2011**, *21*, 937-944.
- (21) Wong, P. T.; Choi, S. K. *Chem. Rev.* **2015**, *115*, 3388-3432.
- (22) Sapsford, K. E.; Algar, W. R.; Berti, L.; Gemmill, K. B.; Casey, B. J.; Oh, E.; Stewart, M. H.; Medintz, I. L. *Chem. Rev.* **2013**, *113*, 1904-2074.
- (23) Hsiao, S.-M.; Peng, B.-Y.; Tseng, Y. S.; Liu, H.-T.; Chen, C.-H.; Lin, H.-M. *Microporous Mesoporous Mater.* **2017**, *250*, 210-220.
- (24) Perez, R. A.; Singh, R. K.; Kim, T.-H.; Kim, H.-W. *Mater. Horiz.* **2017**, *4*, 772-799.
- (25) Singh, R. K.; Patel, K. D.; Leong, K. W.; Kim, H. W. *ACS Appl. Mater. Interfaces* **2017**, *9*, 10309-10337.
- (26) Hennig, A.; Borchering, H.; Jaeger, C.; Hatami, S.; Würth, C.; Hoffmann, A.; Hoffmann, K.; Thiele, T.; Schedler, U.; Resch-Genger, U. *J. Am. Chem. Soc.* **2012**, *134*, 8268-8276.
- (27) Heuer-Jungemann, A.; Feliu, N.; Bakaimi, I.; Hamaly, M.; Alkilany, A.; Chakraborty, I.; Masood, A.; Casula, M. F.; Kostopoulou, A.; Oh, E.; Susumu, K.; Stewart, M. H.; Medintz, I. L.; Stratakis, E.; Parak, W. J.; Kanaras, A. G. *Chem. Rev.* **2019**.
- (28) Hennig, A.; Dietrich, P. M.; Hemmann, F.; Thiele, T.; Borchering, H.; Hoffmann, A.; Schedler, U.; Jäger, C.; Resch-Genger, U.; Unger, W. E. S. *Analyst* **2015**, *140*, 1804-1808.
- (29) Hennig, A.; Hoffmann, A.; Borchering, H.; Thiele, T.; Schedler, U.; Resch-Genger, U. *Chem. Commun.* **2011**, *47*, 7842-7844.
- (30) Gaborieau, M.; Nebhani, L.; Graf, R.; Barner, L.; Barner-Kowollik, C. *Macromolecules* **2010**, *43*, 3868-3875.
- (31) Wolfbeis, O. S. *Chem. Soc. Rev.* **2015**, *44*, 4743-4768.
- (32) Ji, S.; Hoye, T. R.; Macosko, C. W. *Macromolecules* **2005**, *38*, 4679-4686.
- (33) Lorenz, O.; Breidenich, N.; Denter, U.; Reinmüller, K. H.; Rose, G. *Angew. Makromol. Chem.* **1982**, *103*, 159-185.
- (34) Ito, S.; Ogawa, K.; Suzuki, H.; Wang, B.; Yoshida, R.; Kokufuta, E. *Langmuir* **1999**, *15*, 4289-4294.
- (35) Hoare, T.; Pelton, R. *Langmuir* **2004**, *20*, 2123-2133.
- (36) Zhang, L.; He, R.; Gu, H.-C. *Appl. Surf. Sci.* **2006**, *253*, 2611-2617.
- (37) Moser, M.; Nirmalanathan, N.; Behnke, T.; Geissler, D.; Resch-Genger, U. *Anal. Chem.* **2018**, *90*, 5887-5895.
- (38) Leubner, S.; Hatami, S.; Esendemir, N.; Lorenz, T.; Joswig, J. O.; Lesnyak, V.; Recknagel, S.; Gaponik, N.; Resch-Genger, U.; Eychmüller, A. *Dalton Transactions* **2013**, *42*, 12733-12740.
- (39) Fife, D. J.; Bruhn, D. F.; Miller, K. S.; Stoner, D. L. *Appl. Environ. Microbiol.* **2000**, *66*, 2208-2210.
- (40) Sizemore, R. K.; Caldwell, J. J.; Kendrick, A. S. *Appl. Environ. Microbiol.* **1990**, *56*, 2245-2247.
- (41) Crucho, C. I. C.; Baleizão, C.; Farinha, J. P. S. *Anal. Chem.* **2017**, *89*, 681-687.
- (42) Fulmer, G. R.; Miller, A. J. M.; Sherden, N. H.; Gottlieb, H. E.; Nudelman, A.; Stoltz, B. M.; Bercaw, J. E.; Goldberg, K. I. *Organometallics* **2010**, *29*, 2176-2179.
- (43) Holzapfel, V.; Musyanovych, A.; Landfester, K.; Lorenz, M. R.; Mailänder, V. *Macromolecular Chemistry and Physics* **2005**, *206*, 2440-2449.

- (44) Rühle, B.; Datz, S.; Argyo, C.; Bein, T.; Zink, J. I. *Chem. Comm.* **2016**, 52, 1843-1846.
- (45) Rühle, B.; Clemens, D. L.; Lee, B.-Y.; Horwitz, M. A.; Zink, J. I. *J. Am. Chem. Soc.* **2017**, *139*, 6663-6668.
- (46) Cloarec, J.-P.; Chevalier, C.; Genest, J.; Beauvais, J.; Chamas, H.; Chevolot, Y.; Baron, T.; Souifi, A. *Nanotechnology* **2016**, *27*, 295602.
- (47) Sun, Y.; Kunc, F.; Balhara, V.; Coleman, B.; Kodra, O.; Raza, M.; Chen, M.; Brinkmann, A.; Lopinski, G. P.; Johnston, L. J. *Nanoscale Adv.* **2019**, *1*, 1598-1607.
- (48) Huber, A.; Behnke, T.; Würth, C.; Jaeger, C.; Resch-Genger, U. *Anal. Chem.* **2012**, *84*, 3654-3661.
- (49) Nirmalanathan, N.; Behnke, T.; Hoffmann, K.; Kage, D.; Gers-Panther, C. F.; Frank, W.; Müller, T. J. J.; Resch-Genger, U. *J. Phys. Chem. C* **2018**, *122*, 11119-11127.

Supporting Information

Multimodal Cleavable Reporters- Quantification of Amino or Carboxy Groups on Organic and Inorganic Transparent and Fluorescent Nanoparticles with Different Surface Functional Group Densities

Nithiya Nirmalanathan-Budau,^{1,2} Bastian Rühle,¹ Daniel Geißler,¹ Marko Moser,^{1,2} Christopher Kläber,¹ Andreas Schäfer,² Ute Resch-Genger^{1,*}

¹⁾ Federal Institute for Materials Research and Testing (BAM), Richard-Willstätter-Str. 11, D-12489 Berlin, Germany

²⁾ Institut für Chemie und Biochemie, Freie Universität Berlin, Takustrasse 3, 14195, Berlin, Germany
Corresponding Author* U.R.-G.: e-mail, ute.resch@bam.de; phone, ++49(0)30-8104-1134; fax, ++49(0)30-8104-71134.

Table of Content:

I Synthesis and Characterization of polystyrene nanoparticles

Figure S1: Reaction scheme for the synthesis of carboxy PSP	page 2
Figure S2: Change of the particle-size with reaction time.	page 2
Table S1: Characterization of carboxy PSP	page 3
Figure S3: Derivatization scheme of carboxy PSP to amino PSP	page 3
Table S2: Characterization of amino PSP	page 4

II Synthesis and Characterization of mesoporous silica nanoparticles

Figure S4: Reaction scheme for the synthesis of MSN	page 5
Table S3: Characterization of carboxy and amino MSN	page 5
Figure S5: FTIR spectra of sample MSN-COOH-Hi	page 6
Figure S6: Nitrogen sorption data of MSN samples	page 7
Figure S7: TGA data of MSN samples	page 8

III Conductometric titration of carboxylated and aminated PSP and MSN

Figure S8: Conductometric titration of carboxylated and aminated PSP	page 9
Figure S9: Conductometric titration of carboxylated and aminated MSN	page 10

IV Quantitative NMR of aminated and carboxylated MSN

Figure S10: qNMR spectrum of sample MSN-NH ₂ -Hi	page 11
Figure S11: qNMR spectrum of sample MSN-NH ₂ -Lo	page 12
Figure S12: qNMR spectrum of sample MSN-COOH-Hi	page 13
Figure S13: qNMR spectrum of sample MSN-COOH-Lo	page 14

V Amino and Carboxy Group quantification and validation of PSP

Figure S14: PSP-COOH-Me and PSP-COOH-Lo validation with ICP-OES	page 15
Figure S15: FG quantification of PSP with multimodal cleavable reporters	page 15

VI Amino and Carboxy Group quantification and validation of MSN

Figure S16: MSN-COOH-Lo validation with ICP-OES	page 15
Figure S17: FG quantification of MSN with multimodal cleavable reporters	page 16

VII Quantification of dye loaded carboxy PSP

Figure S18: Absorption and emission spectra of dyes in THF and the overlap of NHS-Fluorescein and Fluram	page 16
---	----------------

VIII Biofunctionalization of carboxy PSP

Figure S19: Biomolecule-derivatizable amount of carboxylic functions	page 17
---	----------------

I Synthesis and Characterization of polystyrene nanoparticles

Synthesis of carboxy polystyrene nanoparticles. The carboxylated PSP with different FG densities were synthesized via emulsion polymerization under argon atmosphere. For PSP core synthesis, a 400 μL aqueous solution of the radical starter PPS (0.148 mmol) was added to a mixture of 5200 μL of surfactant SDS (0.042 mmol) and 1300 μL of styrene monomer (11.36 mmol) in aqueous solution at 70°C. After 1 h of stirring at 350 rpm, 10 μL , 30 μL , 120 μL or 300 μL of co-monomer AA (0.146 mmol, 0.437 mmol, 1.75 mmol, 4.37 mmol) were added to the suspension and stirred for further 3 h at 70 °C. After cooling to room temperature (RT), the particle suspension was diluted 6-fold. To remove large chunks, the suspension was centrifugated two times at 15000 g for 2 min and the supernatants were collected. For all further experiment the combined supernatant was used after three further centrifugation and washing steps at 16000 g for 1 h for removing the SDS and KPS containing supernatant.

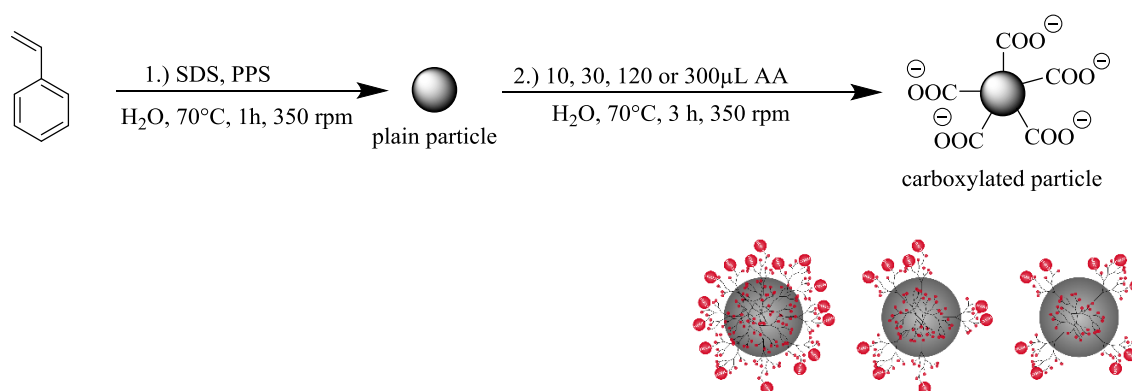


Figure S1: Reaction scheme for the synthesis of carboxy polystyrene nanoparticles with different densities of FGs.

Synthesis screening of carboxy polystyrene nanoparticles. At 70°C the core particles are generated within one hour. By adding different amounts of co-monomer acrylic acid (AA) the surface of the plain core will be grafted with different densities of carboxy functional groups (FGs). The core-shell particles synthesis was quenched by dilution with 35 mL of water after 240 min since the hydrodynamic diameter of the particle did not change significantly any more after 180 min.

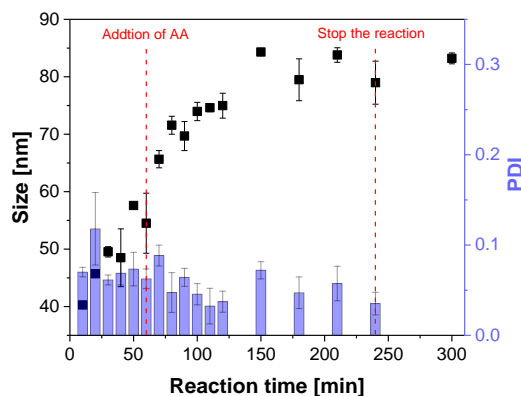
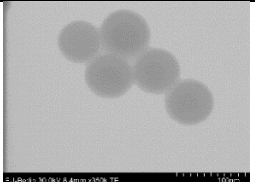
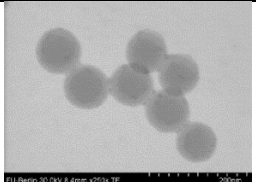
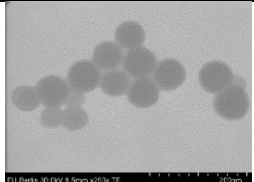
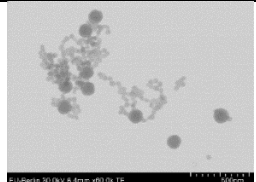


Figure S2: Change of particle size with reaction time.

Characterization of carboxy PSP. The NP with different amounts of co-monomer AA have a hydrodynamic diameter of around 110 nm. While addition of high amounts of AA leads to a polydisperse particle suspension with core-shell particles and smaller acrylic acid particles (see Table S1 last column), a low volume of co-monomer leads to a colloiddally unstable core-shell system in which the particles tend to agglomerate and show a higher hydrodynamic diameter and PDI. As expected, the zeta potential decreased with increasing FG density.

Table S1: Characterization of carboxy PSP.

	PSP-COOH			
	10 μ L AA (PSP-COOH-Lo)	30 μ L AA (PSP-COOH-Me)	120 μ L AA (PSP-COOH-Hi)	300 μ L AA
Hydrodynamic diameter [nm]	148 \pm 27	121 \pm 1	113 \pm 3	polydisperse
PDI	0.280 \pm 0.033	0.090 \pm 0.027	0.142 \pm 0.009	-
Zeta potential	-25 mV	-30 mV	-48 mV	-
SEM				

Synthesis of aminated polystyrene nanoparticles. The aminated PSP with different FG densities were synthesized by derivatization of the carboxy PSP with the highest FG density. 120 μ L of EDC (150 mM) and 60 μ L of s-NHS (300 mM) in MES buffer (0.05 M; pH 5) were added to 100 μ L of carboxylated PSP (5 wt %) after washing the particle three times with MES buffer. The mixture was shaken at 600 rpm for 1 h at RT, followed by one washing step using 480 μ L of phosphate buffer (0.01 M, pH 8). Subsequently, 580 μ L of the activated carboxylated particle suspension (0.86 wt-%) were added to a solution of 200, 1000, 2500 nmol *N*-Boc-ethylendiamine dissolved in 20 μ L of DMSO. The reaction mixture was shaken at 600 rpm for 16 h at RT, followed by centrifugation at 16,000 g for 40 min. The supernatant was removed, and the PSP were deprotected two times with 400 μ L of HCl (0.085 M) and washed two times with phosphate buffer (0.01 M, pH 8).

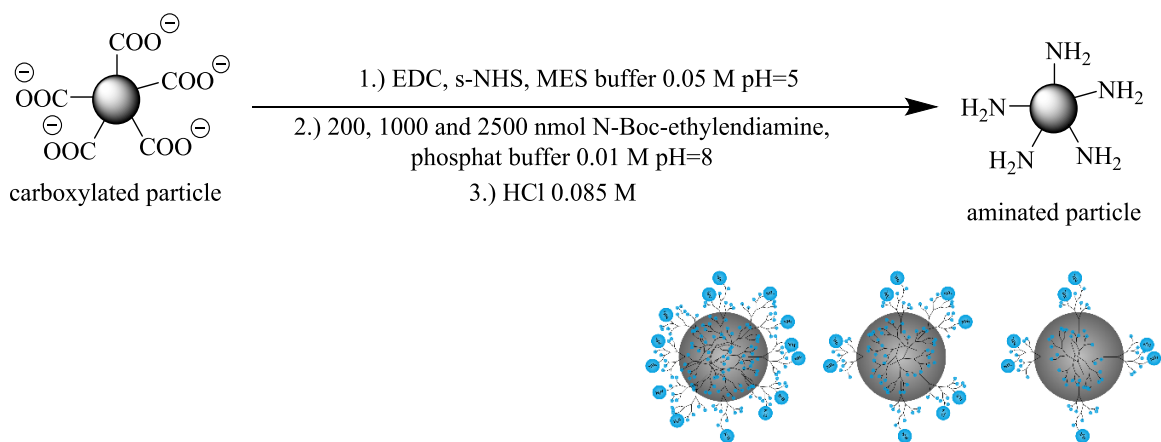


Figure S3: Derivatization scheme of carboxy PSP to amino PSP.

Characterization of amino PSP.

Table S2: Characterization of amino PSP.

	PSP-NH ₂		
	200 nmol EDA (Low)	1000 nmol EDA (Medium)	2500 nmol EDA (High)
Hydrodynamic diameter [nm]	108 ± 3	124 ± 4	135 ± 5
PDI	0.115 ± 0.009	0.148 ± 0.011	0.130 ± 0.012
Zeta potential	-32 mV	-31 mV	-25 mV

II Synthesis and Characterization of mesoporous silica nanoparticles (MSN)

Synthesis of aminated MSN. For the synthesis of aminated MSN with different FG densities, a mixture of 100 mL of Millipore water, 200 mg of hexadecyltrimethylammonium bromide (CTAB; 0.549 mmol) and 1200 µL of NaOH (1.00 M) was prepared and stirred for 20 min @ 80°C. Then, a mixture of 1000 µL of tetraethoxysilane (TEOS; 4.48 mmol) and an appropriate amount of 3-aminopropyl triethoxysilane (APTES; 0.1 mol% or 10 mol%; 1.06 µL or 106 µL) was added dropwise to this mixture under vigorous stirring. The resulting mixture was vigorously stirred for another 2 h at 80°C and afterwards centrifuged for 12 min at 13,640 g. The supernatant was discarded, and the nanoparticles were washed twice with EtOH (2 x 90 mL). To extract the surfactant from the pores, the nanoparticles were resuspended in 90 mL of ethanolic NH₄NO₃ solution (20 mg/mL), refluxed for 2 h, centrifuged again for 12 min at 13,640 g, washed once with 90 mL of EtOH, resuspended in 90 mL of EtOH:HCl (conc) (90:10 v/v) and refluxed again for 2 h. Finally, the suspension was centrifuged for 12 min at 13,640 g, washed twice with EtOH (2 x 90 mL) and stored in 30 mL of EtOH.

Synthesis of carboxylated MSN. For the synthesis of carboxylated MSN with different FG densities, a mixture of 100 mL of Millipore water, 200 mg of hexadecyltrimethylammonium bromide (CTAB; 0.549 mmol) and 1200 µL of NaOH (1.00 M) was prepared and stirred for 20 min @ 80 °C. Then, a mixture of 1000 µL of tetraethoxysilane (TEOS; 4.48 mmol) and an appropriate amount of 2-cyanoethyl triethoxysilane (CETES; 0.1 mol% or 10 mol%; 1.01 µL or 101 µL) was added dropwise to this mixture under vigorous stirring. The resulting mixture was vigorously stirred for another 2 h at 80°C and afterwards centrifuged for 12 min at 13,640 g. The supernatant was discarded, and the nanoparticles were washed twice with EtOH (2 x 90 mL). To extract the surfactant from the pores, the nanoparticles were resuspended in 90 mL of ethanolic NH₄NO₃ solution (20 mg/mL), refluxed for 2 h, centrifuged again for 12 min at 13,640 g, and washed once with 90 mL of EtOH. To further extract the template and to hydrolyze the nitrile groups to carboxylic acid groups, the particles were resuspended in 40 mL of H₂O:HCl (conc) (10:30 v/v) and refluxed for 5 h. Successful hydrolysis of the nitrile groups to carboxy groups was confirmed from ATR-IR spectroscopy (Figure S5; after hydrolysis, new bands appear at $\nu = 1718 \text{ cm}^{-1}$ and $\nu = 1412 \text{ cm}^{-1}$ that can be assigned to C=O stretching and O-H bending vibrations, respectively) and NMR spectroscopy (Figure S10 and S11; the signal at $\delta = 2.44 \text{ ppm}$ from the cyanoethylsilane (peak labeled with a # sign) is negligible after hydrolysis, and a new peak at $\delta = 2.09 \text{ ppm}$ (peak labeled c) that can be assigned to the methylene group of the carboxy-silane is clearly visible). Finally, the suspension was centrifuged for 12 min at 13640 g, washed twice with EtOH (2 x 90 mL) and stored in 30 mL of EtOH.

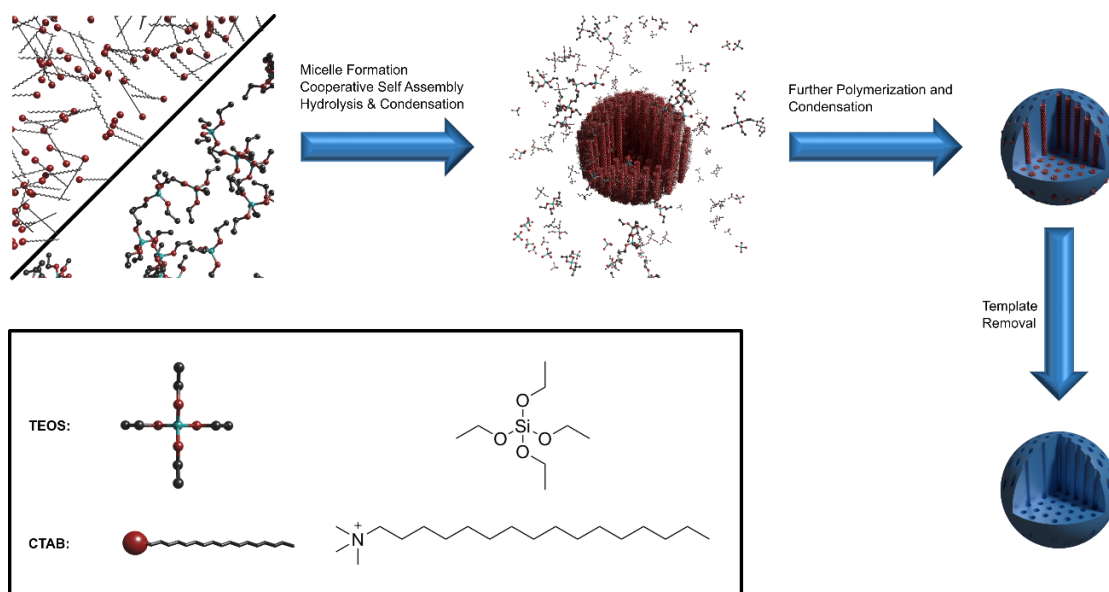


Figure S4: Reaction scheme for the synthesis of mesoporous silica nanoparticles.

Characterization of aminated and carboxylated MSN.

Table S3: Characterization of aminated and carboxylated MSN.

	MSN-COOH		MSN-NH ₂	
	0.1 mol% (low)	10 mol% (high)	0.1 mol% (low)	10 mol% (high)
Hydrodynamic diameter [nm]	252.0 ± 8.9	222.3 ± 1.7	320.6 ± 2.7	216.5 ± 1.8
PDI	0.257 ± 0.010	0.237 ± 0.013	0.228 ± 0.014	0.226 ± 0.006
Zeta potential [mV]	-25.1 ± 3.0	-15.4 ± 1.63	+34.3 ± 1.71	+41.3 ± 0.86
TGA weight loss at 700°C [wt %]	5.4	9.1	10.9	14.4
S_{BET} [m²/g]	738	729	1033	976
V_{tot} [cm³/g]	1.12	1.23	1.58	1.88
d_{BJH} [nm]	2.4	2.3	2.5	2.5
d_{NLDFT} [nm]	3.7	3.4	4.4	4.3

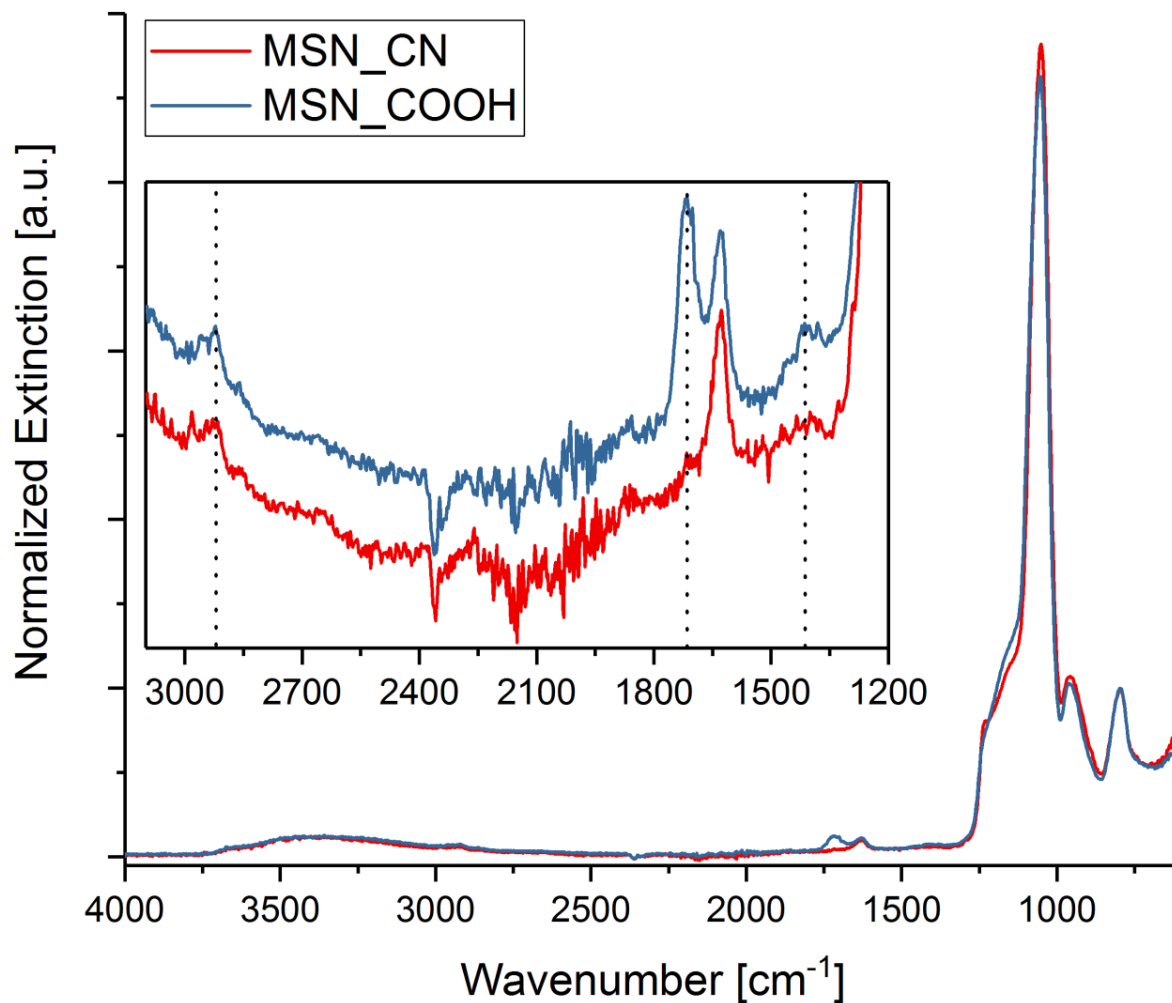


Figure S5: FTIR spectra of sample MSN-COOH-Hi before (red) and after (blue) hydrolysis of the nitrile groups of CETES to carboxy groups. Spectra are normalized to the Si-O-Si vibration at $\nu = 796 \text{ cm}^{-1}$ and slightly vertically offset for clarity. Dotted lines in the inset indicate the C-H stretching vibrations at around 2923 cm^{-1} , C=O stretching vibrations at $\nu = 1718 \text{ cm}^{-1}$, and O-H bending vibrations at $\nu = 1412 \text{ cm}^{-1}$, respectively.

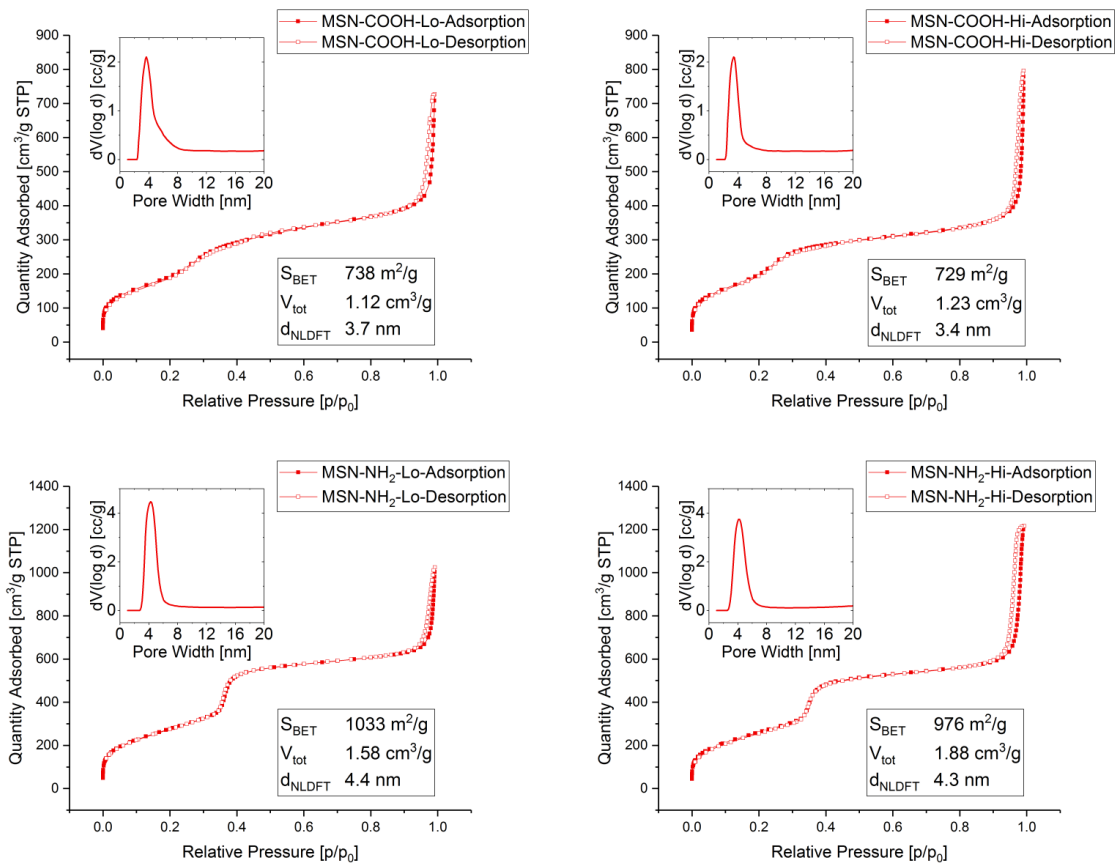


Figure S6: Nitrogen sorption data of samples MSN-COOH-Lo (top left), MSN-COOH-Hi (top right), MSN-NH₂-Lo (bottom left), MSN-NH₂-Hi (bottom right). Insets show the NLDFT pore size distribution. The BET surface area (S_{BET}), the total pore volume (V_{tot}), and the NLDFT pore diameter at the maximum of the pore size distribution (d_{NLDFT}) are also indicated.

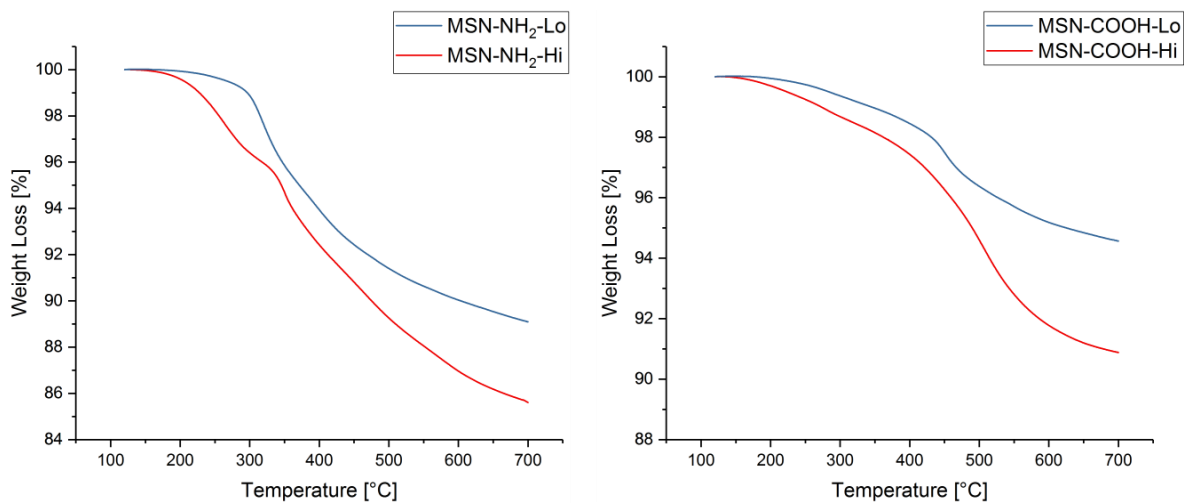


Figure S7: Thermogravimetric analysis of samples MSN-NH₂-Lo and MSN-NH₂-Hi (left) and MSN-COOH-Lo and MSN-COOH-Hi (right).

III Conductometric titration of carboxylated and aminated PSP and MSN

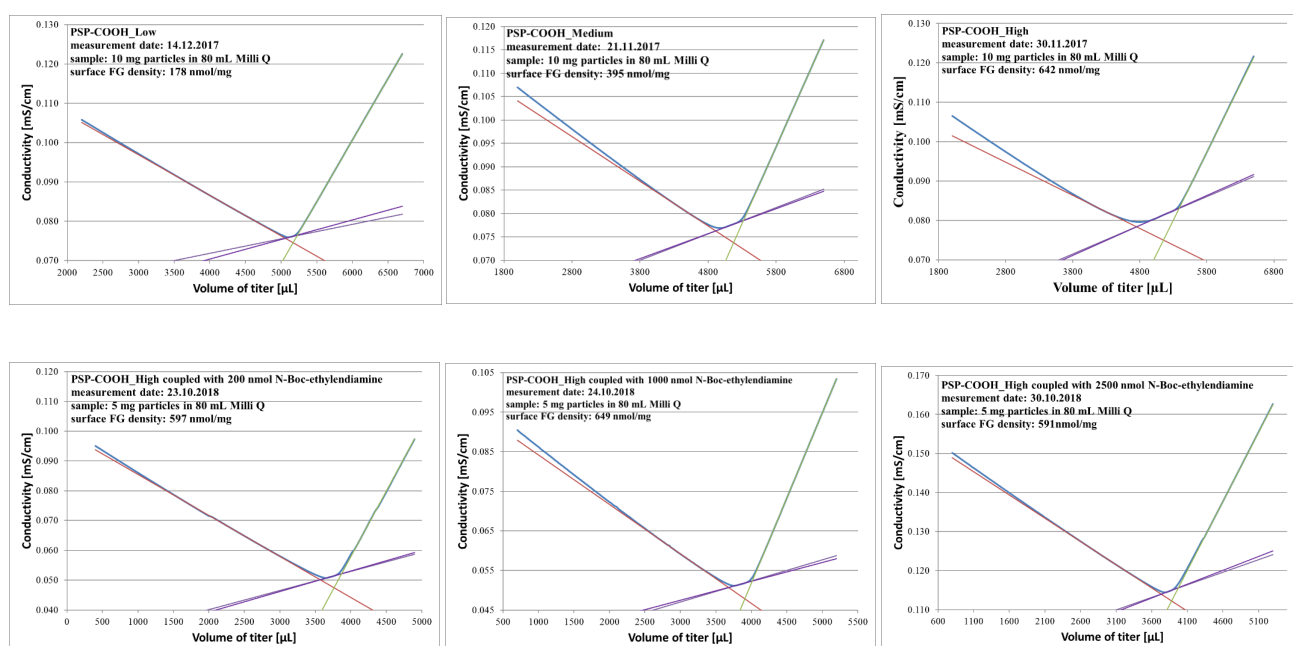


Figure S8: Conductometric titration of carboxylated (top) and aminated (bottom) PSP; 10 mg of PSP-COOH-Lo (top, left), PSP-COOH-Me (top, middle), PSP-COOH-Hi (top, right) and 5 mg of PSP-NH₂-Lo (bottom, left), PSP-NH₂-Me (bottom, middle), PSP-NH₂-Hi (bottom, right) were titrated for the quantification of the total amount of FGs.

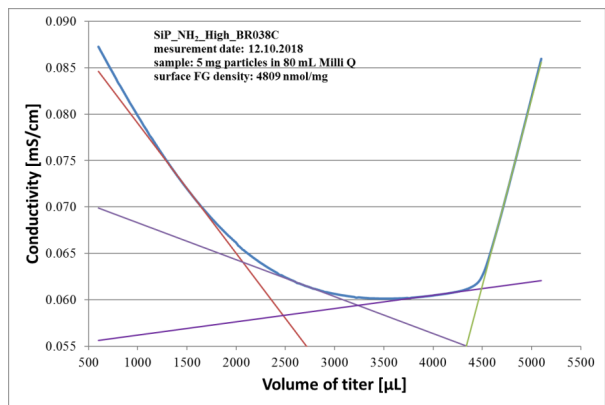
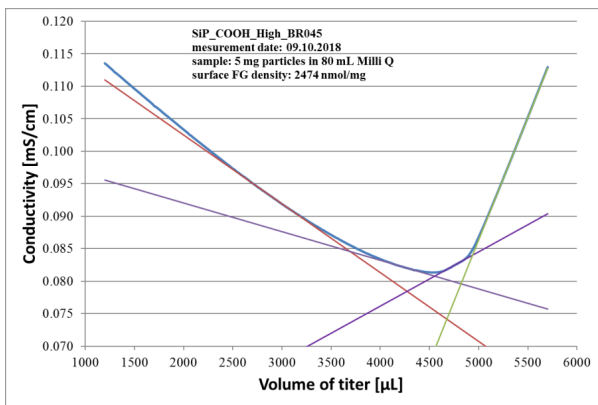


Figure S9: Conductometric titration of carboxylated (left) and aminated (right) MSN.

IV Quantitative NMR of aminated and carboxylated MSN

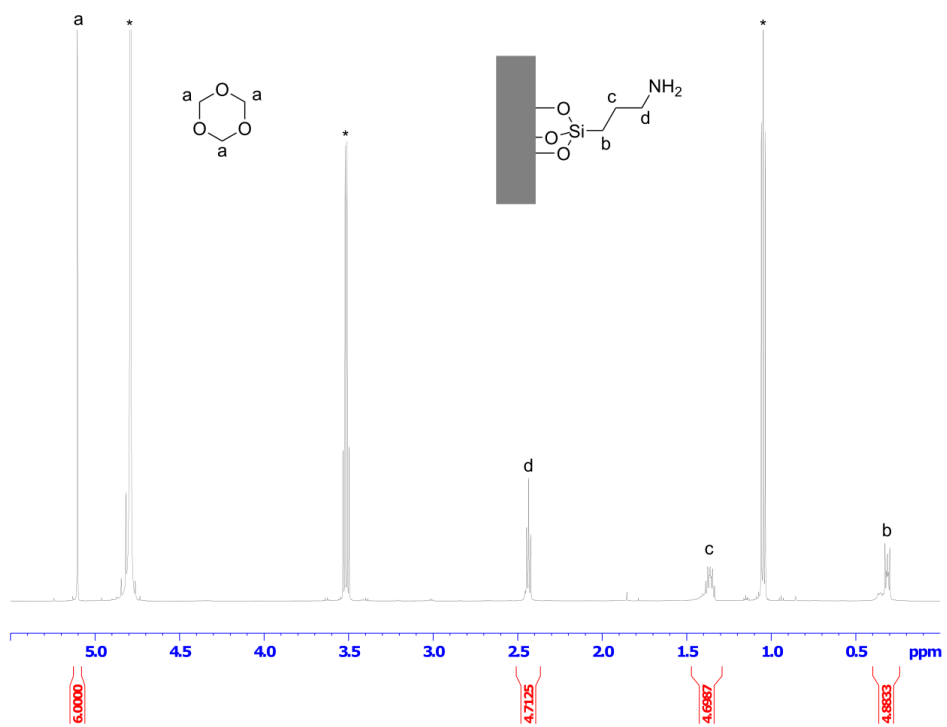


Figure S10: qNMR spectrum of sample MSN-NH₂-Hi. Signals indicated with an asterisk are from the solvent and EtOH.

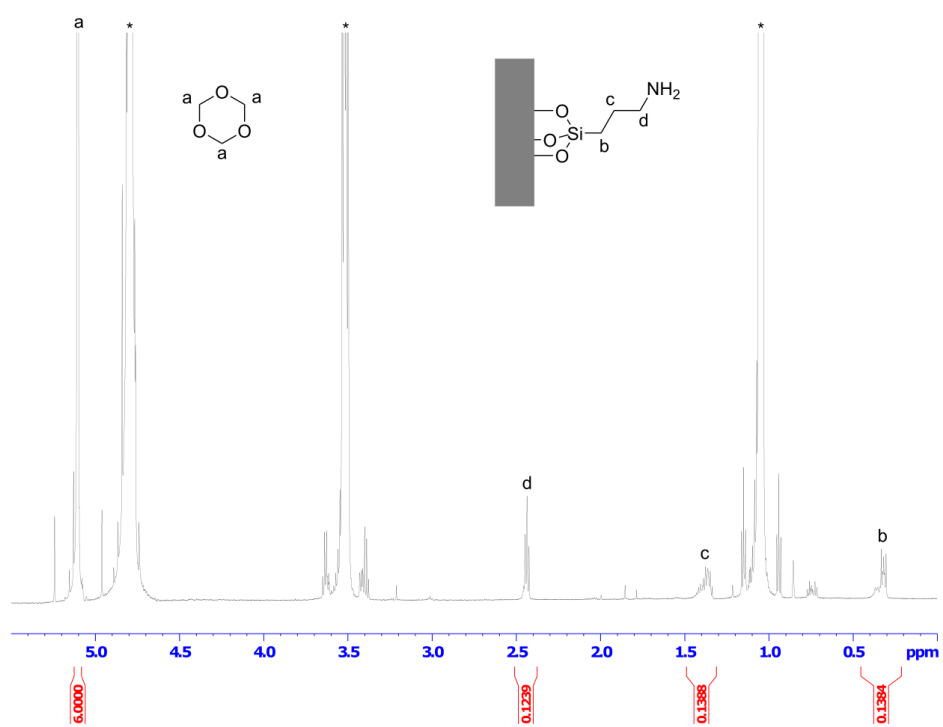


Figure S11: qNMR spectrum of sample MSN-NH₂-Lo. Signals indicated with an asterisk are from the solvent and EtOH.

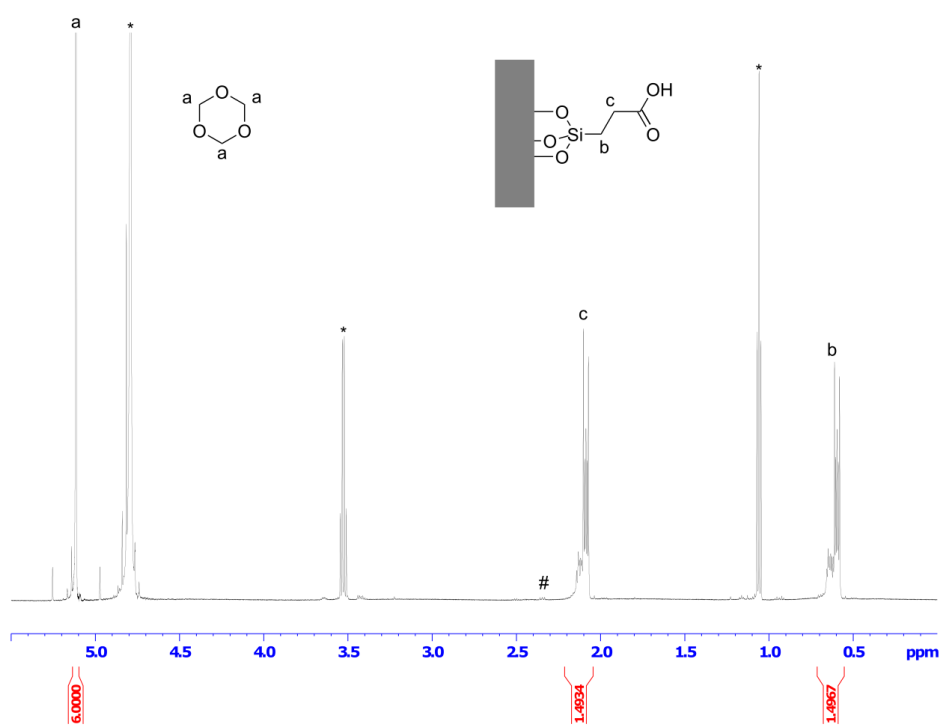


Figure S12: qNMR spectrum of sample MSN-COOH-Hi. Signals indicated with an asterisk are from the solvent and EtOH. The signal indicated with a pound sign can be assigned to the unhydrolyzed precursor (cyanoethylsilane).

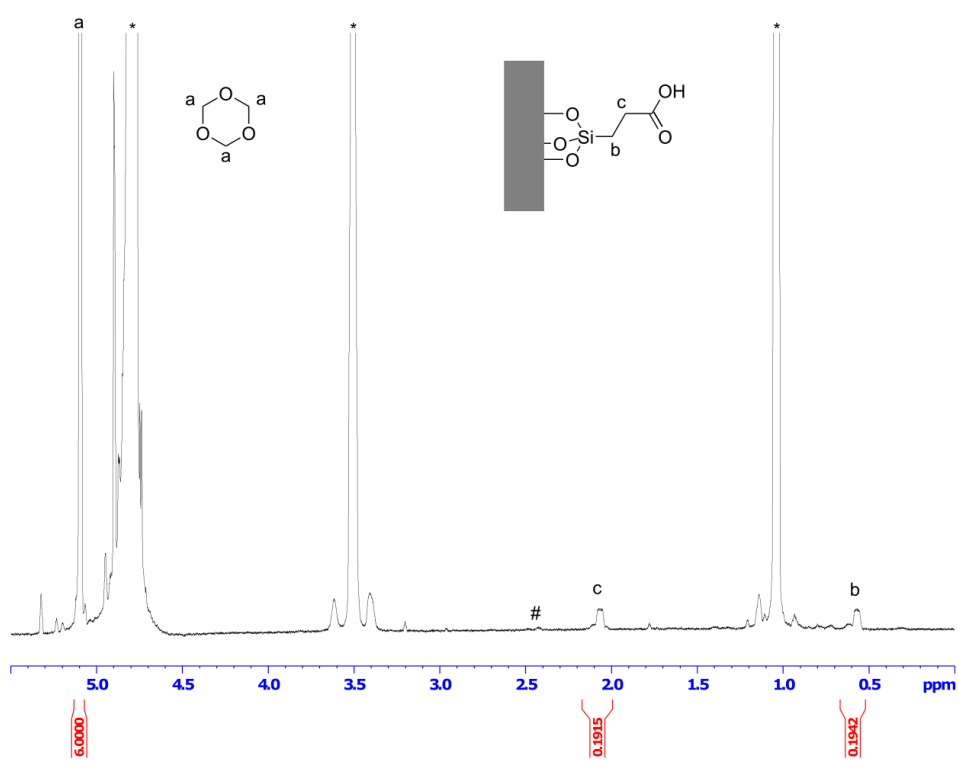


Figure S13: qNMR spectrum of sample MSN-COOH-Lo. Signals indicated with an asterisk are from the solvent and EtOH. The signal indicated with a pound sign can be assigned to the unhydrolyzed precursor (cyanoethylsilane).

V Amino and Carboxy Group quantification and validation of PSP

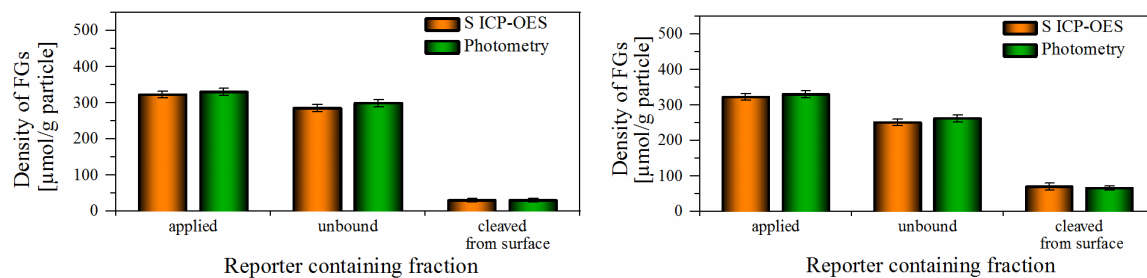


Figure S14: Validation of surface group analysis with *N*-APPA using ICP-OES for low and medium carboxy PSP.

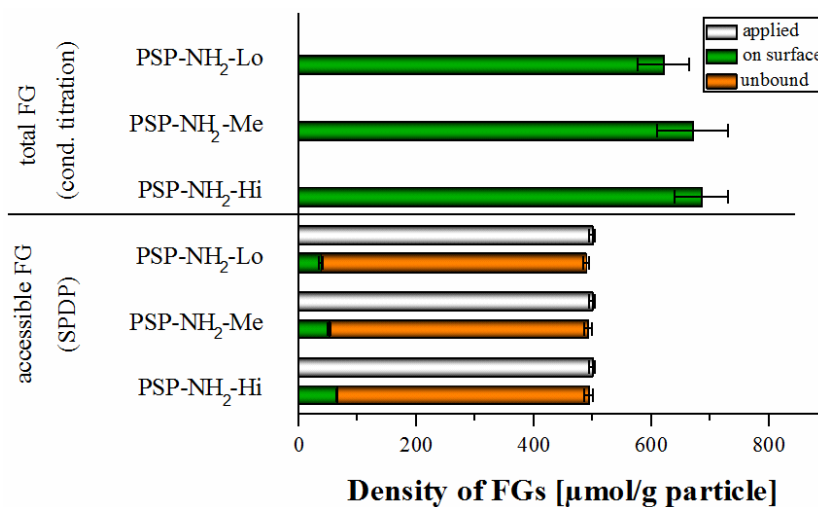


Figure S15: FG quantification with conductometric titration and multimodal cleavable reporter SPDP on self-synthesized amino PSP of different surface functional group densities.

VI Amino and Carboxy Group quantification and validation of MSN

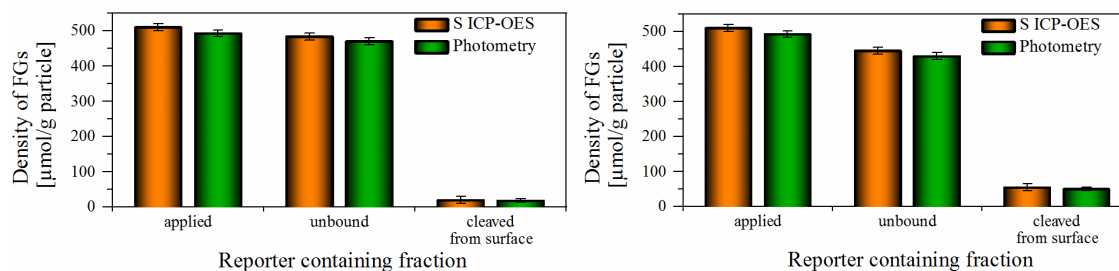


Figure S16: Validation of surface group analysis with *N*-APPA using ICP-OES for low and high carboxy MSN.

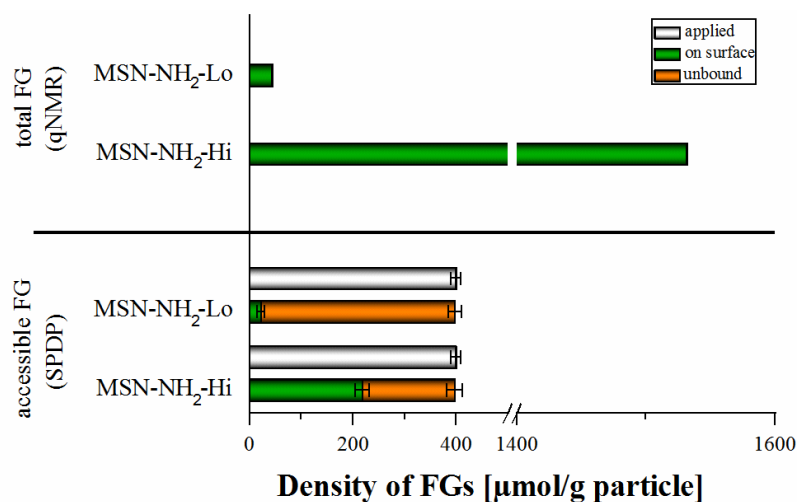


Figure S17: FG quantification with multimodal cleavable reporter SPDP on self-synthesized amino MSN of two different surface functional group densities.

VII Quantification of dye loaded carboxy PSP

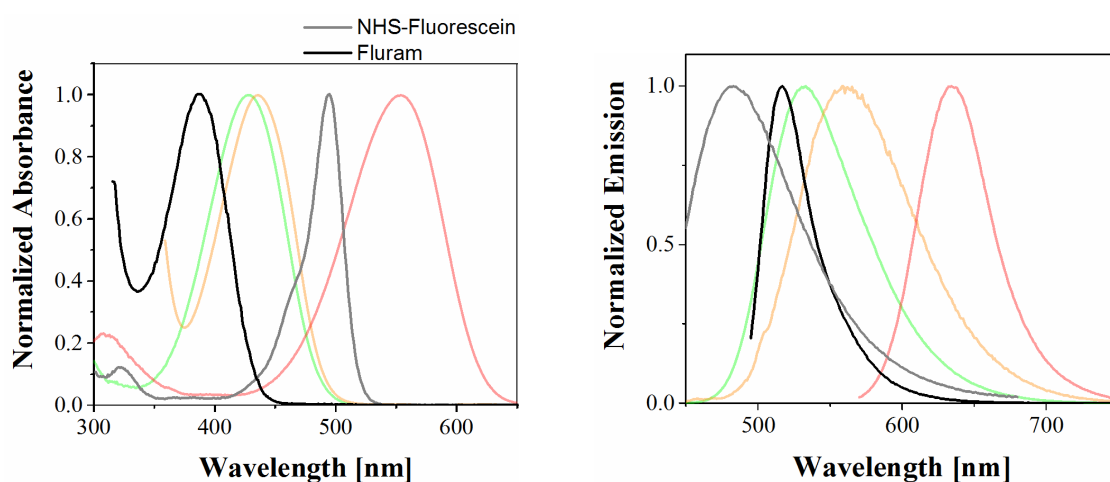
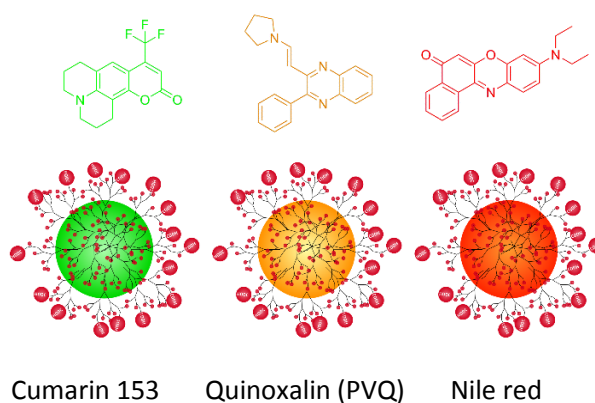


Figure S18: Absorption (left) and emission spectra (right) of Cumarin 153, Nile red and PVQ in THF and the overlap of NHS-Fluorescein and Fluram labels.

VIII Biofunctionalization of carboxy PSP

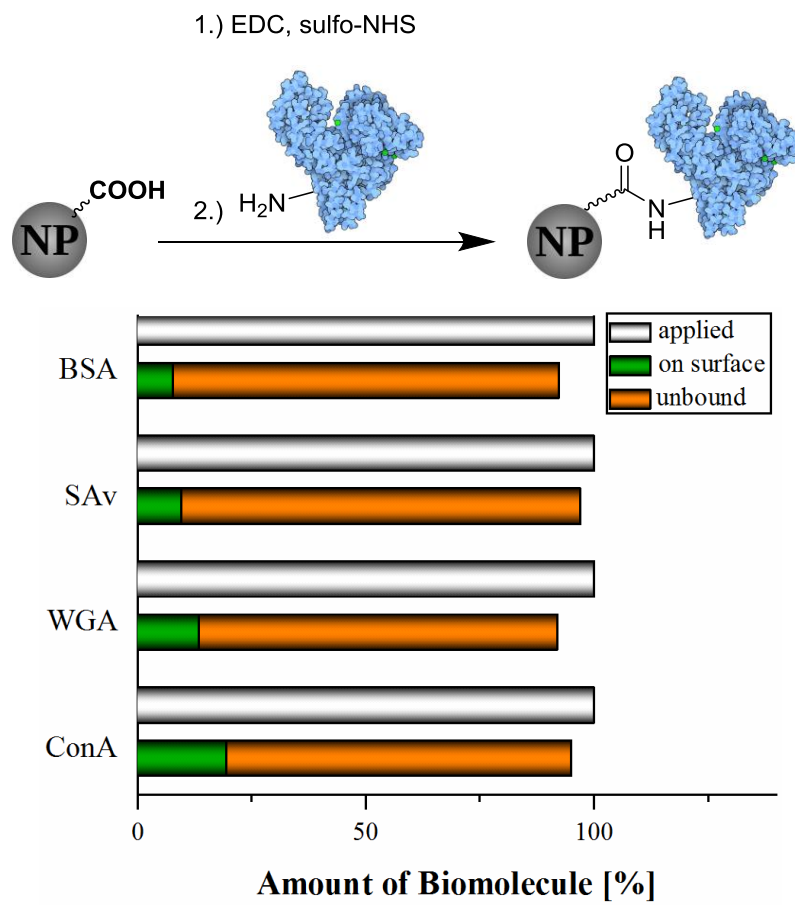


Figure S19. Biomolecule-derivatizable amount of carboxy functions obtained for four differently sized proteins.

3.2 Minor contributions

3.2.1 3-Piperazinyl propenylidene indolone merocyanines: consecutive Three-component Synthesis and Electronic Properties of Solid-state Luminophores with AIE Properties

Melanie Denißen, Nithiya Nirmalananthan, Thomas Behnke, Katrin Hoffmann, Ute Resch-Genger and Thomas J. J. Müller*

Mater. Chem. Front. **2017**, *1*, 2013–2026.

DOI: [10.1039/c7qm00198c](https://doi.org/10.1039/c7qm00198c)

URL: <https://doi.org/10.1039/c7qm00198c>



Figure 21: Adapted with permission from Denißen *et al.* Copyright 2017 Material Chemistry Frontiers.

All 3-piperazinyl propenylidene indolone merocyanines were synthesized and characterized by M. Denißen under supervision of Prof. Dr. T. J. J. Müller at Heinrich-Heine University Düsseldorf. M. Denißen performed also the first photophysical studies with the dye derivatives. N. Nirmalananthan-Budau and her Bachelor student Ella Walczak made aggregation-induced emission studies with three 3-piperazinyl propenylidene indolone merocyanines with -H, -CN, -*tert*-Bu substituents in two different solvent mixtures, evaluated and interpreted the obtained data under the supervision of Dr. T. Behnke. Dr. K. Hoffmann measured the CLSM images of the formed dye crystals for the manuscript.

The manuscript was mainly written by M. Denißen and Prof. Dr. T. J. J. Müller. The AIE part was written by N. Nirmalananthan-Budau and Dr. U. Resch-Genger.

Estimated own contribution: $\approx 15\%$

3.2.2 Quantification of Aldehydes on Polymeric Microbead Surfaces via Catch and Release of Reporter Chromophores

Alexander Roloff, Nithiya Nirmalananthan-Budau, Bastian Rühle, Heike Borchering, Thomas Thiele, Uwe Schedler and Ute Resch-Genger*

Anal. Chem. **2019**, *91*, 8827–8834. Pre-print version of the journal article. Reproduced with permission.

DOI: [10.1021/acs.analchem.8b05515](https://doi.org/10.1021/acs.analchem.8b05515)

URL: <https://doi.org/10.1021/acs.analchem.8b05515>

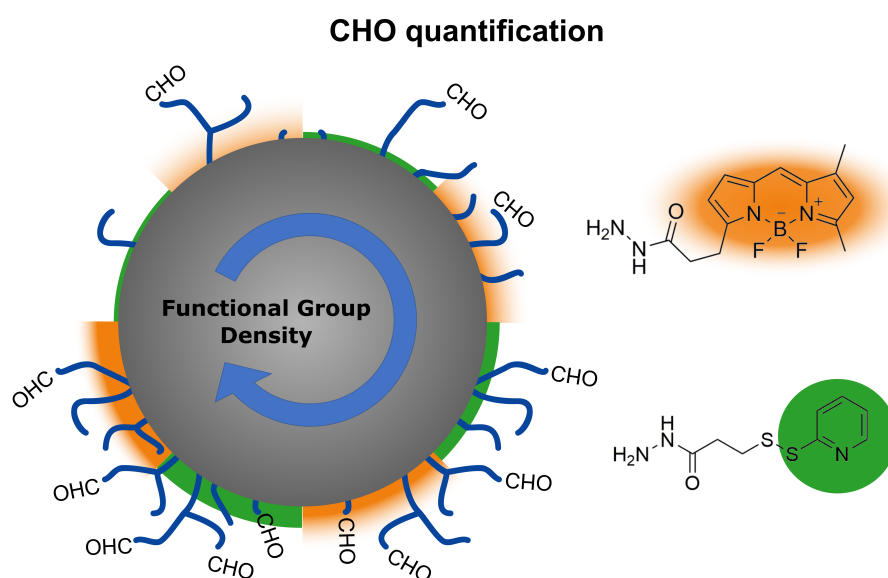


Figure 22: Adapted with permission from Alexander Roloff *et al.* Copyright 2019 Analytical Chemistry.

In this publication Dr. A. Roloff contributed the optical quantification of the accessible aldehyde FGs on micrometer sized PMMA beads with two methods using seven different particle suspensions. Dr. T. Thiele, and Dr. U. Schedler from PolyAn synthesized and characterized the PMMA beads. N. Nirmalananthan-Budau performed the biofunctionalization, biomolecule quantification on the beads with BCA assay and evaluated and interpreted the obtained data. Dr. H. Borchering performed biomolecule quantification on the beads with Biotin assay. Dr. B. Rühle supervised and supported the work.

The manuscript was mainly written by Dr. A. Roloff and Dr. U. Resch-Genger.

Estimated own contribution: $\approx 15\%$

4 Synopsis of the Results, Conclusion & Outlook

Polymer nanoparticles (PNP) are of increasing importance for a wide range of applications, for example, as carriers for functional molecules such as drugs and dye molecules, targeted probes in bioimaging studies, nanosensors, and as reporters for signal enhancement strategies in optical assays. Relevant properties for such applications are – besides the size and shape – the optical properties and the surface chemistry of the PNP. The latter controls the colloidal stability, subsequent biofunctionalization, biocompatibility, and interaction with biological systems including uptake behavior, biodistribution, and toxicity. Based on the knowledge that well-characterized PNP with bright emission are interesting candidates for signal amplification strategies in bioanalytics, the major aim of this thesis was to study differently substituted aggregation-induced emission (AIE) dyes, their encapsulation in preformed polystyrene particles (PSP), and to develop evaluated and validated methods, for quantification of surface functional groups (FGs) on these PSP surfaces.

In ?? and ??, we studied the AIE behavior of two different dye classes: merocyanine and quinoxaline derivatives. Dyes with a twisted skeleton conformation show enhanced emission upon aggregation. This is in contrast to the majority of dyes which exhibit aggregation-caused fluorescence quenching (ACQ). AIE dyes are interesting candidates for signal amplification strategies in optical assays but need to be investigated, since the optical properties of encapsulated dyes can be influenced by the polarity, refractive index, and viscosity of the PNP matrix.

In ?? the AIE behavior of three differently substituted 3-piperazinyl propenylidene indole merocyanine derivatives is summarized. The three substituents used were an -H substituent, an electron donating -*tert*-butyl substituent, and an electron withdrawing -CN substituent attached to the rotatable aryl moiety. All dyes were synthesized in an one-pot reaction using three precursor compounds. All three hydrophobic merocyanine dyes were either barely or completely non-emissive when dissolved in organic solvents such as acetonitrile, THF, or DCM. However, the dyes showed strong fluorescence in the solid state. This enhanced fluorescence was understood to be due to the restriction of the intramolecular motions, such as rotation and vibration of the differently substituted aryl moieties, which favors radiative decay in the solid state. This was a first hint that these dyes should be suitable candidates for AIE. Spectroscopic AIE investigations revealed only a slight emission enhancement of the dye aggregates formed in acetonitrile-water mixtures containing 75% to 80% water and in

THF-water mixtures containing more than 75% water relative to the isolated dye molecule in pure organic solvent. The fluorescence quantum yield and fluorescence lifetime of the dye aggregates was measured. In the acetonitrile-water mixtures, the strongest enhancement of the quantum yield was observed for the electron withdrawing -CN and the weakest enhancement was observed for the electron donating *-tert*-butyl substituent. The fluorescence lifetime measurements showed the opposite trend, with the *-tert*-butyl substituted dye having the longest lifetime and the -CN substituted dye having the shortest. If only emissive species were present, the fluorescence lifetime and quantum yield should be directly proportional to each other. The contradictory lifetime and quantum yield measurements indicates that both emissive and non-emissive aggregates were formed. In the less polar THF-water mixture the aggregates formed by the -H substituted dye had the strongest quantum yield enhancement, while the *-tert*-butyl substituted dye exhibited the longest lifetime and the -CN substituted dye did not show AIE behavior. In general, no systematic trends were observed for the three merocyanine derivatives. Additionally, all changes in the fluorescence characteristics were too small to reflect an influence of the different substituents on the AIE effect. Increasing the energy of the aggregate suspension by ultrasonication revealed highly fluorescent 5 μm crystalline needles that are colloidally unstable in aqueous solution. Stabilization by encapsulating the dyes into preformed PSP was not useful because the highly fluorescent crystals were too large to be formed in the PSP matrix during the encapsulation.

In ?? the influence of the substitution pattern on the AIE behavior was investigated for four differently substituted quinoxaline derivatives, which were easily accessible synthetically through a four- or five component one pot synthesis approach. Unlike the merocyanine dyes, the quinoxaline derivatives have a completely different rotatable aromatic moiety. These moieties have completely different angles relative to the coplanar quinoxaline ring and vinylic double bond in the crystal structure. While the heterocyclic and electron-rich methoxythienyl-substituted derivative shows a nearly coplanar orientation, the electron-neutral phenyl-substituted quinoxaline has an orthogonal arrangement. The other two heterocyclic electron-rich pyrrolyl- and indolyl-substituted dyes show angles in between the first two dyes. Like the merocyanine dyes, all quinoxaline derivatives showed intense solid-state fluorescence. Spectroscopic studies of the dyes in EtOH-water mixtures with increasing water content revealed dye aggregation for all mixtures containing more than 80% water. The formed aggregates became smaller in diameter and the suspension became more emissive with increasing water fraction up to 98%. Detailed investigations confirmed a systematic trend in both parameters. The torsion angle (dihedral angle) of the different substituents and the water content of the EtOH-water mixtures not only controls the aggregate size, but also the aggregation induced fluorescence enhancement. The phenyl-substituted quinoxaline with the largest torsion angle showed the highest enhancement in fluorescence intensity and the heterocyclic methoxythienyl-substituted derivative with the smallest torsion angle the

lowest one. The good correlation between the size of the torsion angle and the **AIE** effect underlined the structural control of **AIE** in this dye class.

The phenyl-substituted quinoxaline dye formed nm-sized aggregates and showed strongest **AIE** effect with a quantum yield enhancement by a factor of 6.8 and a fluorescence lifetime increase by a factor of 23. This dye was exemplarily incorporated into 1 μm -sized carboxy-functionalized **PSP** using a simple swelling procedure which is well established for conventional **ACQ** dyes in literature to circumvent the colloidal instability of the dye aggregates.

This **AIE** dye encapsulation enabled high dye loading concentrations, demonstrated a way to circumvent the low colloidal stability of the dye aggregates, and improved the fluorescence properties compared to the dye aggregates in suspension. This is reflected by an up to 3-fold increase in quantum yield and a 1.5-fold increase in lifetime. Beyond that, this entrapping strategy enables subsequent surface functionalization of the **PSP**, for example, with biomolecules for applications as nanoscale reporters in bioanalysis. Moreover, this demonstrates the potential of **AIE** dyes for signal enhancement strategies using preformed **PNP**, as these dyes can be encapsulated in a much higher concentration than conventional **ACQ** dyes.

In ??, ?? and ??, we studied different quantification methods for the determination of the total and the accessible amount of **FGs** on **PNP** functionalized with carboxy, amine, and aldehyde groups and presented the concept of multimodal cleavable probes for catch-and-release assays.

The reliable quantification of accessible surface **FGs** of fluorescent nanoparticles (**NPs**) is a prerequisite for sophisticated and versatile applications. In ?? three different optical assays for **FG** quantification were developed, optimized, and compared using commercial 100 nm- and 1 μm -sized carboxy- and amino-functionalized **PSP**. As a basic requirement for the assay comparison, the total amount of (de)protonatable **FGs** on these aminated or carboxylated **PSP** was determined with conductometric titration. The first optical assay for the quantification of the accessible **FGs** used conventional and commercial dyes with reactive groups, for example, 6-aminofluorescein or **NHS**-fluorescein for the covalent functionalization of the **PSP** surface **FGs**. This approach required the quantification of unbound dyes in the supernatant after several time-consuming washing steps, whereas the direct quantification of the bound dye was hampered by particle scattering and dye-dye interactions on the particle surface that result in fluorescence quenching. Only an irreversible dissolution of the **PSP** could enable the direct determination. The second assay was based on dye precursors that become strongly absorptive and/or emissive upon reaction with the respective **FGs**, like Fluram, or color changing dyes like IR797. This approach allowed for a spectral discrimination between reacted and unreacted labels, and could thereby omit tedious washing steps. However, the direct quantification of particle-bound dyes was still hampered by particle-induced light

scattering and dye-dye interactions. Moreover, as Fluram is unstable in aqueous solutions, only the amount of surface-bound dyes could be determined after particle dissolution in an organic solvent such as THF, whereas the amount of unreacted Fluram was not measured. IR797 enabled the spectroscopic determination of both the unreacted dye and the bound dye after particle dissolution. However, both the Fluram and IR797 assays required calibration with a model system (molecule) that has similar spectroscopic properties and target-specific changes in ϵ and Φ to the reaction products.

As the first two assays clearly show some drawbacks for the quantification of FGs on particles, a new approach was developed using the cleavable labels *N*-succinimidyl-3-(2-pyridyldithio)propionate (SPDP) and *N*-(aminoethyl)-3-(pyridin-2-yl)disulfanylpropanamide trifluoroacetate (*N*-APPA). These reporters consist of a cleavable disulfide linker, a reactive group, and an optically detectable reporter unit. These labels can be quantitatively cleaved off from the NP surface using a reducing agent such as tris(2-carboxyethyl)phosphine hydrochloride (TCEP), and thus enable both the quantification of unbound reporters in the supernatant and reporters cleaved off from the particle surface. Additionally, the thiol groups formed on the particle surface upon reductive cleavage allow for validation with ICP-OES and the Ellman's assay, an already evaluated and established optical assay for thiol groups. This assay comparison underlines the general advantages of our cleavable reporters SPDP and *N*-APPA for the quantification of FGs on particle surfaces. First, a mass balance can be obtained from measurements of the unreacted reporter and the cleaved off reporter. Second, the choice of a disulfide cleavable reporter enables a straightforward and simple validation with established analytical methods relying on different detection schemes. Furthermore, this versatile concept circumvents distortion of optical signals by particle-induced light scattering and reporter-reporter interactions. With all three assays we could quantify the accessible FGs on the surface to be around 12-16% of the total amount of FGs for 100 nm-sized PSP and to 2-4% of the total FGs for 1 μ m-sized PSP. The first two dye-based methods, besides the aforementioned drawbacks, also exhibit higher standard deviations. The cleavable reporter-based assay is not only beneficial to obtain a complete mass balance and to enable straightforward method validation, but also offers lower standard deviations.

In ?? the application of the straightforward spectrophotometrical cleavable reporter assay was expanded, by applying *N*-APPA and SPDP to the quantification of accessible surface FGs on custom made 100 nm-sized PSP with three different densities of either carboxy or amino surface groups. As for the commercial PSP, a mass balance could be obtained by quantifying the unbound reporters in the supernatant and the reporters cleaved off from the particle surface. Again, the amount of accessible groups quantified optically also correlated very well with the ICP-OES validation measurements of sulfur. This quantification method using cleavable labels is not only restricted to polystyrene materials. For example, we could show that a quantification of FGs on mesoporous silica nanoparticles (MSN) is also possible as demonstrated by the validation of the method results with ICP-OES data.

Moreover, for dye-loaded **PSP** the dyes used in conventional labelling-based **FG** quantification strategies could interfere with signals originating from the dyes encapsulated in the **NPs**. However, such a problem can be easily circumvented by using the cleavable reporter labeling method, since all quantification steps of the reporter are performed in the supernatant after particle separation. We could demonstrate this advantage for **PSP** loaded with the conventional dyes coumarin 153 and Nile red as well as for **PSP** loaded with the **AIE** dye phenyl-quinoxaline.

The quantification of the accessible amount of **FGs** with **SPDP** and **N-APPA** allowed the reduction of the necessary **PSP**-coupling biomolecule amount for bio analytics by up to 8-fold compared to the total amount of **FGs** on surface.

In ?? we demonstrated that the cleavable reporter method is not limited to carboxy and amino groups but rather can be adapted to other surface functionalities and other quantitatively cleavable units. The commercial cleavable reporter 3-(2-pyridyldithio)propionyl hydrazide (**PDPH**) was successfully used to quantify the accessible aldehyde **FGs** on the surface of 5.6 μm -sized **PMMA** particles. The results of these measurements were compared with the results from the catch-and-release BODIPY-hydrazide (**BDP-hzd**) assay that employs a fluorescent BODIPY dye as reporter unit. In both assays, the aldehyde particles were conjugated with hydrazine-bearing labels (differing in size and signal read out) by forming hydrazone bonds. Unspecific adsorbed and unbound reporters could be easily separated by washing. Subsequently, the particle-bound reporter molecules were chemically cleaved off with **TCEP** for the **PDPH** assay and with formaldehyde to shift the equilibrium to the cleaved BODIPY reporter to guarantee quantitative release for the **BDP-hzd** assay. Quantification of the cleaved reporter was performed optically in the supernatant after removal of the particles by centrifugation. Due to the sensitive fluorescence-based detection of the released reporter, this assay is especially useful in quantifying low aldehyde densities on small sample quantities. Comparing the results obtained with both assays to the amount of the bead-bound model protein streptavidin following reductive amination reveals a good correlation between the aldehyde and protein-labeling densities. However, differences in the absolute amount of streptavidin, quantified with the BCA assay, and the cleavable reporters utilized in the assays, underline the importance of label size and charge for surface group quantification methods.

In summary, the systematic investigation of different substituent patterns of the **AIE** dyes showed that substituents affecting the molecule's planarity can influence the **AIE** behavior significantly. It was also shown that **AIE** dyes can also be entrapped in preformed **PSP**. This enables high dye loading concentrations and optimizes **AIE** dye fluorescence features. A reliable quantification of accessible **FGs** on simple and encoded **PSP** can be achieved with cleavable reporters in catch-and-release assays. The application of this strategy to particles of different material composition such as **PNP** and **MSN** as well as **FGs** such as amine, carboxy, and aldehyde showed the versatility of these assays.

To extend the cleavable probes strategy, we are currently evaluating cleavable reporters with fluorescent groups and fluorine-containing reporter parts, which allow for surface group quantification with optical assays, elemental analysis, [ICP-OES](#), [qNMR](#), [XPS](#), and reference-free total reflection X-ray fluorescence.

5 Reference

- (1) Algar, W. R.; Prasuhn, D. E.; Stewart, M. H.; Jennings, T. L.; Blanco-Canosa, J. B.; Dawson, P. E.; Medintz, I. L. *Bioconjugate Chem.* **2011**, *22*, 825–858.
- (2) Cao, G.; Wang, Y., *Nanostructures and nanomaterials : synthesis, properties, and applications*, Second edition; World scientific series in nanoscience and nanotechnology, xiii, 581 pages.
- (3) Turkevich, J. *Gold Bull.* **1985**, *18*, 86–91.
- (4) Nagarajan, S.; Yong, Z. *Recent Pat. Biomed. Eng. (Discontinued)* **2008**, *1*, 34–42.
- (5) Perrault, S. D.; Chan, W. C. W. *J. Am. Chem. Soc.* **2009**, *131*, 17042–17043.
- (6) Nikoobakht, B.; El-Sayed, M. A. *Chem. Mater.* **2003**, *15*, 1957–1962.
- (7) Perezjuste, J.; Pastorizasantos, I.; Lizmarzan, L.; Mulvaney, P. *Coord. Chem. Rev.* **2005**, *249*, 1870–1901.
- (8) Chen, J. et al. *Nano Lett.* **2005**, *5*, 473–477.
- (9) Song, Q.; Zhang, Z. J. *J. Am. Chem. Soc.* **2004**, *126*, 6164–6168.
- (10) Wang, Z. L.; Ahmad, T. S.; El-Sayed, M. A. *Surf. Sci.* **1997**, *380*, 302–310.
- (11) Qu, X.; Omar, L.; Le, T. B. H.; Tetley, L.; Bolton, K.; Chooi, K. W.; Wang, W.; Uchegbu, I. F. *Langmuir* **2008**, *24*, 9997–10004.
- (12) Ren, T.-Z.; Yuan, Z.-Y.; Hu, W.; Zou, X. *Microporous Mesoporous Mater.* **2008**, *112*, 467–473.
- (13) Ren, X.; Han, D.; Chen, D.; Tang, F. *Mater. Res. Bull.* **2007**, *42*, 807–813.
- (14) Suematsu, N. J.; Ogawa, Y.; Yamamoto, Y.; Yamaguchi, T. *J. Colloid Interface Sci.* **2007**, *310*, 648–652.
- (15) Hu, J.-S.; Guo; Liang, H.-P.; Wan, L.-J.; Jiang, L. *J. Am. Chem. Soc.* **2005**, *127*, 17090–17095.
- (16) Jitianu, M.; Goia, D. V. *J. Colloid Interface Sci.* **2007**, *309*, 78–85.
- (17) Collins, G.; Holmes, J. D. *J. Mater. Chem.* **2011**, *21*, 11052–11069.
- (18) Lebedeva, I. V.; Chamberlain, T. W.; Popov, A. M.; Knizhnik, A. A.; Zoberbier, T.; Biskupek, J.; Kaiser, U.; Khlobystov, A. N. *Nanoscale* **2014**, *6*, 14877–14890.
- (19) Lynch, I.; Cedervall, T.; Lundqvist, M.; Cabaleiro-Lago, C.; Linse, S.; Dawson, K. A. *Adv. Colloid Interface Sci.* **2007**, *134-135*, 167–174.

-
- (20) Prakash, S.; Chakrabarty, T.; Singh, A. K.; Shahi, V. K. *Biosens. Bioelectron.* **2013**, *41*, 43–53.
- (21) Sedlák, J.; Kuřitka, I.; Machovský, M.; Šuly, P.; Bažant, P.; Sedláček, T. *Adv. Powder Technol.* **2015**, *26*, 1064–1071.
- (22) Zhu, S.-G. et al. *Biotechnol. Appl. Biochem.* **2004**, *39*, 179–187.
- (23) Delplace, V.; Couvreur, P.; Nicolas, J. *Polym. Chem.* **2014**, *5*, 1529–1544.
- (24) Twibanire, J.; Grindley, T. B. *Polymers* **2014**, *6*, 179.
- (25) Vauthier, C.; Bouchemal, K. *Pharm. Res.* **2009**, *26*, 1025–1058.
- (26) Behnke, T.; Würth, C.; Hoffmann, K.; Hübner, M.; Panne, U.; Resch-Genger, U. *J. Fluoresc.* **2011**, *21*, 937–944.
- (27) Behnke, T.; Würth, C.; Laux, E.-M.; Hoffmann, K.; Resch-Genger, U. *Dyes Pigm.* **2012**, *94*, 247–257.
- (28) Quevedo, P. D.; Behnke, T.; Resch-Genger, U. *Anal. Bioanal. Chem.* **2016**, *408*, 4133–4149.
- (29) Napp, J.; Behnke, T.; Fischer, L.; Würth, C.; Wottawa, M.; Katschinski, D. M.; Alves, F.; Resch-Genger, U.; Schäferling, M. *Anal. Chem.* **2011**, *83*, 9039–9046.
- (30) Markus, M. A.; Napp, J.; Behnke, T.; Mitkovski, M.; Monecke, S.; Dullin, C.; Kilfeather, S.; Dressel, R.; Resch-Genger, U.; Alves, F. *ACS Nano* **2015**, *9*, 11642–11657.
- (31) Behnke, T.; Mathejczyk, J. E.; Brehm, R.; Würth, C.; Gomes, F. R.; Dullin, C.; Napp, J.; Alves, F.; Resch-Genger, U. *Biomaterials* **2013**, *34*, 160–170.
- (32) Oltra, N. S.; Nair, P.; Discher, D. E. *Annu. Rev. Chem. Biomol. Eng.* **2014**, *5*, 281–299.
- (33) Holzapfel, V.; Musyanovych, A.; Landfester, K.; Lorenz, M. R.; Mailänder, V. *Macromol. Chem. Phys.* **2005**, *206*, 2440–2449.
- (34) Delair, T.; Marguet, V.; Pichot, C.; Mandrand, B. *Colloid. Polym. Sci.* **1994**, *272*, 962–970.
- (35) Gibaud, S.; Demoy, M.; Andreux, J. P.; Weingarten, C.; Gouritin, B.; Couvreur, P. *J. Pharm. Sci.* **1996**, *85*, 944–950.
- (36) Nemmar, A.; Hoylaerts, M. F.; Hoet, P. H. M.; Dinsdale, D.; Smith, T.; Xu, H.; Vermynen, J.; Nemery, B. *Am. J. Respir. Crit. Care Med.* **2002**, *166*, 998–1004.
- (37) Sun, X.; Rossin, R.; Turner, J. L.; Becker, M. L.; Joralemon, M. J.; Welch, M. J.; Wooley, K. L. *Biomacromolecules* **2005**, *6*, 2541–2554.
- (38) Petros, R. A.; DeSimone, J. M. *Nat. Rev. Drug Discov.* **2010**, *9*, 615.
- (39) Zhang, Z.; Tsai, P.-C.; Ramezanli, T.; Michniak-Kohn, B. B. *Nanomed. Nanobiotechnol.* **2013**, *5*, 205–218.

-
- (40) Bahadar, H.; Maqbool, F.; Niaz, K.; Abdollahi, M. *Iran. Biomed. J.* **2016**, *20*, 1–11.
- (41) Vijayan, V.; Reddy, K. R.; Sakthivel, S.; Swetha, C. *Colloids Surf., B: Biointerfaces* **2013**, *111*, 150–155.
- (42) Peer, D.; Karp, J. M.; Hong, S.; Farokhzad, O. C.; Margalit, R.; Langer, R. *Nat. Nanotechnol.* **2007**, *2*, 751.
- (43) Rao, J. P.; Geckeler, K. E. *Prog. Polym. Sci.* **2011**, *36*, 887–913.
- (44) Kulkarni, S. A.; Feng, S.-S. *Pharm. Res.* **2013**, *30*, 2512–2522.
- (45) Shang, L.; Nienhaus, K.; Nienhaus, G. U. *J. Nanobiotechnology* **2014**, *12*, 5.
- (46) Jiang, W.; Kim, B. Y. S.; Rutka, J. T.; Chan, W. C. W. *Nat. Nanotechnol.* **2008**, *3*, 145.
- (47) Champion, J. A.; Katare, Y. K.; Mitragotri, S. *PNAS* **2007**, *104*, 11901–11904.
- (48) Champion, J. A.; Mitragotri, S. *Pharm. Res.* **2009**, *26*, 244–249.
- (49) Cox, A. J.; DeWeerd, A. J.; Linden, J. *Am. J. Phys.* **2002**, *70*, 620–625.
- (50) Howes, P. D.; Chandrawati, R.; Stevens, M. M. *Science* **2014**, *346*, 1247390–1–1247390–10.
- (51) De, M.; Ghosh, P. S.; Rotello, V. M. *Adv. Mater.* **2008**, *20*, 4225–4241.
- (52) Wang, M.; Thanou, M. *Pharmacol. Res.* **2010**, *62*, 90–99.
- (53) Michalet, X.; Pinaud, F. F.; Bentolila, L. A.; Tsay, J. M.; Doose, S.; Li, J. J.; Sundaresan, G.; Wu, A. M.; Gambhir, S. S.; Weiss, S. *Science* **2005**, *307*, 538–544.
- (54) Pinaud, F.; Clarke, S.; Sittner, A.; Dahan, M. *Nat. Methods* **2010**, *7*, 275.
- (55) Gnach, A.; Bednarkiewicz, A. *Nano Today* **2012**, *7*, 532–563.
- (56) Chen, O. et al. *Nat. Mater.* **2013**, *12*, 445.
- (57) Chen, Y.; Vela, J.; Htoon, H.; Casson, J. L.; Werder, D. J.; Bussian, D. A.; Klimov, V. I.; Hollingsworth, J. A. *J. Am. Chem. Soc.* **2008**, *130*, 5026–5027.
- (58) Wolfbeis, O. S. *Chem. Soc. Rev.* **2015**, *44*, 4743–4768.
- (59) Monguzzi, A.; Frigoli, M.; Larpent, C.; Meinardi, F. *RSC Advances* **2012**, *2*, 11731–11736.
- (60) Sun, G.; Berezin, M. Y.; Fan, J.; Lee, H.; Ma, J.; Zhang, K.; Wooley, K. L.; Achilefu, S. *Nanoscale* **2010**, *2*, 548–558.
- (61) Chen, J.; Xu, B.; Ouyang, X.; Tang, B. Z.; Cao, Y. *J. Phys. Chem. A* **2004**, *108*, 7522–7526.
- (62) Shustova, N. B.; Ong, T.-C.; Cozzolino, A. F.; Michaelis, V. K.; Griffin, R. G.; Dincă, M. *J. Am. Chem. Soc.* **2012**, *134*, 15061–15070.

- (63) Pauli, J.; Grabolle, M.; Brehm, R.; Spieles, M.; Hamann, F. M.; Wenzel, M.; Hilger, I.; Resch-Genger, U. *Bioconjugate Chem.* **2011**, *22*, 1298–1308.
- (64) Hennig, A.; Borchering, H.; Jaeger, C.; Hatami, S.; Würth, C.; Hoffmann, A.; Hoffmann, K.; Thiele, T.; Schedler, U.; Resch-Genger, U. *J. Am. Chem. Soc.* **2012**, *134*, 8268–8276.
- (65) Hennig, A.; Hatami, S.; Spieles, M.; Resch-Genger, U. *Photochem. Photobiol. Sci.* **2013**, *12*, 729–737.
- (66) Qin, W.; Li, K.; Feng, G.; Li, M.; Yang, Z.; Liu, B.; Tang, B. Z. *Adv. Funct. Mater.* **2014**, *24*, 635–643.
- (67) Genovese, D.; Rampazzo, E.; Bonacchi, S.; Montalti, M.; Zaccheroni, N.; Prodi, L. *Nanoscale* **2014**, *6*, 3022–3036.
- (68) Ning, Z.; Chen, Z.; Zhang, Q.; Yan, Y.; Qian, S.; Cao, Y.; Tian, H. *Adv. Funct. Mater.* **2007**, *17*, 3799–3807.
- (69) Qin, W.; Ding, D.; Liu, J.; Yuan, W. Z.; Hu, Y.; Liu, B.; Tang, B. Z. *Adv. Funct. Mater.* **2012**, *22*, 771–779.
- (70) Zheng, Z.; Yu, Z.; Yang, M.; Jin, F.; Zhang, Q.; Zhou, H.; Wu, J.; Tian, Y. *J. Org. Chem.* **2013**, *78*, 3222–3234.
- (71) Luo, J. et al. *Chem. Commun.* **2001**, 1740–1741.
- (72) Huang, J.; Sun, N.; Yang, J.; Tang, R.; Li, Q.; Ma, D.; Li, Z. *Adv. Funct. Mater.* **2014**, *24*, 7645–7654.
- (73) Hong, Y.; Lam, J. W. Y.; Tang, B. Z. *Chem. Commun.* **2009**, 4332–4353.
- (74) Kokado, K.; Chujo, Y. *J. Org. Chem.* **2011**, *76*, 316–319.
- (75) Tong, H.; Hong, Y.; Dong, Y.; Ren, Y.; Häußler, M.; Lam, J. W. Y.; Wong, K. S.; Tang, B. Z. *J. Phys. Chem. A* **2007**, *111*, 2000–2007.
- (76) Zhao, Z.; He, B.; Tang, B. Z. *Chem. Sci.* **2015**, *6*, 5347–5365.
- (77) Chen, M. et al. *Chem. Sci.* **2015**, *6*, 1932–1937.
- (78) Li, Y.; Shao, A.; Wang, Y.; Mei, J.; Niu, D.; Gu, J.; Shi, P.; Zhu, W.; Tian, H.; Shi, J. *Adv. Mater.* **2016**, *28*, 3187–3193.
- (79) Zhang, J.; Ma, S.; Fang, H.; Xu, B.; Sun, H.; Chan, I.; Tian, W. *Mater. Chem. Front.* **2017**, *1*, 1422–1429.
- (80) Yu, C. Y. Y.; Xu, H.; Ji, S.; Kwok, R. T. K.; Lam, J. W. Y.; Li, X.; Krishnan, S.; Ding, D.; Tang, B. Z. *Adv. Mater.* **2017**, *29*, 1606167.
- (81) Li, K.; Liu, B. *Chem. Soc. Rev.* **2014**, *43*, 6570–6597.
- (82) Chen, S.; Wang, H.; Hong, Y.; Tang, B. Z. *Mater. Horiz.* **2016**, *3*, 283–293.

-
- (83) Yang, B.; Zhang, X.; Zhang, X.; Huang, Z.; Wei, Y.; Tao, L. *Mater. Today* **2016**, *19*, 284–291.
- (84) Yan, L.; Zhang, Y.; Xu, B.; Tian, W. *Nanoscale* **2016**, *8*, 2471–2487.
- (85) Li, K. et al. *Sci. Rep.* **2013**, *3*, 1150.
- (86) Feng, G.; Tay, C. Y.; Chui, Q. X.; Liu, R.; Tomczak, N.; Liu, J.; Tang, B. Z.; Leong, D. T.; Liu, B. *Biomaterials* **2014**, *35*, 8669–8677.
- (87) Jayaram, D. T.; Ramos-Romero, S.; Shankar, B. H.; Garrido, C.; Rubio, N.; Sanchez-Cid, L.; Gómez, S. B.; Blanco, J.; Ramaiah, D. *ACS Chem. Biol.* **2016**, *11*, 104–112.
- (88) Chen, Y.; Han, H.; Tong, H.; Chen, T.; Wang, H.; Ji, J.; Jin, Q. *ACS Appl. Mater. Interfaces* **2016**, *8*, 21185–21192.
- (89) Hennig, A.; Dietrich, P. M.; Hemmann, F.; Thiele, T.; Borcharding, H.; Hoffmann, A.; Schedler, U.; Jager, C.; Resch-Genger, U.; Unger, W. E. S. *Analyst* **2015**, *140*, 1804–1808.
- (90) Hennig, A.; Hoffmann, A.; Borcharding, H.; Thiele, T.; Schedler, U.; Resch-Genger, U. *Anal. Chem.* **2011**, *83*, 4970–4974.
- (91) Holländer, A. *Surf. Interface Anal.* **2004**, *36*, 1023–1026.
- (92) Chen, G.; Roy, I.; Yang, C.; Prasad, P. N. *Chem. Rev.* **2016**, *116*, 2826–85.
- (93) Sato, T.; Ruch, R., *Stabilization of colloidal dispersions by polymer adsorption*; Surfactant science series; Dekker: New York, **1980**, xi, 155 p.
- (94) Charron, G.; Hühn, D.; Perrier, A.; Cordier, L.; Pickett, C. J.; Nann, T.; Parak, W. J. *Langmuir* **2012**, *28*, 15141–15149.
- (95) Hermanson, G. T., *Bioconjugate techniques*, 2nd ed; Academic Press: Amsterdam; Boston, **2008**, xxx, 1202 p.
- (96) Ivanov, V. B.; Behnisch, J.; Holländer, A.; Mehdorn, F.; Zimmermann, H. *Surf. Interface Anal.* **1996**, *24*, 257–262.
- (97) Lockett, M. R.; Phillips, M. F.; Jarecki, J. L.; Peelen, D.; Smith, L. M. *Langmuir* **2008**, *24*, 69–75.
- (98) Valeur, E.; Bradley, M. *Chem. Soc. Rev.* **2009**, *38*, 606–631.
- (99) Felbeck, T.; Hoffmann, K.; Lezhnina, M. M.; Kynast, U. H.; Resch-Genger, U. *J. Phys. Chem. C* **2015**, *119*, 12978–12987.
- (100) Moser, M.; Behnke, T.; Hamers-Allin, C.; Klein-Hartwig, K.; Falkenhagen, J.; Resch-Genger, U. *Anal. Chem.* **2015**, *87*, 9376–9383.
- (101) Moser, M.; Schneider, R.; Behnke, T.; Schneider, T.; Falkenhagen, J.; Resch-Genger, U. *Anal. Chem.* **2016**, *88*, 8624–8631.

- (102) West, K. R.; Otto, S. *Curr. Drug Discov. Technol.* **2005**, *2*, 123–160.
- (103) Whitesides, G. M.; Lilburn, J. E.; Szajewski, R. P. *J. Org. Chem.* **1977**, *42*, 332–338.
- (104) Dirksen, A.; Dawson, P. E. *Bioconjugate Chem.* **2008**, *19*, 2543–2548.
- (105) Carrico, I. S.; Carlson, B. L.; Bertozzi, C. R. *Nat. Chem. Biol.* **2007**, *3*, 321–322.
- (106) Sapsford, K. E.; Algar, W. R.; Berti, L.; Gemmill, K. B.; Casey, B. J.; Oh, E.; Stewart, M. H.; Medintz, I. L. *Chem. Rev.* **2013**, *113*, 1904–2074.
- (107) Fukukawa, K.-i.; Rossin, R.; Hagooley, A.; Pressly, E. D.; Hunt, J. N.; Messmore, B. W.; Wooley, K. L.; Welch, M. J.; Hawker, C. J. *Biomacromolecules* **2008**, *9*, 1329–1339.
- (108) Sun, G.; Hagooley, A.; Xu, J.; Nyström, A. M.; Li, Z.; Rossin, R.; Moore, D. A.; Wooley, K. L.; Welch, M. J. *Biomacromolecules* **2008**, *9*, 1997–2006.
- (109) Saei, A. A. et al. *Chem. Mater.* **2017**, *29*, 6578–6595.
- (110) Fröhlich, E. *Int. J. Nanomed.* **2012**, *7*, 5577–5591.
- (111) Xia, T.; Kovichich, M.; Brant, J.; Hotze, M.; Sempf, J.; Oberley, T.; Sioutas, C.; Yeh, J. I.; Wiesner, M. R.; Nel, A. E. *Nano Letters* **2006**, *6*, 1794–1807.
- (112) Cismaru, L.; Popa, M. *Rev. Roum. Chim.* **2010**, *55*, 433–442.
- (113) Nasir, A.; Kausar, A.; Younus, A. *Polym. Plast. Technol. Eng.* **2015**, *54*, 325–341.
- (114) Eastoe, J.; Hollamby, M. J.; Hudson, L. *Adv. Colloid Interface Sci.* **2006**, *128-130*, 5–15.
- (115) Ballauff, M.; Lu, Y. *Polymer* **2007**, *48*, 1815–1823.
- (116) Ni, K. F.; Shan, G. R.; Weng, Z. X.; Sheibat-Othman, N.; Fevotte, G.; Lefebvre, F.; Bourgeat-Lami, E. *Macromolecules* **2005**, *38*, 7321–7329.
- (117) Jiang, J.; Thayumanavan, S. *Macromolecules* **2005**, *38*, 5886–5891.
- (118) Li, P.; Zhu, J.; Sunintaboon, P.; Harris, F. W. *Langmuir* **2002**, *18*, 8641–8646.
- (119) Foyer, G.; Barriol, M.; Negrell, C.; Caillol, S.; David, G.; Boutevin, B. *Prog. Org. Coat.* **2015**, *84*, 1–8.
- (120) Li, G.; Zheng, H.; Bai, R. *Macromol. Rapid Commun.* **2009**, *30*, 442–447.
- (121) Hoffmann, K.; Mix, R.; Friedrich, J.; Buschmann, H.-J.; Resch-Genger, U. *J. Fluoresc.* **2009**, *19*, 229–237.
- (122) Wang, C.; Otto, S.; Dorn, M.; Heinze, K.; Resch-Genger, U. *Anal. Chem.* **2019**, *91*, 2337–2344.
- (123) Liu, Q.-H.; Liu, J.; Guo, J.-C.; Yan, X.-L.; Wang, D.-H.; Chen, L.; Yan, F.-Y.; Chen, L.-G. *J. Mater. Chem.* **2009**, *19*, 2018–2025.
- (124) Greenspan, P.; Mayer, E. P.; Fowler, S. D. *J. Cell Biol.* **1985**, *100*, 965–973.

-
- (125) Klymchenko, A. S.; Roger, E.; Anton, N.; Anton, H.; Shulov, I.; Vermot, J.; Mely, Y.; Vandamme, T. F. *RSC Advances* **2012**, *2*, 11876–11886.
- (126) Li, H.; Zhang, X.; Zhang, X.; Yang, B.; Yang, Y.; Wei, Y. *Macromol. Rapid Commun.* **2014**, *35*, 1661–1667.
- (127) Zhang, X.; Zhang, X.; Yang, B.; Hui, J.; Liu, M.; Chi, Z.; Liu, S.; Xu, J.; Wei, Y. *Polym. Chem.* **2014**, *5*, 683–688.
- (128) Liu, M.; Zhang, X.; Yang, B.; Liu, L.; Deng, F.; Zhang, X.; Wei, Y. *Macromol. Biosci.* **2014**, *14*, 1260–1267.
- (129) Zhang, X.; Zhang, X.; Yang, B.; Liu, M.; Liu, W.; Chen, Y.; Wei, Y. *Polym. Chem.* **2014**, *5*, 399–404.
- (130) Zhang, X.; Zhang, X.; Yang, B.; Yang, Y.; Wei, Y. *Polym. Chem.* **2014**, *5*, 5885–5889.
- (131) Wang, K.; Zhang, X.; Zhang, X.; Ma, C.; Li, Z.; Huang, Z.; Zhang, Q.; Wei, Y. *Polym. Chem.* **2015**, *6*, 4455–4461.
- (132) Wan, Q.; Xu, D.; Mao, L.; He, Z.; Zeng, G.; Shi, Y.; Deng, F.; Liu, M.; Zhang, X.; Wei, Y. *Macromol. Rapid Commun.* **2017**, *38*, 1600752.
- (133) Geng, J.; Li, K.; Qin, W.; Ma, L.; Gurzadyan, G. G.; Tang, B. Z.; Liu, B. *Small* **2013**, *9*, 2012–2019.
- (134) Chávez, J. L.; Wong, J. L.; Duran, R. S. *Langmuir* **2008**, *24*, 2064–2071.
- (135) Qian, L.; Sha, Y.; Yang, X. *Thin Solid Films* **2006**, *515*, 1349–1353.
- (136) Kuo, K.-T.; Chen, S.-Y.; Cheng, B.-M.; Lin, C.-C. *Thin Solid Films* **2008**, *517*, 1257–1261.
- (137) Kawahashi, N.; Shiho, H. *J. Mater. Chem.* **2000**, *10*, 2294–2297.
- (138) Lu, L.; Sun, G.; Zhang, H.; Wang, H.; Xi, S.; Hu, J.; Tian, Z.; Chen, R. *J. Mater. Chem.* **2004**, *14*, 1005–1009.
- (139) Richman, E. K.; Hutchison, J. E. *ACS Nano* **2009**, *3*, 2441–2446.
- (140) Song, C.; Yu, W.; Zhao, B.; Zhang, H.; Tang, C.; Sun, K.; Wu, X.; Dong, L.; Chen, Y. *Catal. Commun.* **2009**, *10*, 650–654.
- (141) Cui, X.; Zhong, S.; Yan, J.; Wang, C.; Zhang, H.; Wang, H. *Colloids Surf. A: Physicochemical and Engineering Aspects* **2010**, *360*, 41–46.
- (142) Green, D. L.; Lin, J. S.; Lam, Y.-F.; Hu, M. Z. C.; Schaefer, D. W.; Harris, M. T. *J. Colloid Interface Sci.* **2003**, *266*, 346–358.
- (143) Reimer, L., *Scanning electron microscopy: physics of image formation and microanalysis*; Springer series in optical sciences, **1998**, xviii, 457 pages.
- (144) Atkins, P. W.; De Paula, J., *Physical chemistry*, 9th; W.H. Freeman: New York, **2010**, xxi, 1139 p.

- (145) Klein, T.; Buhr, E.; Georg Frase, C. In *Advances in Imaging and Electron Physics*, Hawkes, P. W., Ed.; Elsevier: 2012, pp 297–356.
- (146) Santos, N. C.; Castanho, M. A. *Biophys. J.* **1996**, *71*, 1641–1650.
- (147) Cho, E. J.; Holback, H.; Liu, K. C.; Abouelmagd, S. A.; Park, J.; Yeo, Y. *Mol. Pharm.* **2013**, *10*, 2093–2110.
- (148) Schmidt, W., *Optische Spektroskopie: Eine Einführung*, 2. Auflage; Wiley-VCH: Weinheim, **2000**, 320 p.
- (149) Valeur, B., *Molecular fluorescence: principles and applications*; Wiley-VCH: Weinheim ; New York, **2002**, xiv, 387 p.
- (150) Lakowicz, J. R., *Principles of fluorescence spectroscopy*; Springer: New York, **2006**, xxvi, 954 p.
- (151) Würth, C.; Pauli, J.; Lochmann, C.; Spieles, M.; Resch-Genger, U. *Anal. Chem.* **2012**, *84*, 1345–1352.
- (152) Würth, C.; Grabolle, M.; Pauli, J.; Spieles, M.; Resch-Genger, U. *Anal. Chem.* **2011**, *83*, 3431–3439.
- (153) Würth, C.; Grabolle, M.; Pauli, J.; Spieles, M.; Resch-Genger, U. *Nat. Protoc.* **2013**, *8*, 1535–1550.
- (154) Hennig, A.; Hoffmann, A.; Borchering, H.; Thiele, T.; Schedler, U.; Resch-Genger, U. *Chem. Commun.* **2011**, *47*, 7842–7844.
- (155) Wen, C.-Y.; Sun, J.-Y. *ChemistrySelect* **2017**, *2*, 10885–10888.
- (156) Klučáková, M. *React. Funct. Polym.* **2018**, *128*, 24–28.
- (157) Beck, S.; Méthot, M.; Bouchard, J. *Cellulose* **2015**, *22*, 101–116.
- (158) Fras, L.; Laine, J.; Stenius, P.; Stana-Kleinschek, K.; Ribitsch, V.; Doleček, V. *J. Appl. Polym. Sci.* **2004**, *92*, 3186–3195.
- (159) Martín-Domínguez, A.; Lara-Sánchez, A.; Hansen-Hansen, A. M.; Alarcón-Herrera, M. T. *Environ. Sci. Pollut. Res.* **2016**, *23*, 12085–12094.
- (160) Selitrenikov, A. V.; Zevatskii, Y. E. *Russ. J. Gen. Chem.* **2015**, *85*, 7–13.
- (161) Mousseau, F.; Vitorazi, L.; Herrmann, L.; Mornet, S.; Berret, J. F. *J. Colloid Interface Sci.* **2016**, *475*, 36–45.
- (162) Cloarec, J.-P.; Chevalier, C.; Genest, J.; Beauvais, J.; Chamas, H.; Chevolot, Y.; Baron, T.; Souifi, A. *Nanotechnology* **2016**, *27*, 295602.
- (163) Kawaguchi, S.; Yekta, A.; Winnik, M. A. *J. Colloid Interface Sci.* **1995**, *176*, 362–369.
- (164) Sauzedde, F.; Ganachaud, F.; Elaïssari, A.; Pichot, C. *J. Appl. Polym. Sci.* **1997**, *65*, 2331–2342.

-
- (165) Henglein, A.; Meisel, D. *J. Phys. Chem. B* **1998**, *102*, 8364–8366.
- (166) Randelović, M.; Momčilović, M.; Purenović, M.; Zarubica, A.; Bojić, A. *Environ. Earth Sci.* **2016**, *75*, 764.
- (167) Gorris, H. H.; Saleh, S. M.; Groegel, D. B. M.; Ernst, S.; Reiner, K.; Mustroph, H.; Wolfbeis, O. S. *Bioconjugate Chem.* **2011**, *22*, 1433–1437.
- (168) Saleh, S. M.; Ali, R.; Wolfbeis, O. S. *Microchim. Acta* **2011**, *174*, 429–434.
- (169) Wetzl, B. K.; Yarmoluk, S. M.; Craig, D. B.; Wolfbeis, O. S. *Angew. Chem. Int. Ed.* **2004**, *43*, 5400–5402.
- (170) Yang, Y.; Verhelst, S. H. L. *Chem. Commun.* **2013**, *49*, 5366–5368.
- (171) Smith, P. K.; Krohn, R. I.; Hermanson, G. T.; Mallia, A. K.; Gartner, F. H.; Provenzano, M. D.; Fujimoto, E. K.; Goeke, N. M.; Olson, B. J.; Klenk, D. C. *Anal. Biochem.* **1985**, *150*, 76–85.
- (172) Olson, B. J.; Markwell, J. *Curr. Protoc. Protein Sci.* **2007**, *48*, 3.4.1–3.4.29.
- (173) Cammann, K., *Instrumentelle Analytische Chemie: Verfahren, Anwendungen, Qualitätssicherung*; Spektrum Akademischer Verlag GmbH: Heidelberg, Berlin, **2010**, 617 p.
- (174) Cazes, J.; Ewing, G. W., *Ewing's analytical instrumentation handbook*, 3rd ed.; Marcel Dekker: New York, **2005**, xxiv, 1037 p.
- (175) Luan, J.; Feng, R.; Yu, C.; Wu, X.; Shen, W.; Chen, Y.; Di, B.; Su, M. *Anal. Sci.* **2018**, *34*, 1093–1098.
- (176) Khatun, R.; Hunter, H. N.; Sheng, Y.; Carpick, B. W.; Kirkitadze, M. D. *J. Pharm. Biomed. Anal.* **2018**, *159*, 166–172.
- (177) Owczarek, A.; Klys, A.; Olszewska, M. A. *Talanta* **2019**, *192*, 263–269.
- (178) Morris-Cohen, A. J.; Malicki, M.; Peterson, M. D.; Slavin, J. W. J.; Weiss, E. A. *Chem. Mater.* **2012**, *25*, 1155–1165.
- (179) Zeng, B.; Palui, G.; Zhang, C.; Zhan, N.; Wang, W.; Ji, X.; Chen, B.; Mattoussi, H. *Chem. Mater.* **2017**, *30*, 225–238.
- (180) Ji, X.; Copenhaver, D.; Sichmeller, C.; Peng, X. *J. Am. Chem. Soc.* **2008**, *130*, 5726–5735.
- (181) Crucho, C. I.; Baleizao, C.; Farinha, J. P. *Anal. Chem.* **2017**, *89*, 681–687.
- (182) Melanson, J. E.; Thibeault, M.-P.; Stocks, B. B.; Leek, D. M.; McRae, G.; Meija, J. *Anal. Bioanal. Chem.* **2018**, *410*, 6719–6731.

A Appendix

A.1 Publications and planned publications

Publications

- 1) M. R. Shreykar, N. Scholz, A. Jadhav, T. Behnke, N. Nirmalananthan, S. Kothavale, U. Resch-Genger, N. Sekar, “Fluorescent Coumarin-Rhodamine Hybrids - Synthesis and spectroscopic properties “, *J. Fluoresc.* **2017**, *27*, 1949–1956. (not included in the thesis)
- 2) M. Denißen, N. Nirmalananthan, T. Behnke, K. Hoffmann, U. Resch-Genger, T. J. J. Müller, “3-Piperazinyl propenylidene indolone merocyanines – consecutive three-component synthesis and electronic properties of solid state luminophores with AIE properties“, *Mater. Chem. Front.* **2017**, *1*, 2013-2026. (included in the thesis)
- 3) N. Nirmalananthan, T. Behnke, K. Hoffmann, D. Kage, C. F. Gers-Panther, W. Frank, T. J. J. Müller, U. Resch-Genger, “Crystallization and Aggregation-Induced Emission in a Series of Pyrrolidinylvinylquinoxaline Derivatives”, *J. Phys. Chem. C* **2018**, *122*, 11119–11127. (included in the thesis)
- 4) M. Moser,[§] N. Nirmalananthan,[§] T. Behnke, D. Geißler, U. Resch-Genger, “Multimodal Cleavable Reporters versus Conventional Labels for Optical Quantification of Accessible Amino and Carboxy Groups on Nano- and Microparticles”, *Anal. Chem.* **2018**, *90*, 5887–5895. (included in the thesis, [§] equal contribution)
- 5) A. Roloff, N. Nirmalananthan-Budau, B. Rühle, H. Borcharding, T. Thiele, U. Schedler and U. Resch-Genger, “Quantification of Aldehydes on Polymeric Microbead Surfaces via Catch and Release of Reporter Chromophores”, submitted to *Anal. Chem.* (included in the thesis)
- 6) N. Nirmalananthan-Budau, J. Horst Budau, D. Moldenhauer, W. Kraus, K. Hoffmann, B. Paulus, and U. Resch-Genger, “Control of Aggregation-induced Emission in Donor-Acceptor-Donor Dyes: Dual Propeller-like Donors vs. Propeller-like and Planar Donors”, submitted to *Phys. Chem. Chem. Phys.* (not included in the thesis)

7) N. Nirmalanathan-Budau, B. Rühle, D. Geißler, M. Moser, C. Kläber, A. Schäfer, U. Resch-Genger, “Multimodal Cleavable Reporters for Quantifying Carboxy and Amino Groups on Organic and Inorganic Nanoparticles”, submitted to *Sci. Rep.* (included in the thesis)

Planned publications

1) M. Denißen, R. Hannen, D. Itskalov, N. Nirmalanathan-Budau, K. Hoffmann, G. J. Reiss, U. Resch-Genger, T. J. J. Müller, “Dually Aggregation-induced White-light Emissive Bichromophore by Consecutive Four-component Synthesis”, in preparation.

2) N. Nirmalanathan-Budau, D. Geißler, B. Rühle, A. Schäfer, U. Resch-Genger, “Optical Quantification of Accessible Carboxy and Amino Surface Functional Groups on Polystyrene Nanoparticles with New Generation Multimodal Cleavable Reporter”, in preparation.

3) A. Müller, T. Heinrich, V. Kunz, J. Radnik, J. M. Stockmann, N. Nirmalanathan-Budau, D. Geißler, K. Sparnacci, W. E. S. Unger, “Studying PTFE-PS core-shell Nanoparticles with incomplete Shell: PCA assisted ToF-SIMS clearly distinguishes different Degrees of Core Encapsulation by the Shell Material ”, in preparation.

4) Z. You, N. Nirmalanathan-Budau, B. Rühle, U. Resch-Genger, S. Weidner “Separation and Surface Groups Quantification of Polystyrene and Silica Nanoparticles using Capillary Electrophoresis (CE) and asymmetrical Flow-Field-Flow Fractionation (AF4)”, in preparation.

A.2 Conference contributions

1) N. Nirmalanathan, T. Behnke, U. Resch-Genger, C. Gers, H. Fischer, T.J.J. Müller, A Series of New Pyrrolidinylvinylquinoxaline Derivatives as possible fluorescent nanoreporters with Aggregation-Induced Emission (AIE), **Poster Presentation** at the 14th Conference on methods and applications of fluorescence, Würzburg, 2015

2) N. Nirmalanathan, T. Behnke, C. Gers, H. Fischer, T.J.J. Müller, U. Resch-Genger, A Series of New Pyrrolidinylvinylquinoxaline Derivatives as possible fluorescent nanoreporters with Aggregation-Induced Emission (AIE), **Poster Presentation** at Potsdam Days Bioanalysis, Potsdam, 2015

- 3) N. Nirmalanathan, T. Behnke, K. Hoffmann, D. Kage, C. F. Gers, T.J.J. Müller, U. Resch-Genger, New pyrrolidinylvinylquinoxaline derivatives with aggregation-induced emission as possible fluorescent nanoreporters, **Poster Presentation** at Innovation Forum Senftenberg, Senftenberg, 2016
- 4) N. Nirmalanathan, M. Moser, T. Behnke, U. Resch-Genger, Optical Methods for the Quantification of Functional Groups on Particle Surfaces, **Oral Presentation** at the 10th German BioSensor Symposium, Potsdam, 2017
- 5) N. Nirmalanathan, M. Moser, T. Behnke, U. Resch-Genger, New Approaches for the Quantification of Functional Groups on Micro- and Nanoparticle Surfaces, **Oral Presentation** at ANAKON, Tübingen, 2017
- 6) N. Nirmalanathan, M. Moser, T. Behnke, U. Resch-Genger, Quantification of Surface Groups on Core-Shell Polymer Particles with Optical Spectroscopy, **Poster Presentation** at Analytik bewegt, Berlin, 2017
- 7) T. Behnke, M. Moser, N. Nirmalanathan, U. Resch-Genger, Spectroscopic quantification of surface groups on micro- and nanoparticles, **Oral Presentation** at 253rd ACS National Meeting, San Francisco, 2017
- 8) N. Nirmalanathan, M. Moser, T. Behnke, R. Schneider, U. Resch-Genger, Functional group analysis on 3D carrier materials with simple optical assays, **Oral Presentation** at the Colloquium of Optical Spectrometry, Berlin, 2017
- 9) N. Nirmalanathan, M. Moser, T. Behnke, D. Geißler, U. Resch-Genger, Multimodal cleavable reporters vs conventional labels for optical quantification of amino and carboxy groups on nanomaterials and microparticles, **Oral Presentation** at BAM-BfR Seminar, Berlin, 2018
- 10) N. Nirmalanathan, M. Moser, T. Behnke, D. Geißler, U. Resch-Genger, Multimodal cleavable reporters for the optical quantification of functional groups on nano- and microparticles, **Poster Presentation** at INNANOPART Open day, London, 2018
- 11) D. Geißler, N. Nirmalanathan, M. Moser, U. Resch-Genger, Synthesis of polymeric nanoparticles with different surface group densities and their characterisation using multimodal cleavable reporters and lanthanide tags, **Poster Presentation** at INNANOPART Open day, London, 2018

- 12) U. Resch-Genger, N. Nirmalanathan, M. Moser, D. Geißler, T. Behnke, R. Schneider, Simple and Versatile Methods for Quantifying Functional Groups, Ligands, and Biomolecules on Nanomaterials, **Oral Presentation** at INNANOPART Open day, London, 2018
- 13) N. Nirmalanathan, M. Moser, T. Behnke, D. Geißler, U. Resch-Genger, Functional group analysis on Nanoparticles with simple optical assays, **Poster Presentation** at PTB-BAM Nanoworkshop, Berlin, 2018
- 14) N. Nirmalanathan, M. Moser, D. Geißler, T. Behnke, R. Schneider, U. Resch-Genger, Simple and Validated Methods for Quantifying Functional Groups, Ligands, and Biomolecules on Nanomaterials, **Poster Presentation** at PTB-BAM Nanoworkshop, Berlin, 2018
- 15) N. Nirmalanathan-Budau, M. Moser, T. Behnke, D. Geißler, U. Resch-Genger, Optical Quantification of Surface Groups on Nanoparticles with Multimodal Cleavable Reporters, **Poster Presentation** at NanoTox 2018 - 9th International Conference on Nanotoxicology, Neuss, 2018
- 16) U. Resch-Genger, N. Nirmalanathan-Budau, M. Moser, A. Roloff, D. Moldenhauer, Quantification of Surface Groups on Nanomaterials with Simple Optical Methods, **Oral Presentation** at JRC-NIST Workshop, Italy, 2018